Damping Effects of Drogue Parachutes on Orion Crew Module Dynamics

Vanessa V. Aubuchon

Thesis submitted to the faculty of the Virginia Polytechnic Institute and State University
in partial fulfillment of the requirements for the degree of

Master of Science
In
Aerospace Engineering

Dr. Mayuresh Patil, Committee Chair
Dr. Craig Woolsey
Dr. D. Bruce Owens

July 1, 2013
Blacksburg, VA

Keywords: Parachutes, Forced Oscillation, Damping, Blunt Body Reentry Vehicle,
Dynamic Derivatives

Damping Effects of Drogue Parachutes on Orion Crew Module Dynamics

Vanessa V. Aubuchon

ABSTRACT

Currently, simulation predictions of the Orion Crew Module (CM) dynamics with drogue parachutes deployed are under-predicting the amount of damping as seen in free-flight tests. The Apollo Legacy Chute Damping model has been resurrected and applied to the Orion system. The legacy model has been applied to predict CM damping under drogue parachutes for both Vertical Spin Tunnel free flights and the Pad Abort-1 flight test. Comparisons between the legacy Apollo prediction method and test data are favorable. A key hypothesis in the Apollo legacy drogue damping analysis is that the drogue parachutes' net load vector aligns with the CM drogue attachment point velocity vector. This assumption seems reasonable and produces good results, but has never been quantitatively proven. The wake of the CM influences the drogue parachutes, which makes performance predictions of the parachutes difficult. Many of these effects are not currently modeled in the simulations.

A forced oscillation test of the CM with parachutes was conducted in the NASA LaRC 20-Ft Vertical Spin Tunnel (VST) to gather additional data to validate and refine the Apollo legacy drogue model. A second loads balance was added to the original Orion VST model to measure the drogue parachute loads independently of the CM. The objective of the test was to identify the contribution of the drogues to CM damping and provide additional information to quantify wake effects and the interactions between the CM and parachutes. The drogue parachute force vector was shown to be highly dependent on the CM wake characteristics. Based on these wind tunnel test data, the Apollo Legacy Chute Damping model was determined to be a sufficient approximation of the parachute dynamics in relationship to the CM dynamics for preliminary entry vehicle system design. More wake effects should be included to better model the system. These results are being used to improve simulation model fidelity of CM flight with drogues deployed, which has been identified by the project as key to a successful Orion Critical Design Review.

Dedication

For my husband, Kahlil Stubbs, who stood by my side and offered enormous amounts of encouragement and support throughout the course of this research, despite life's discouragements and distractions.

Acknowledgements

Foremost, I would like to express my sincere thanks to my mentor, Dr. Bruce Owens. I cannot imagine where I would be without his expert guidance and unwavering support over the last 9 years.

I thank Sue Grafton, Earl Harris, Clinton Duncan, Wes O'Neal, Lee Pollard, and Gene Adams of the NASA Langley Flight Dynamics Branch for their technical support of the wind tunnel test.

I thank Joe Gamble who resurrected the Apollo chute damping model and provided his expertise.

I thank Mike Fremaux who, as my supervisor, has encouraged me strongly to get this thesis finished.

I thank Pete Macaluso and Reggie Riddle at AEDC. They never complained once as they navigated through the red tape and bureaucracy to loan me the hardware instrumental in accomplishing this research.

Table of Contents

List of Figures

List of Tables

Chapter 1

Introduction

The objective of the research presented in this paper is to examine clustered drogue parachute behavior in a blunt-body reentry vehicle's wake and the effect of the parachute behavior on the vehicle's dynamics. Specifically, this research is needed to validate a simple Apollo-era mathematical model of the drogue parachute's effect on the Orion Crew Module (CM) dynamics.

Currently, simulation predictions of the CM dynamics with drogue parachutes deployed are under-predicting the amount of damping compared to that seen in free-flight tests. The Apollo Legacy Chute Damping model has been resurrected and applied to the Orion system. The legacy model has been applied to predict CM damping under drogue parachutes for both NASA Langley 20-Foot Vertical Spin Tunnel free flights and the Pad Abort-1 flight test. Comparisons between the legacy Apollo prediction method and test data are favorable.

A key hypothesis in the Apollo legacy drogue damping model is that the drogue parachutes' net load vector aligns with the CM drogue attachment point velocity vector. This assumption seems reasonable and produces good results, but has never been quantitatively proven.

A forced oscillation test of the CM with parachutes was conducted in the NASA LaRC 20-Foot Vertical Spin Tunnel (VST) to gather additional data to validate and refine the Apollo legacy drogue model. A second loads balance was added to the original VST model to measure the drogue parachute loads independently of the CM. The wake of the CM influences the drogue parachutes, which makes performance predictions of the parachutes difficult. Significant interactions exist between the CM and the drogue parachutes, which vary with CM angle of attack. Many of these effects are not currently modeled in the simulations, and what is modeled is not anchored to test data. The objective of the test was to identify the contribution of the drogues to CM damping and provide additional information to quantify wake effects and the interactions between the CM and parachutes. These results are being used to improve simulation model fidelity of CM flight with drogues deployed, which has been identified by the project as key to a successful Critical Design Review.

1.1 Overview of Orion Multi-Purpose Crew Vehicle

NASA's plan for human space exploration calls for a long term exploration to an asteroid and eventually to Mars. These goals require the development of a new spacecraft known as the Orion Multi-Purpose Crew Vehicle (MPCV), which is based on the cancelled Crew Exploration Vehicle design requirements for traveling beyond Low Earth Orbit [1]. The Orion MPCV is based on a design similar to the Apollo program's Command and Service Modules and is composed of four main elements: the Launch Abort System, the Crew Module, the Service Module, and the Spacecraft Adapter as shown in Figure 1-1 [2]. The

Launch Abort System provides a reliable abort capability for aborts that occur within the atmosphere. The Launch Abort System is jettisoned after the launch vehicle exits the Earth's atmosphere. The Crew Module (CM) provides a safe habitable volume for the crew during launch, spaceflight, and return through the atmosphere. The Service Module provides additional resources necessary to support the primary mission, including power and maneuvering capability. The Service Module is also used to provide abort capability for exo-atmospheric aborts. The Spacecraft Adapter provides the interface between the spacecraft and the launch vehicle.

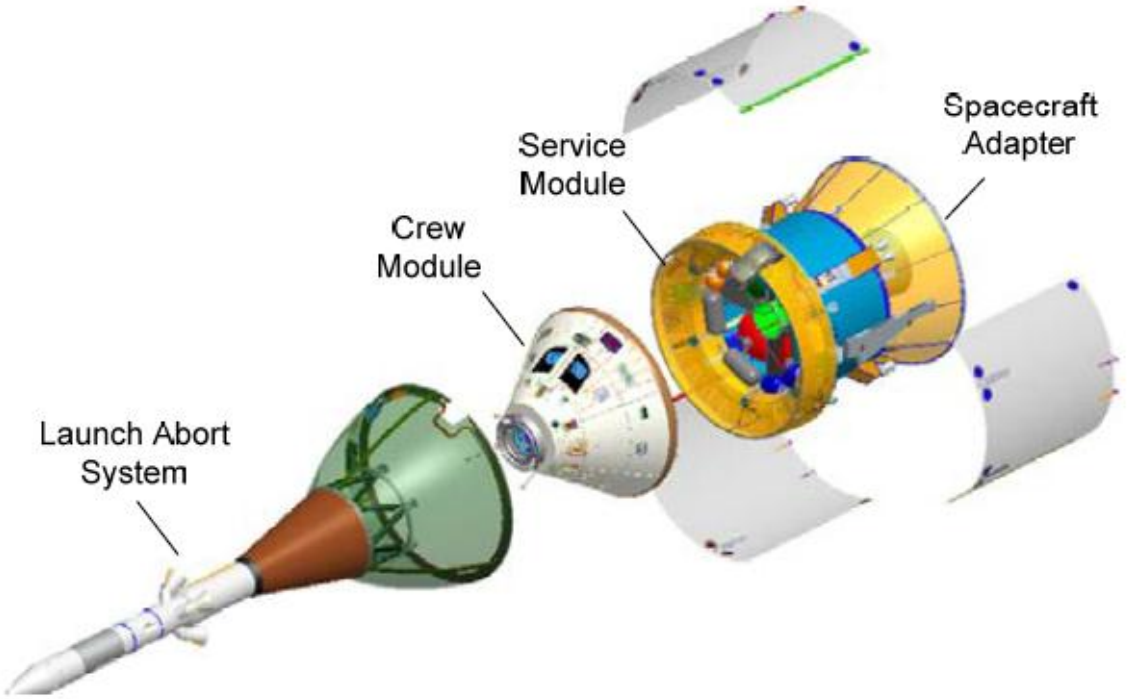

Figure 1-1: Orion Multi-Purpose Crew Vehicle (MPCV).

During reentry, the drogue parachutes provide damping of vehicle oscillations and drag to slow down the vehicle for successful deployment of main parachutes. The CM is shown in Figure 1-2 with a cutout to display the crew position. The reentry parachute

sequence is presented in Figure 1-3. CM flight under the drogue parachutes occurs both during nominal reentry and during reentry after an abort from a failed launch. First, a mortar is deployed and three Forward Bay Cover parachutes (FBCPs) are released to remove the Forward Bay Cover (FBC). Then, a mortar deploys two drogue parachutes, which have two reefing stages before they are fully open. The drogues are released and the pilot chutes are deployed to pull out three large main parachutes. The main parachutes go through two reefing stages before they are fully open and slow the CM for a gentle water landing. The fully-open drogue parachute part of the sequence is the focus of this research.

Figure 1-2: Orion Crew Module (CM).

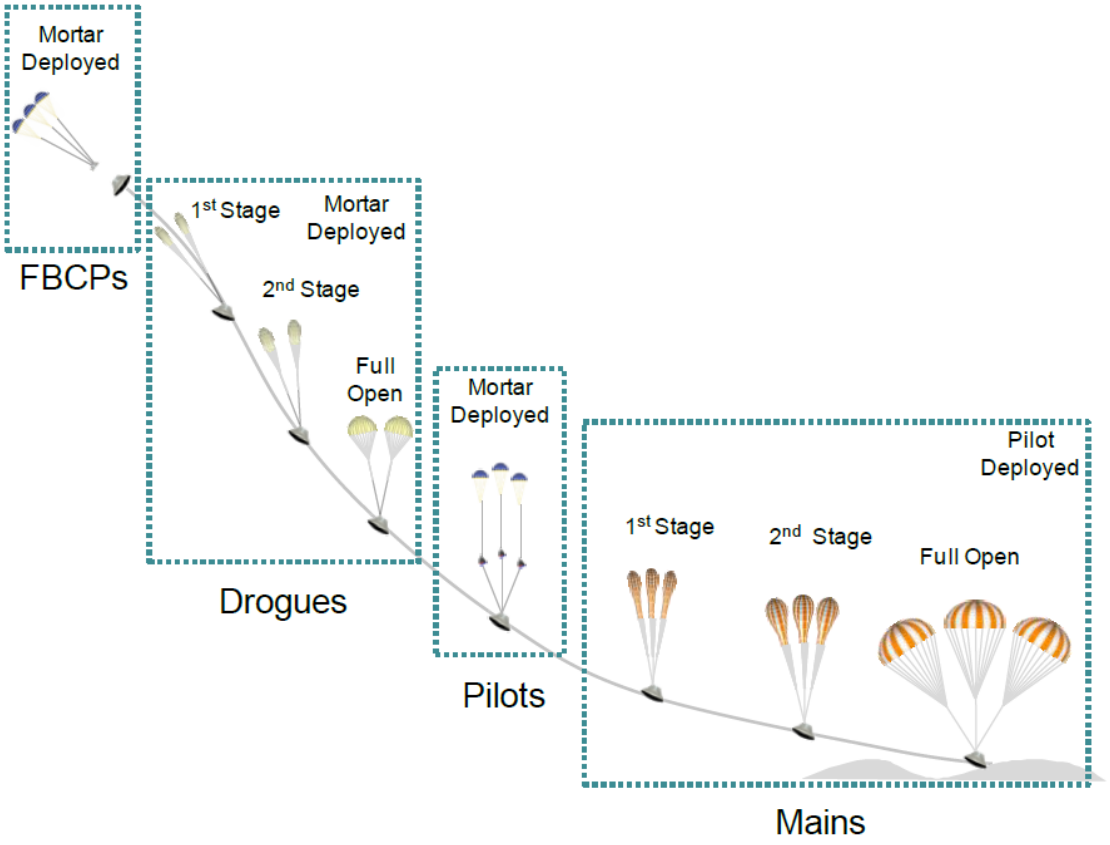

Figure 1-3: Reentry parachute sequence for Crew Module.

1.2 Overview of Simulation Modeling of Crew Module Dynamics with Drogue Parachutes

Simulation results have predicted more severe dynamics of the CM with drogues fully deployed than was seen in full-scale flight tests, including Orion's Pad Abort-1, as well as dynamically-scaled model tests in the NASA Langley 20-Foot Vertical Spin Tunnel [3] [4] [5]. A concern is that the simulations are not accurately calculating the total system damping.

One of the simulations used to model the CM-parachute system is called Decelerator System Simulation (DSS) [6]. DSS is a multi-body simulation that models vehicle and parachute dynamics, as well as parachute deployment. Both the parachute and CM are modeled as six degree-of-freedom bodies attached by an elastic riser. DSS does not directly model the total system damping. Damping behavior is instead captured through the elastic coupling of the parachutes and CM. The two drogue parachutes are treated as one with an equivalent surface area and drag. DSS's heritage includes the Solid Rocket Booster recovery system, X-38, and Orion Capsule Parachute Assembly Team (CPAS) testing. The DSS prediction of CM dynamics under drogue parachutes is compared to motions observed in the Pad Abort-1 and VST free-flight tests. Those tests are described below and followed by a comparison of the DSS predictions to a VST free-flight run.

The Pad Abort-1 (PA-1) [7] flight test was conducted at White Sands Missile Range, New Mexico on May 6, 2010. This test was designed to demonstrate the viability of the Orion Launch Abort System (LAS) to perform an abort from a launch vehicle on the pad. The PA-1 flight profile is shown in Figure 1-4. The LAS is initiated on the ground by igniting the Abort Motor (AM), which provides the thrust to pull the vehicle away from the pad during an abort, and the Attitude Control Motor (ACM), which provides the yaw and pitch control of the LAS during an abort. After the steering and coast phases, the launch abort vehicle is reoriented in order to jettison the launch abort tower. The re-entry parachutes are then deployed from the CM. The portion of the flight when the drogue parachutes are fully deployed, shown in Figure 1-5, is compared to simulation models of the CM-drogue parachute system dynamics.

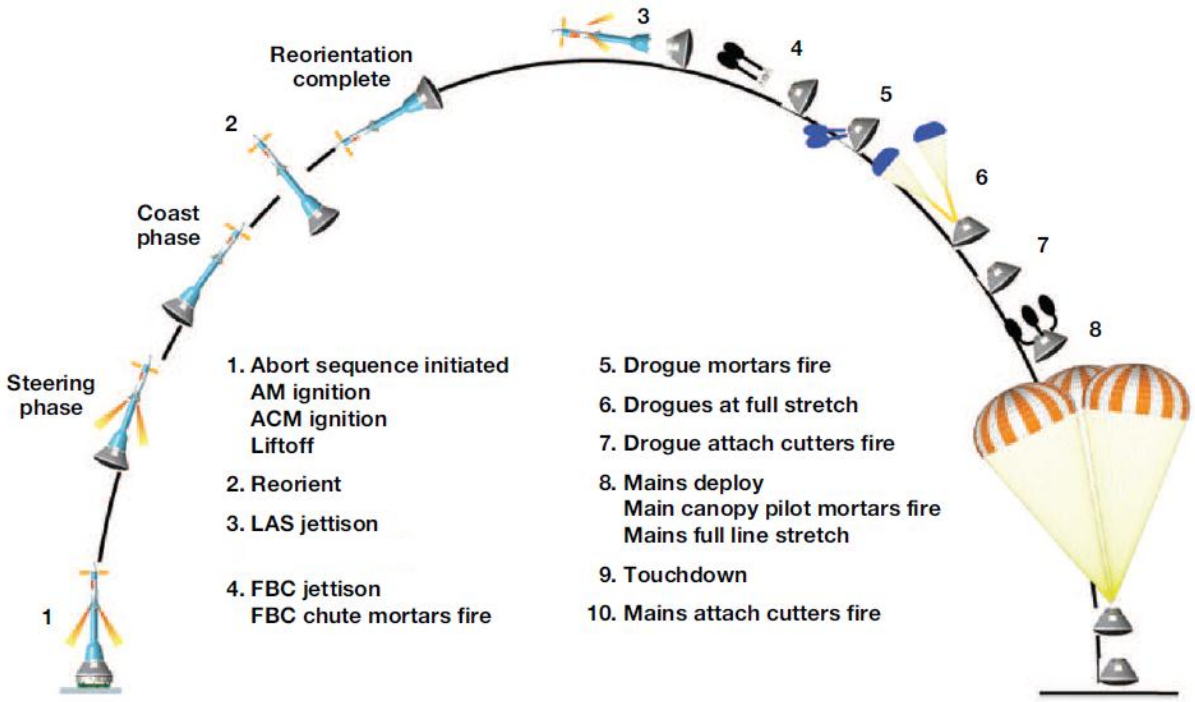

Figure 1-4: Launch Abort System PA-1 flight profile.

Figure 1-5: PA-1 CM flight with drogue parachutes.

The low-speed, subscale free-flight test of the CM-drogue parachute system was conducted in the NASA Langley 20-Foot Vertical Spin Tunnel (VST) [5]. A $1/16^{th}$-scale model of the CM was dynamically scaled to represent the full-scale vehicle in center of gravity location, weight, and moments of inertia. Attitude and position time histories were recorded with an optical data acquisition system. The attitude time history data from this test was used to compare to simulation models of the system dynamics.

DSS, along with other simulation models, do not accurately predict CM dynamics under drogue parachutes when compared to motions observed in the free-flight tests discussed above. An angle of attack time history of a VST subscale free-flight test compared to the DSS prediction is shown in Figure 1-6 [8]. The VST free-flight test shows that the CM

oscillatory motion is more damped than DSS predicts. Since the center of gravity of the CM is offset from the vehicle centerline in the pitch plane, and the drogue parachutes are offset in the pitch plane, the majority of the oscillatory motion is in the pitch plane. For this reason, most of the data presented in this paper will focus on pitch plane motion.

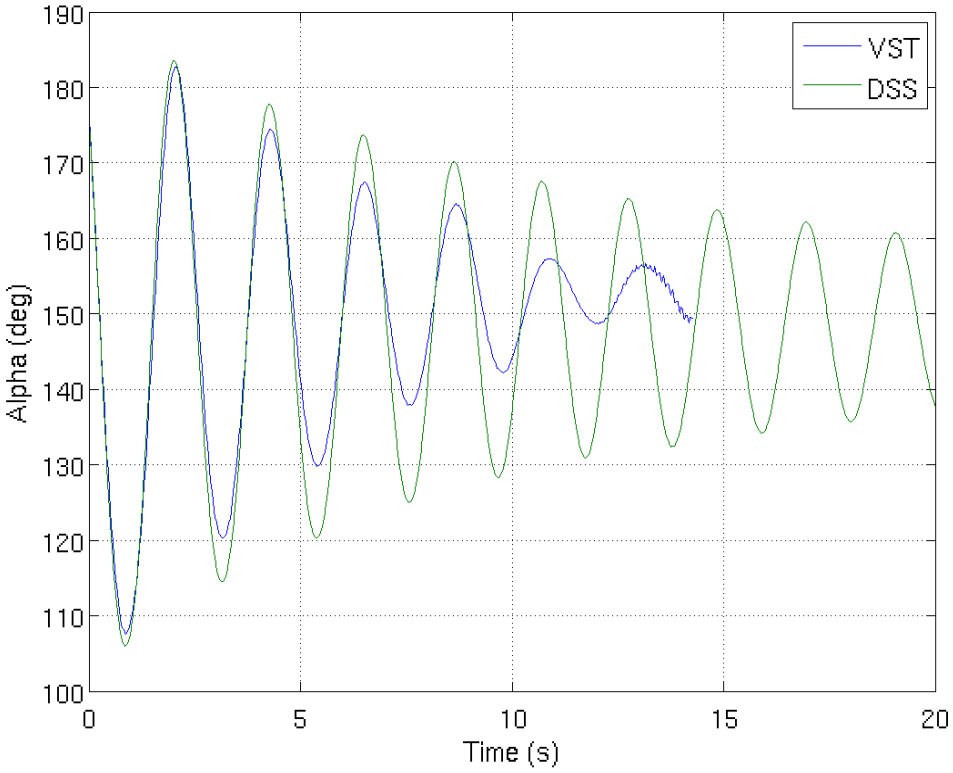

Figure 1-6: Angle of attack time history: DSS analytical simulation versus VST subscale free-flight test [8].

1.3 Apollo Legacy Chute Damping Model

The Apollo program implemented a simple chute damping model that coupled the CM dynamics to the drogue parachute behavior. The model is described in this section, and equations for the chute contribution to the system dynamics are derived in [8]. This model's assumptions will be compared to wind tunnel test measurements presented later in this paper.

The Apollo Legacy Chute Damping model is based on the hypothesis that the drogue parachute force vector aligns with the resultant velocity of the parachute attach point on the CM. Drogue damping is provided by a hysteresis in the moment arm of the drogue parachute force as the drogue aligns with the resultant velocity of the attach point during cyclic motion [8]. The two drogue parachutes are treated as one with an equivalent surface area and drag.

First, the static moment provided by the drogue parachutes is examined. The Apollo drogue model makes the assumption that the drogue force vector aligns with the freestream velocity vector. The moment provided by the chutes is shown in (1.1).

$$M_{chute} = (C_D S)_{chute} * \bar{q}_{chute} * L \tag{1.1}$$

The force produced by the chutes is the full-scale drag area, $(C_D S)_{chute}$, multiplied by the dynamic pressure, $\bar{q}_{chute}$. The full-scale drag area is the drag coefficient, C_D, multiplied

by the circular area of the flat parachute, S. The moment arm, L, is the perpendicular distance from the parachute force vector to the center of gravity of the CM. This is illustrated in Figure 1-7. The moment arm, L, is equal to the distance from the CM center of gravity to the parachute attach point, R, multiplied by the sine of the angle, Δα, between the R vector and the freestream velocity vector, V_∞. The moment provided by the chutes can be rewritten as in (1.2).

$$M_{chute} = (C_D S)_{chute} * \bar{q}_{chute} * R * \sin \Delta\alpha \tag{1.2}$$

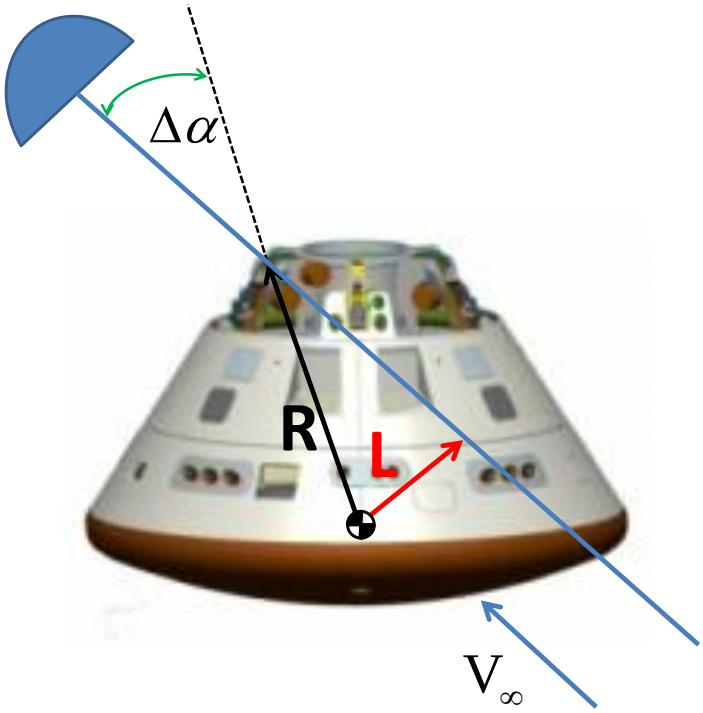

Figure 1-7: Diagram of parachute pitching moment components for static CM used in the Apollo Legacy Chute Damping model.

The rate derivative of the pitching moment provided by the drogue parachutes in oscillatory motion is examined next. The Apollo drogue model uses the assumption that the drogue force vector aligns with the vector sum of the freestream velocity and the rotational velocity at the drogue attach point, $R \times \dot{\alpha}$. $\dot{\alpha}$ is the rate of change of angle of attack of the CM. This is illustrated in Figure 1-8. The additional moment provided by the chutes in oscillatory motion can be written as in (1.3).

$$M_{chute} = (C_D S)_{chute} * \bar{q}_{chute} * R * \sin \Delta\theta \tag{1.3}$$

$\Delta\theta$ is the angle between V_∞ and the rotated parachute due to the lag of the chute with respect to the CM angle of attack. $\Delta\theta$ can be defined as in (1.4). For small angles (less than 30°), $\tan\Delta\theta \approx \Delta\theta \approx \sin\Delta\theta$. Using the small angle approximation, the moment provided by the chutes as the CM is rotating can be rewritten as shown in (1.5).

$$tan\Delta\theta = \frac{R\dot{\alpha}}{V_\infty} \tag{1.4}$$

$$M_{chute} = (C_D S)_{chute} * \bar{q}_{chute} * \frac{R^2\dot{\alpha}}{V_\infty} \tag{1.5}$$

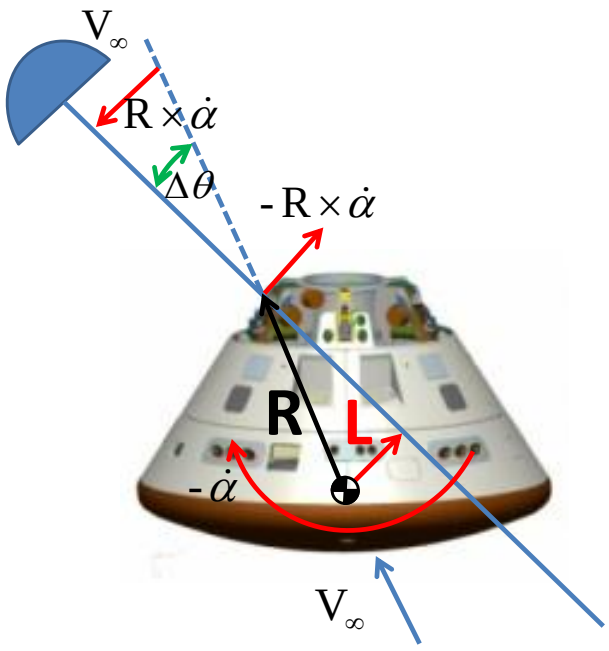

Figure 1-8: Diagram of Parachute Pitching Moment Components for Rotating CM.

The total moment provided by the drogue parachutes is calculated by adding the moments in (1.3) and (1.5). In other words, the total moment arm of the drogue parachutes force vector is $R * sin(\Delta\alpha + \Delta\theta)$, and the force magnitude is $(C_D S)_{chute} * \bar{q}_{chute}$.

An alternate method of computing the pitching moment provided by the drogue parachutes is using the equivalent Cm_α and Cm_q provided by the drogues and adding those components to the CM Cm_α and Cm_q. Cm_α is the pitching moment derivative with respect to angle of attack, α, and Cm_q is the pitching moment derivative with respect to

the non-dimensional pitch rate, $\frac{ql_{ref}}{2V_\infty}$. Reference [8] shows the derivation of these equations in detail.

The equivalent chute pitching moment coefficient slope with angle of attack is in (1.6), and can be simply added to the CM pitching moment to produce a total CM-chute pitching moment.

$$Chute\ Cm_\alpha = -\frac{(C_D S)_{chute} * \bar{q}_{chute} * R}{\bar{q}_{CM} * (S_{ref} l_{ref})_{CM}} \tag{1.6}$$

The equivalent chute pitch damping coefficient is in (1.7), and can be added to the CM pitch damping to produce a total CM-chute pitch damping coefficient.

$$Chute\ Cm_q = -\frac{2(C_D S)_{chute} * \bar{q}_{chute} * R^2}{(\bar{q} S_{ref} l_{ref}^2)_{CM}} \tag{1.7}$$

These simple Cm_α and Cm_q equations for the drogue parachute contribution could be used in preliminary design of drogue parachute damping systems. As demonstrated in Reference [8], simulation results show that using either of these equations or the build-up of the moment resulting from $\Delta\alpha$ and $\Delta\theta$ produce the same results, verifying a correct derivation.

The Apollo model has been compared to both the Pad Abort-1 and VST subscale free-flight test data [8]. The drogue parachute pitch angle from Pad Abort-1 and a simulation

utilizing the Apollo drogue parachute model is shown in Figure 1-9. The simulation used for this particular comparison is named GEMASS. Two different data sets for the drogue parachute pitch angle are plotted. One is from a computer program that tracked the average angle of the drogue parachutes relative to the CM via a camera mounted in the top of the CM looking up at the parachutes. The other is from a manual method of analyzing each video frame from that same camera. The merits of both are discussed in [8]. The simulation-predicted angle matches the measured angle very well with the exception of a small time bias and magnitude bias. These biases are corrected in the simulation data and shown in Figure 1-10. The time bias, or time shift, correction needed is 0.05 seconds. The magnitude bias, or pitch angle bias, correction is 7°. Many limitations could account for these adjustments, one of which is the wake behind the CM biasing the chutes.

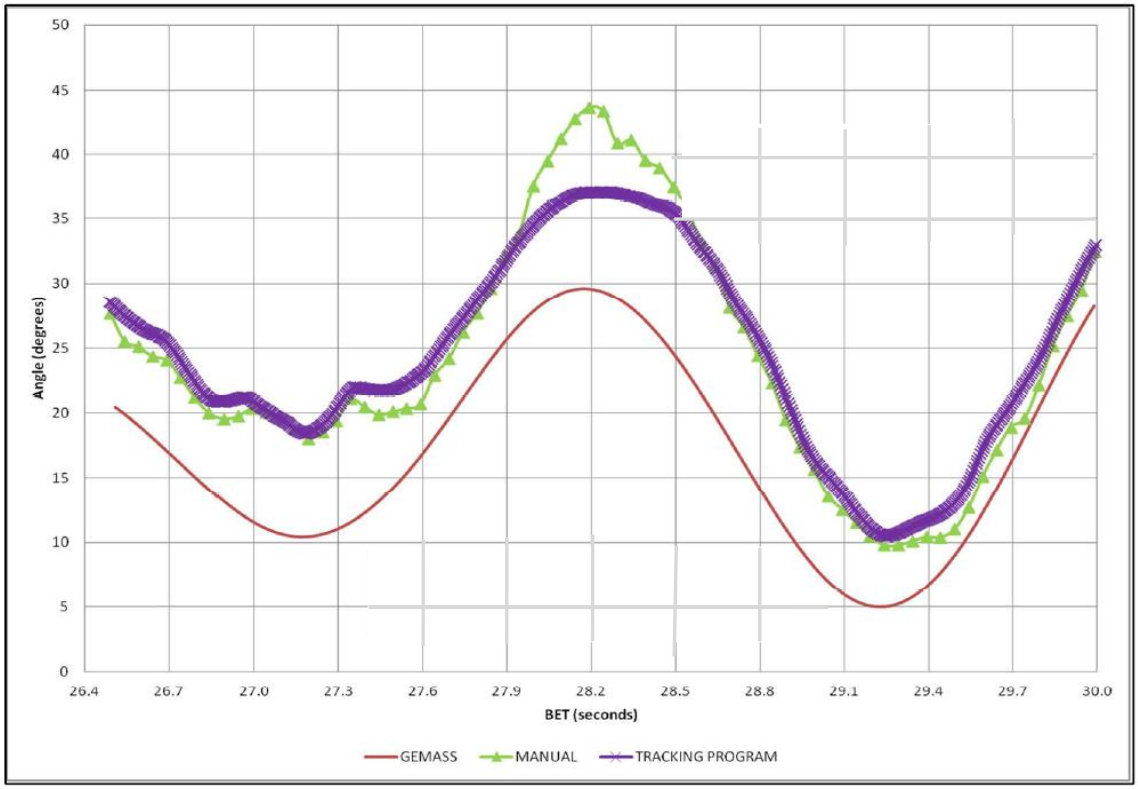

Figure 1-9: Apollo model comparison to Pad Abort-1 drogue parachute pitch angle [7].

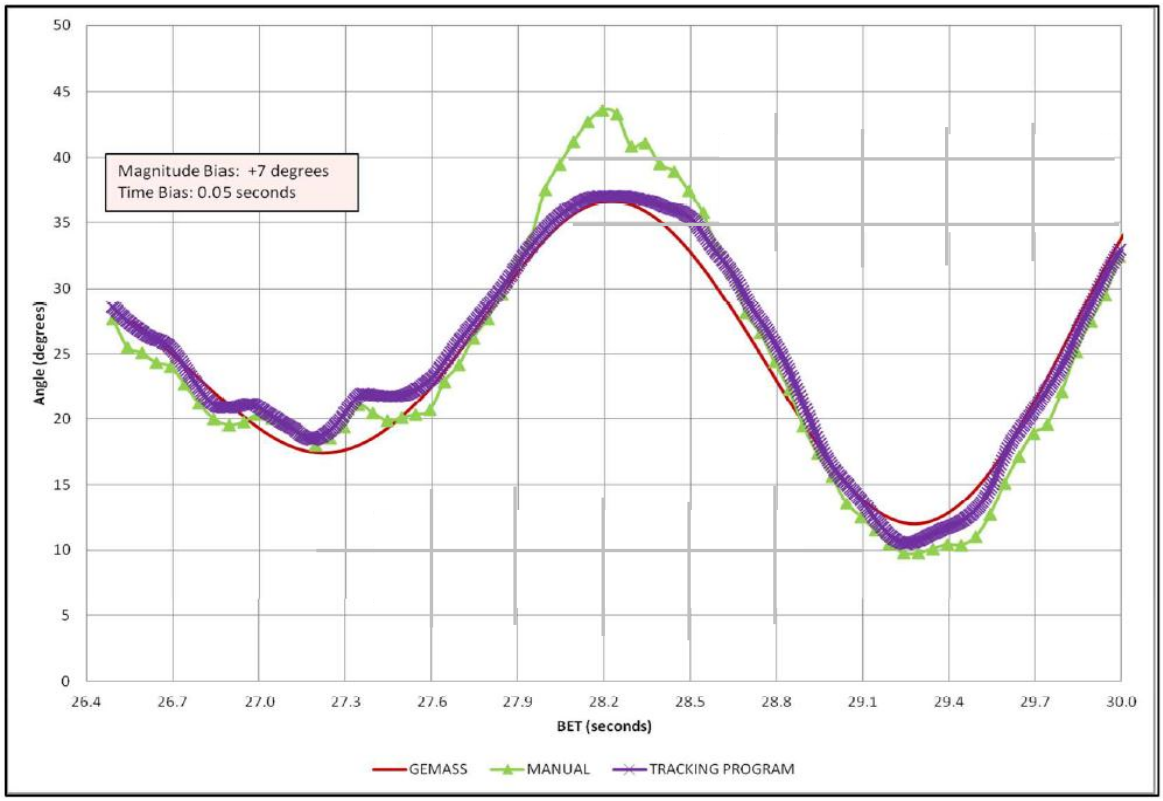

Figure 1-10: Apollo model comparison to Pad Abort-1 drogue parachute pitch angle with bias and time shift [7].

The pitch rate and angle of attack of the CM from the previous VST subscale free-flight tests is compared to simulation results with the Apollo drogue model in Figure 1-11 and Figure 1-12. A slight adjustment was made to the drogue attach point location to achieve the proper trim angle of attack. One possible explanation for this adjustment is that the translational velocity of the model in free flight in the VST was ignored in modeling. A bias in the parachute force vector will also have an effect on the trim angle of attack.

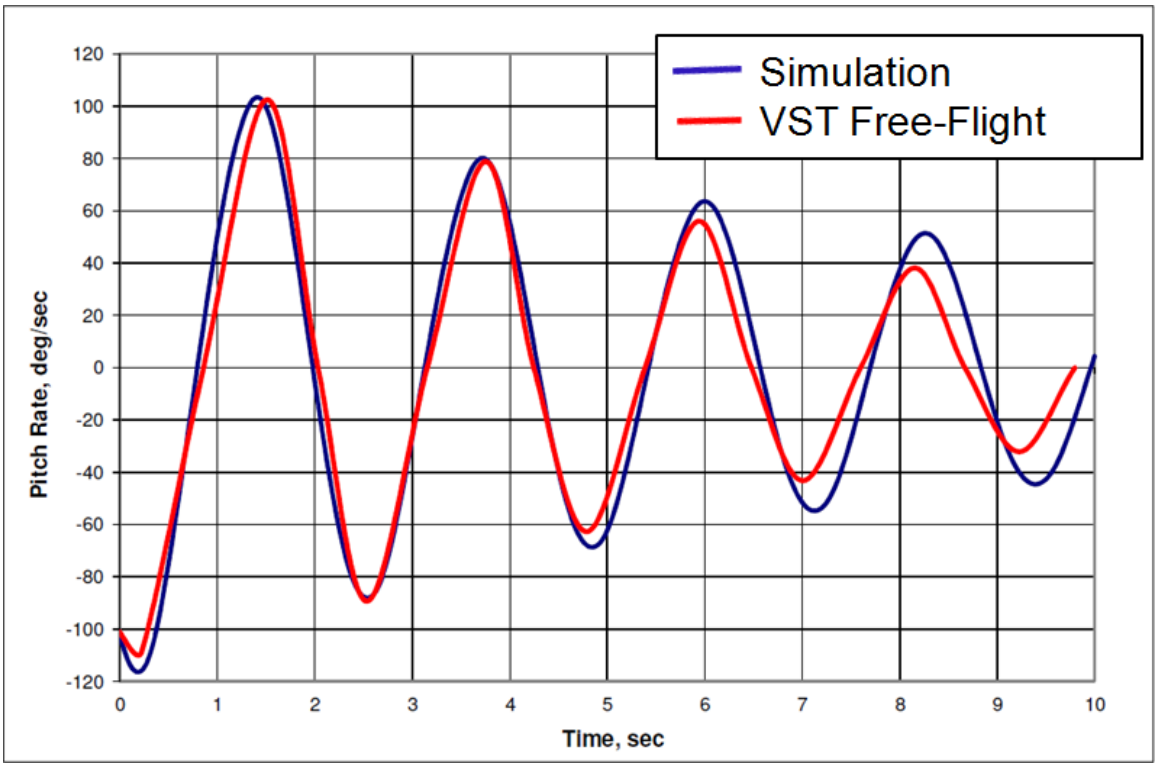

Figure 1-11: CM pitch rate time history comparison between Apollo drogue model and VST free-flight CM pitch rate [8].

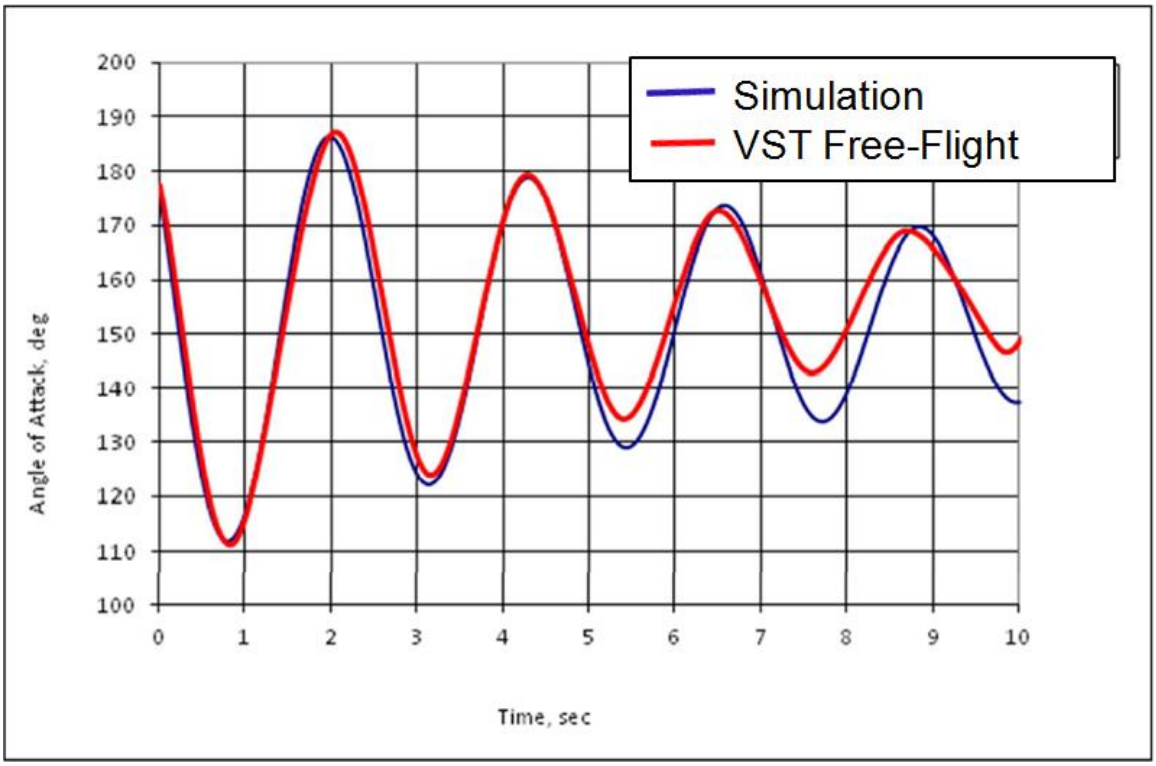

Figure 1-12: CM angle of attack time history comparison between Apollo drogue model and VST free-flight CM angle of attack [8].

The Apollo drogue model produces CM dynamics that are more representative of the damped vehicle oscillations seen in free-flight tests than the two-body parachute simulations are currently producing. If the Apollo drogue model assumptions can be validated, the Apollo model can be used to enhance the high-fidelity two-body simulations, such as DSS, so that the CM dynamics with drogue parachutes are correctly modeled.

Validation of Apollo Drogue Model through Wind Tunnel Testing

In order to validate the Apollo drogue model, an additional wind tunnel test of the CM-drogue system was conducted in the VST. The purpose of this wind tunnel test was to quantify the combined, as well as individual components, of the damping of the CM-drogue system (in the form of dynamic derivatives) using the forced oscillation technique. The data obtained from this wind tunnel test were used to assess the effectiveness of the drogue chutes in providing rate damping for the CM. Both static and dynamic aerodynamics, including the effect of sideslip, reduced frequency, and non-dimensional angular rate, were collected. The parachute riser line force vector was measured to validate the Apollo model assumptions. The Pressure Recovery Fraction (PRF), or drag loss of the parachutes caused by the CM wake having a reduced dynamic pressure, was also measured to ensure correct modeling of parachute drag in the simulation. The induced effect of drogues on CM aerodynamics was also assessed. In addition, the test provided data to assess the static and dynamic effects of a one-drogue-out scenario and provided insight into the caveats associated with modeling two drogues as one in the simulation. It is believed that this is the first time since the Apollo program that dynamic aerodynamics of an integrated capsule-drogue system have been measured directly [9].

The unique combination of dynamic testing capabilities and specialized technician skills at the VST were used to quickly adapt an existing model and parachutes for this test. Note that the Reynolds number for this test was much lower than the flight Reynolds

number, and there is a Reynolds number effect on dynamic derivatives as discussed in Ref. [10]. However, as the first step in correctly modeling the flight dynamics of the CM-drogue system, the data gathered in this test will be used to aid in reproducing similar dynamics in a simulation as was seen in free flight tests in the VST—utilizing the same tunnel, test conditions, model, and parachutes. The simulation will be populated with static and dynamic aerodynamic data gathered from this test. This allows a rapid, inexpensive method of potentially identifying a simulation modeling problem that may also apply at higher Reynolds numbers. Utilizing the VST in this manner also allows for an inexpensive method of identifying challenges and best practices for working with the drogue parachutes in a more expensive wind tunnel if necessary.

Chapter 2

Wind Tunnel Test Setup

The experimental wind tunnel test was performed in the NASA Langley 20-Foot Vertical Spin Tunnel (VST). The VST is a low speed, annular return tunnel that operates at atmospheric conditions. The closed, 12-sided test section is 20 feet across and 25 feet high. The VST has provided key subsonic, dynamic stability data for many atmospheric entry vehicles, including the Pioneer Venus, Stardust, and Mars Sample Return planetary probes and the Mercury, Gemini, and Apollo space capsules. The VST has more recently been utilized to assess subsonic dynamic stability of the Orion Launch Abort System, CM, and drogue parachute performance. The tunnel's rotary balance system has a forced oscillation capability that is used to measure body axis rate damping characteristics [11].

A $1/16^{th}$-scale CM was modified from a free-flight model [5] to accept a 6-component strain gage balance. The model was built using an automated polycarbonate fabrication system in the NASA Langley Research Center rapid prototyping lab. The model with drogues attached is shown in Figure 2-1. The model reference length and reference area used to compute aerodynamic coefficients are based on capsule diameter.

Figure 2-1: Orion Crew Module with drogue parachutes in

Langley 20-Foot Vertical Spin Tunnel.

The parachutes used for this test were acquired from an inventory at the VST that is used for airplane spin recovery and entry vehicle drogue parachute testing. The 18-inch diameter flat, circular parachutes have a full-scale drag area (C_DS) of 221 ft^2 based on a C_D of 0.55, and are constructed of high permeability nylon that results in good stability and a near-zero trim angle. The model towline length—defined as the length from the attachment point to the canopy skirt—was 62.5 inches (1,000 inches full-scale). The parachute towlines are attached to the zero-degree gusset, or the gusset aligned with the +Z body axis as shown in Figure 2-2 [12], at the "down and out" attachment point, shown in Figure 2-3.

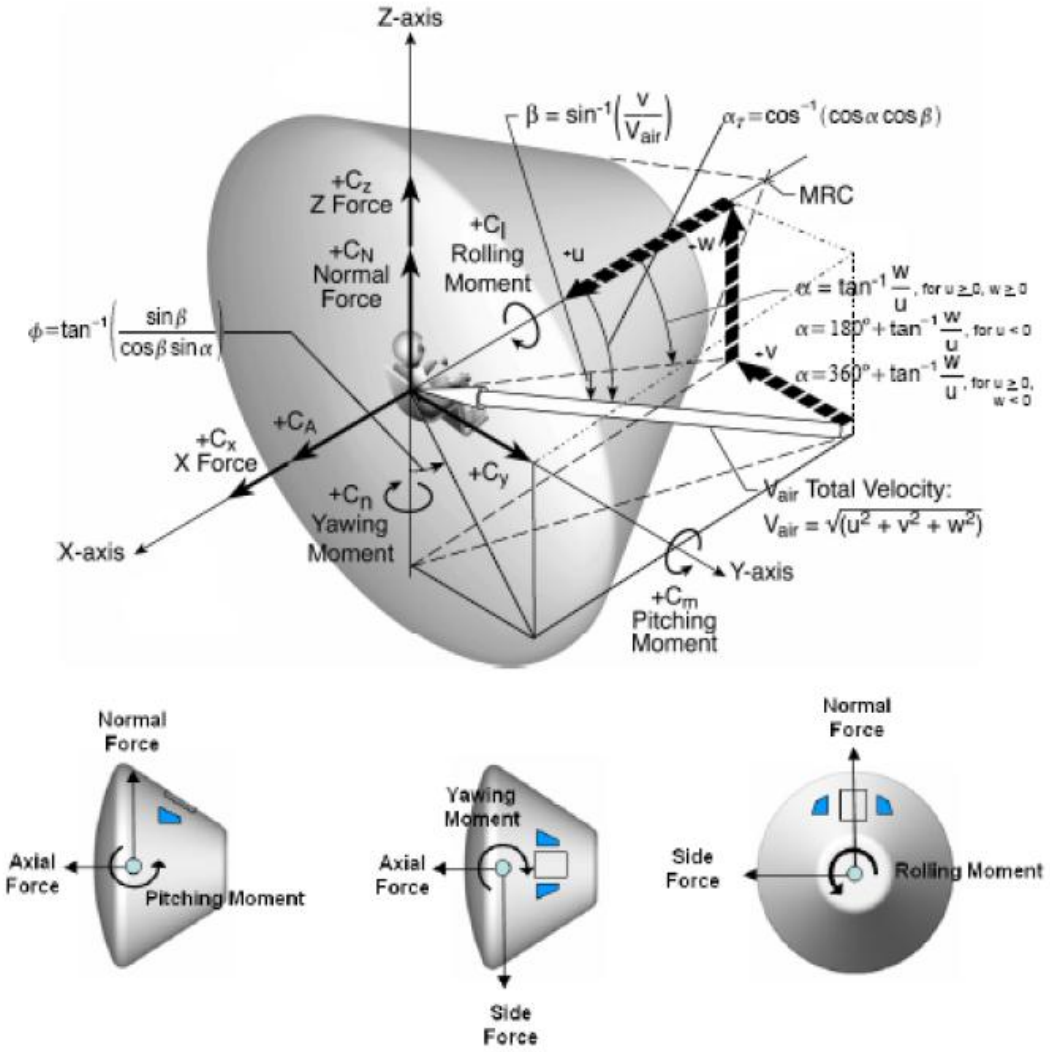

Figure 2-2: Coordinate system for the Orion Crew Module [12].

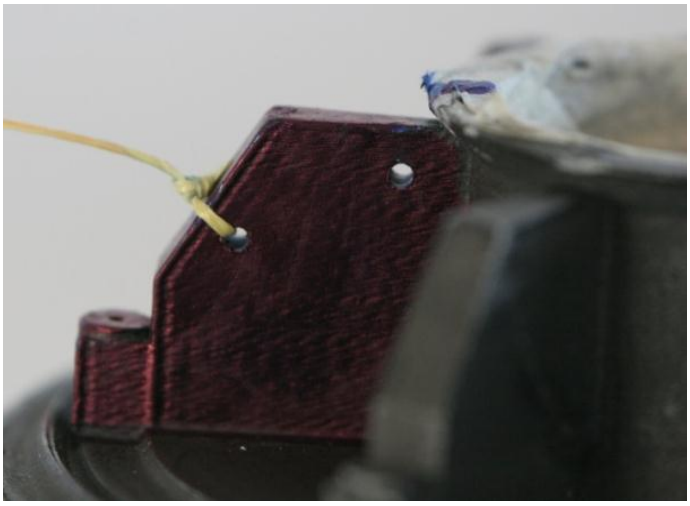

Figure 2-3: "Down and Out" drogue parachute attachment point on the zero degree gusset.

A six-component, 1.110-inch diameter strain gage balance was used to measure forces and moments on the model. During the rapid model modification from free-flight to a captive configuration, a compromise was made which exposed a portion of the balance to the flow. This exposed portion was covered with a thin membrane (highly flexible "dental dam" material). No significant effect was noted in the balance signal due to the membrane. The balance was mounted on the axis of rotation at the center of gravity (CG) location. Taking advantage of model symmetry, internal model hardware was designed to be shifted to the correct CG location when changing from pitch to yaw configurations, leaving one sting entry in the model.

A position potentiometer was used to measure model position for the forced oscillation technique. The model sting was rotated to set the model at the desired angle of attack and

then oscillated about that point to obtain force and moment time history data necessary to calculate damping derivatives.

For the first part of the wind tunnel test, drogue line forces were measured with an Omega in-line load cell (model LCFD-10). The load cell has a load limit of 10 pounds and a diameter of 0.75 inches and weighs 1.48 ounces. The Omega load cell is shown in Figure 2-4. Initially, the primary objective of the test was to measure the total CM-parachute system damping derivatives to compare to the Apollo model derived equivalent damping derivatives. The load cell was to measure the drag reduction at the parachutes due to the wake deficit behind the CM. Upon inconclusive findings, the assumption of the Apollo model about the parachute force vector relative to the CM attitude needed to be verified. Since only the magnitude of the drogue force vector could be measured with the load cell, additional wind tunnel testing was conducted to measure the drogue force vector to validate the Apollo drogue model assumption of the force vector aligning with the velocity at the drogue attachment point. This measurement was accomplished with a small six-component balance mounted at the drogue attachment point. The six-component balance is shown mounted in the CM in Figure 2-5.

In order to assess any CM forces and moments under the upstream influence of the drogues, a separate "drogue sting" was fabricated to attach the drogues at the correct location over the CM for both pitch and yaw motions in order to assess the possible influence of the drogues on CM aerodynamics. The drogue sting rotated with the CM for the forced oscillation technique, allowing the drogue attachment point to remain at the

proper location over the CM. A conceptual drawing of the pitch and yaw configurations for this drogue sting is shown in Figure 2-6. This sting with drogues attached in the pitch configuration is pictured in Figure 2-4.

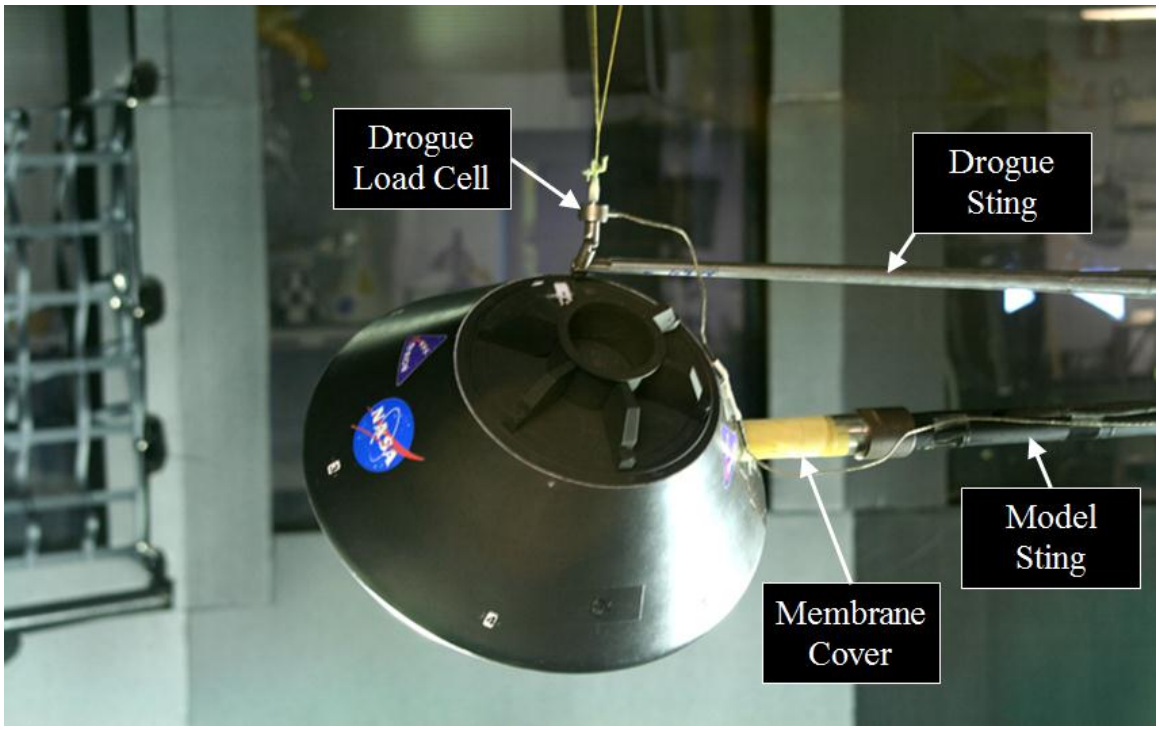

Figure 2-4: Crew Module model with drogues attached to the drogue sting in pitch configuration.

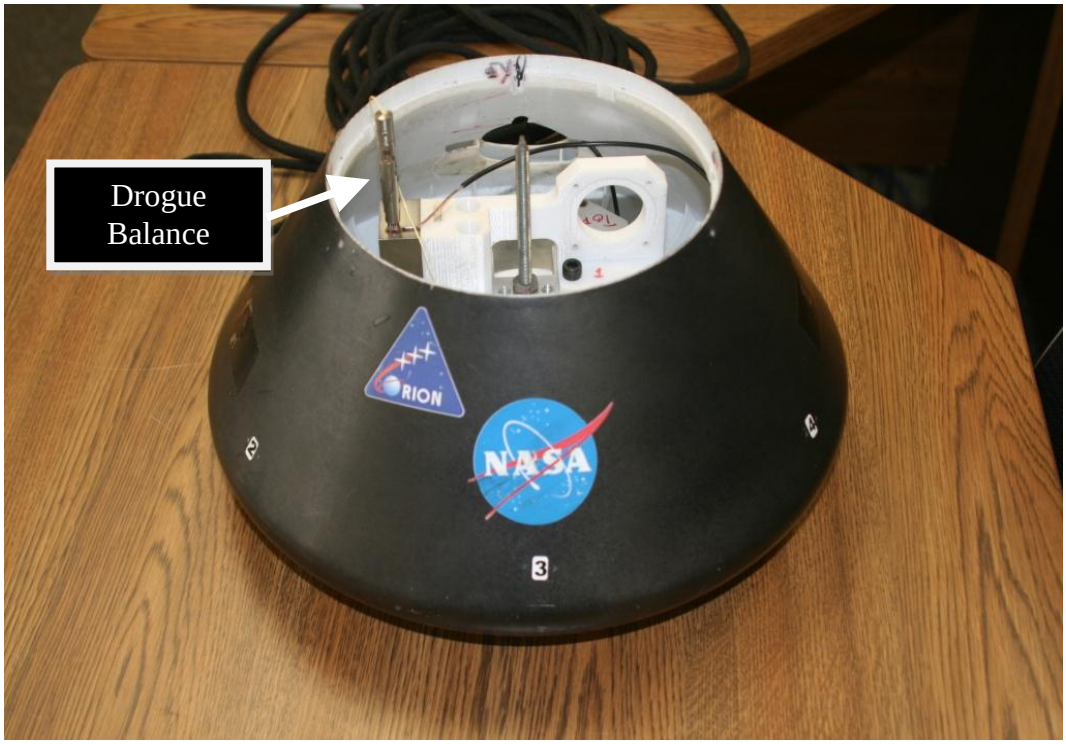

Figure 2-5: Crew Module with six-component balance to measure drogue force vector.

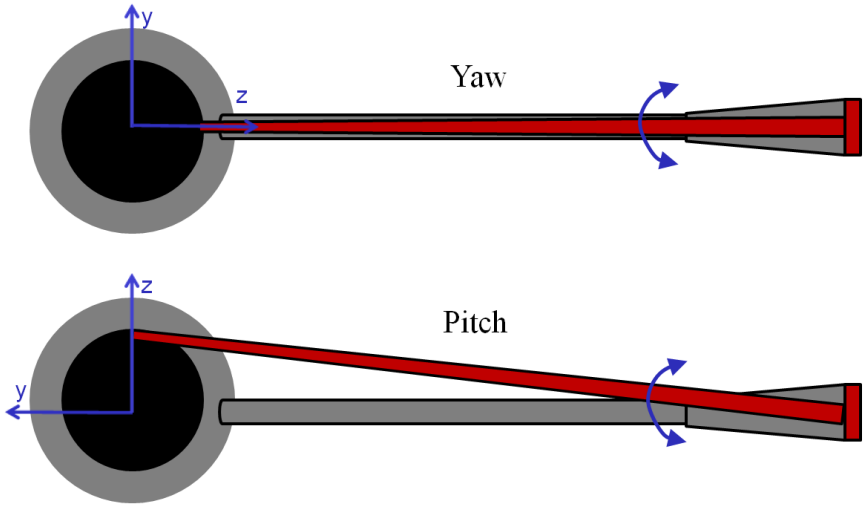

Figure 2-6: Top view illustration of pitch and yaw drogue sting configurations (red) and model sting (grey).

The majority of the test was focused on measuring the pitching moment, but some data were collected for the yaw configuration as well, and is presented in the Results section of this paper. Test data were gathered for the heatshield-forward condition, which is the orientation that the vehicle is intended to descend through the atmosphere. Reduced frequency and angular rates for the forced oscillation testing were chosen based on dynamics observed in model free-flight tests of the CM with drogues [5].

The majority of the wind tunnel test was conducted at a dynamic pressure of 3 psf and a Reynolds number of 310,000 based on the CM diameter. A small portion of the test was performed at a dynamic pressure of 1.5 psf (Reynolds number of 230,000 based on CM diameter) in order to achieve desired reduced frequency and non-dimensional angular rate variations.

The angle-of-attack range used in the test was 100° to 220°. Angle of attack of 180° is the heatshield forward attitude for the CM. Sideslip angle was varied from -40° to 40° at various angles of attack. Sinusoidal motion with amplitudes of up to ±40° and frequencies of up to 2 Hz was used for the forced oscillation technique.

Seven model configurations were tested and are summarized in Table 2.1. These seven configurations provided data to assess many important effects, such as the interference effect of the drogue sting by comparing configuration 1 with 2 and 3 with 6; induced influence of drogues on CM aerodynamics by comparing configuration 2 with 4; and effect of drogues on total system damping by comparing configuration 1 with 6 (or 2 with

3). The drogue riser line force without the CM wake was measured with configuration 5. Configuration 7 was used to model a drogue-out case and to obtain additional data to aid in validating the simulation's modeling of two drogues as a single drogue. Figure 2-7 and Figure 2-8 show the CM and drogues with and without the drogue sting, respectively.

Table 2.1: Wind tunnel model configurations.

Configuration	Description	Purpose
1	CM alone	Baseline for comparing CM dynamics with and without the drogues
2	CM alone with the drogue sting	Aerodynamic effect of the drogue sting on CM
3	Two fully-deployed drogues attached to CM plus drogue sting	Total system static and dynamic aerodynamics with drogue sting in place
4	Two fully-deployed drogues attached to drogue sting	CM forces and moments under the aerodynamic influence of the drogues
5	Two fully-deployed drogues alone mounted to the drogue sting	Drogues alone riser line forces
6	Two fully-deployed drogues attached to CM with no drogue sting	Total system static and dynamic aerodynamics without the drogue sting
7	Single fully-deployed drogue attached to CM with no drogue sting	Direct analogy to current two-body simulations of the CM and drogues, which model two drogues as a single drogue

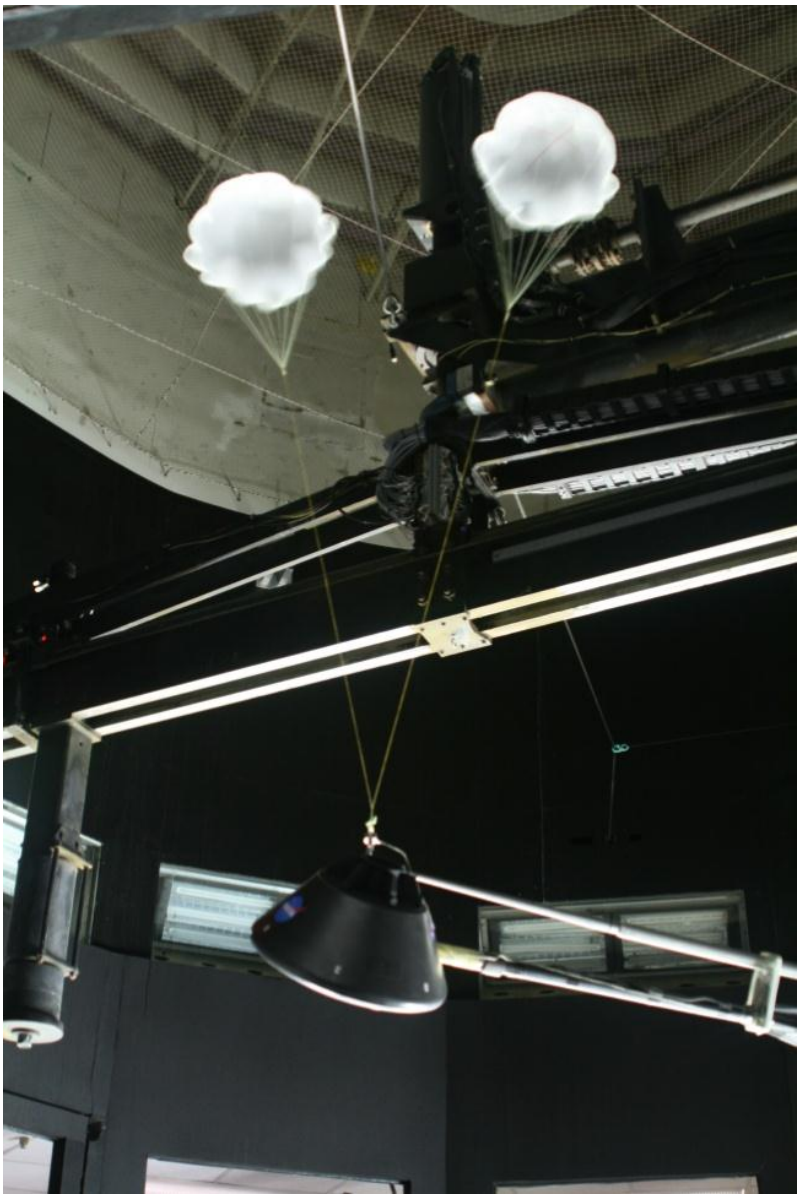

Figure 2-7: Crew Module with drogue sting.

Figure 2-8: Crew Module without drogue sting.

Chapter 3

Wind Tunnel Test Results

The results of the wind tunnel test are organized in terms of the objectives of the research presented in this paper. This chapter covers the first three objectives: 1) damping effects of drogue parachutes on the CM-parachute system, 2) upstream influence of the drogue parachutes on CM aerodynamics, and 3) drogue parachute drag reduction due to CM wake. The fourth objective, measuring the riser line force vector, is presented in Chapter 4, where the experimentally obtained riser line force vector angle is compared to the Apollo drogue model predictions.

3.1 Damping Effects of Drogue Parachutes on Crew Module Dynamics

Other than providing additional drag, a major purpose of the drogue chutes is to stabilize and orient the CM to enable proper main parachute deployment and inflation. The results from this wind tunnel test show that the drogue chutes are providing stability to the CM. However, the degree of stability is currently in question based on conflicting data from flight tests and simulation results. Since the aerodynamic forces and moments are a build-up of the static and dynamic components, the results discussed below focus on quantifying the both static and dynamic stability. The oscillatory motion of the CM is defined by the oscillation frequency and amplitude growth or decay. The oscillation

frequency is primarily dependent on the vehicle inertia and static aerodynamic moments. The CM static and dynamic aerodynamics without parachutes are discussed in detail in References [13] and [14].

3.1.1 Longitudinal Static Aerodynamic Characteristics

Figure 3-1 shows the static pitching moment at a range of angle of attack values around the heatshield-forward attitude for the CM alone, CM with one drogue, and CM with two drogues. Comparing the *CM alone* with the *CM with two drogues* configurations shows a significant increase in static stability Cm_α (i.e., increased negative slope of the linearized curves about trim in Figure 3-1) due to the restoring moment of the drogues. The drogue chutes also cause the trim angle of attack to move from about 167° to 151° due to their laterally-offset attachment point.

Also shown in Figure 3-1 is the effect of only one drogue, a scenario that occurs when one of the two drogues does not inflate properly. The drogue-out case still provides considerable static stability compared to the CM alone.

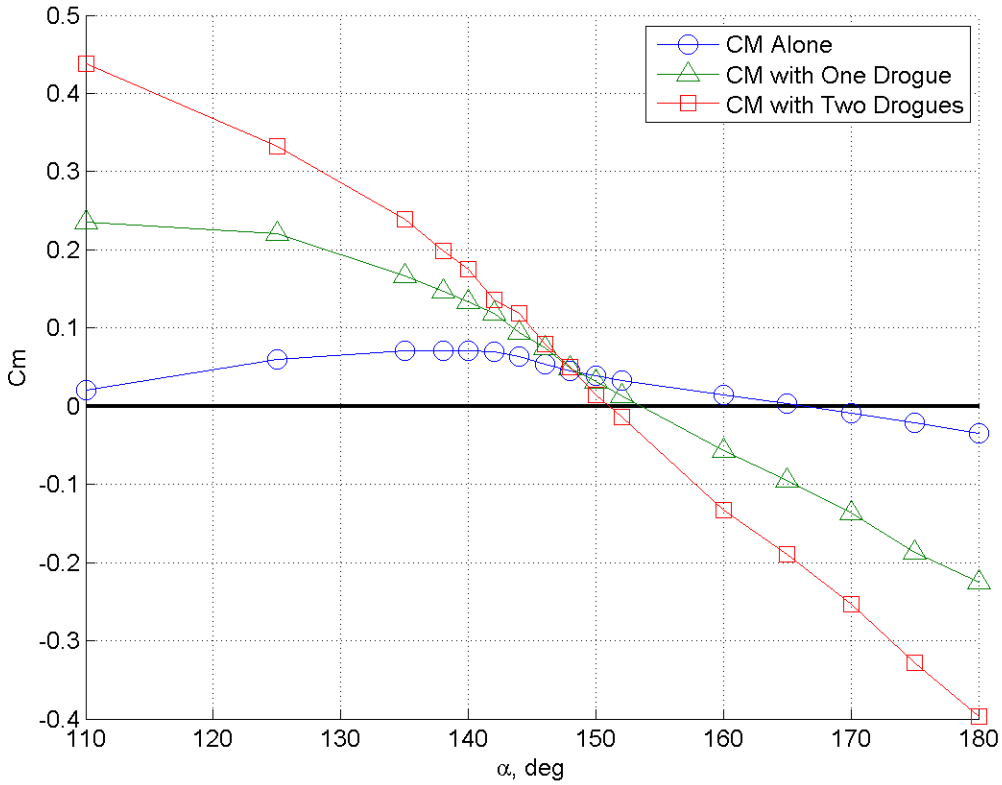

Figure 3-1: Static stability for CM alone, CM with one drogue,

and CM with two drogues.

3.1.2 Damping Characteristics

The damping characteristics of the CM-drogue system will be described in five sections: pitch damping, one drogue out, oscillation frequency effects, rate effects, and yaw damping characteristics. Each of these sections describes a particular aspect of the damping characteristics of the CM-drogue parachute system that is important in modeling the dynamics of the system. Reduced frequency, k, and maximum non-dimensional

angular rate, $\hat{q}_{max}$, are two similarity parameters used to match frequency and rate of oscillations seen in free-flight. The equations for non-dimensional angular rate and reduced frequency are shown in (3.1) and (3.2) below, respectively. q_{max} is the maximum pitch rate, and ω is the oscillation frequency.

$$\hat{q}_{max} = \frac{q_{max} \cdot L_{ref}}{2V_{\infty}} \tag{3.1}$$

$$k = \frac{\omega \cdot L_{ref}}{2V_{\infty}} \tag{3.2}$$

The forced oscillation data were reduced using the single point method. Cm_q is calculated by differencing the measured pitching moment at the points of maximum and minimum rate on the averaged hysteresis loop (pitching moment versus model position as measured by potentiometer) and dividing by the non-dimensional pitch rate. The forced oscillation technique, including data reduction, are described in detail in Ref. [15], and the single point method is summarized in the Appendix of this paper. Stable damping is indicated by negative values of Cm_q. The equation for Cmq is in (3.3) below.

$$Cm_q = \frac{\partial Cm}{\partial \hat{q}} \tag{3.3}$$

3.1.2.1 Quantitative Effect of Two Drogue Parachutes on Pitch Damping Derivatives

The pitch damping derivatives, Cm_q, versus CM angle of attack for the CM without drogues and the CM with two fully-deployed drogues is shown in Figure 3-2: Dynamic stability for CM alone and with two drogues. Figure 3-2. The data plotted are for a frequency that is representative of VST free-flight with drogues (reduced frequency of 0.125 and non-dimensional angular rate of 0.022). The CM-drogue system exhibited this frequency of motion in the earlier free-flight test in the VST [5]. Larger amplitudes of oscillation were desired but could not be achieved due to amplitude and frequency combination limitations of the forced oscillation rig. A few calculated Cm_q values in Figure 3-2 do not appear to follow the damping trend. There are several possible explanations for this phenomenon, including sensitivity to the data reduction method and repeatability concerns due to the unsteady nature of the drogues. The drogues have a relatively constant damping effect from an angle of attack of 144° to 180°. Below 144°, the drogues significantly increase their contribution to system damping. With the two drogues attached, the CM oscillates about its trim angle of about 151°.

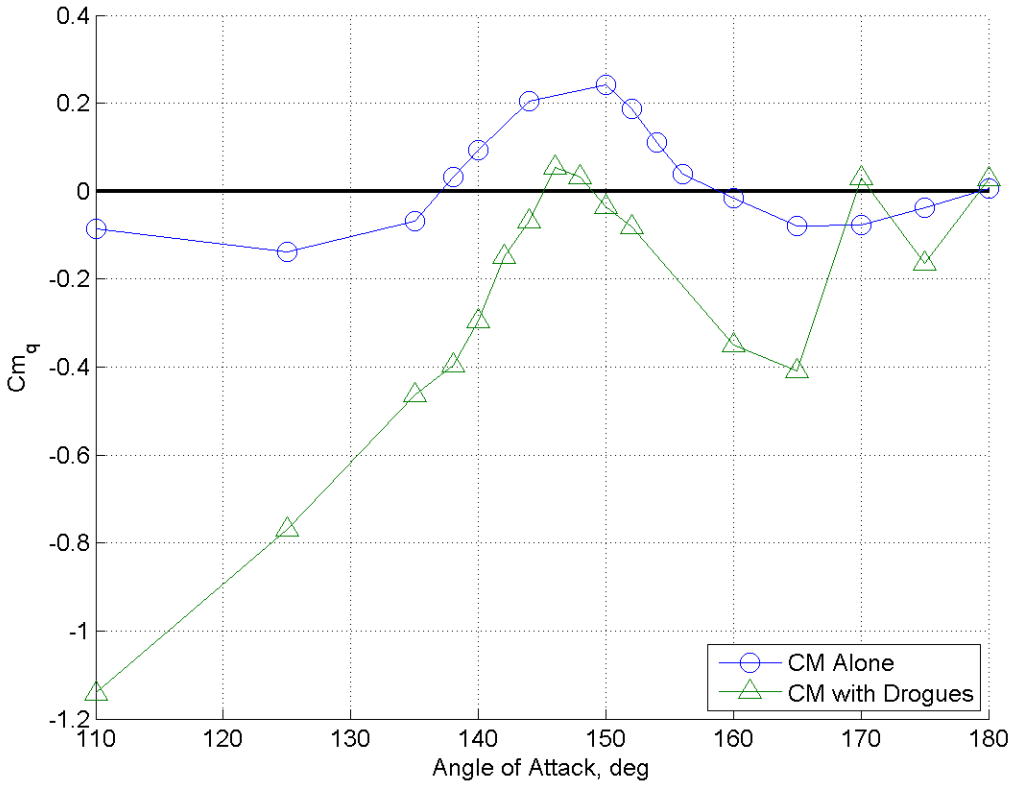

Figure 3-2: Dynamic stability for CM alone and with two drogues.

3.1.2.2 Quantitative Effect of One Drogue Parachute on Pitch Damping Derivatives

Examining one fully-deployed drogue parachute instead of two sheds light on a failure scenario where one drogue does not deploy correctly, also called "one drogue out" and provides information necessary to confirm that modeling two parachutes as one in the simulations is being done properly. Figure 3-3 shows the effect of one drogue out on dynamic pitch stability. The data compared were computed from oscillations with a reduced frequency of 0.091 and non-dimensional angular rate of 0.016. This is representative of the oscillation frequency seen in VST free-flight tests of the CM with

one drogue. Cm_q decreases for one drogue versus two, indicating the drag force from two drogues is more stabilizing to the CM-drogue system than one drogue, as expected.

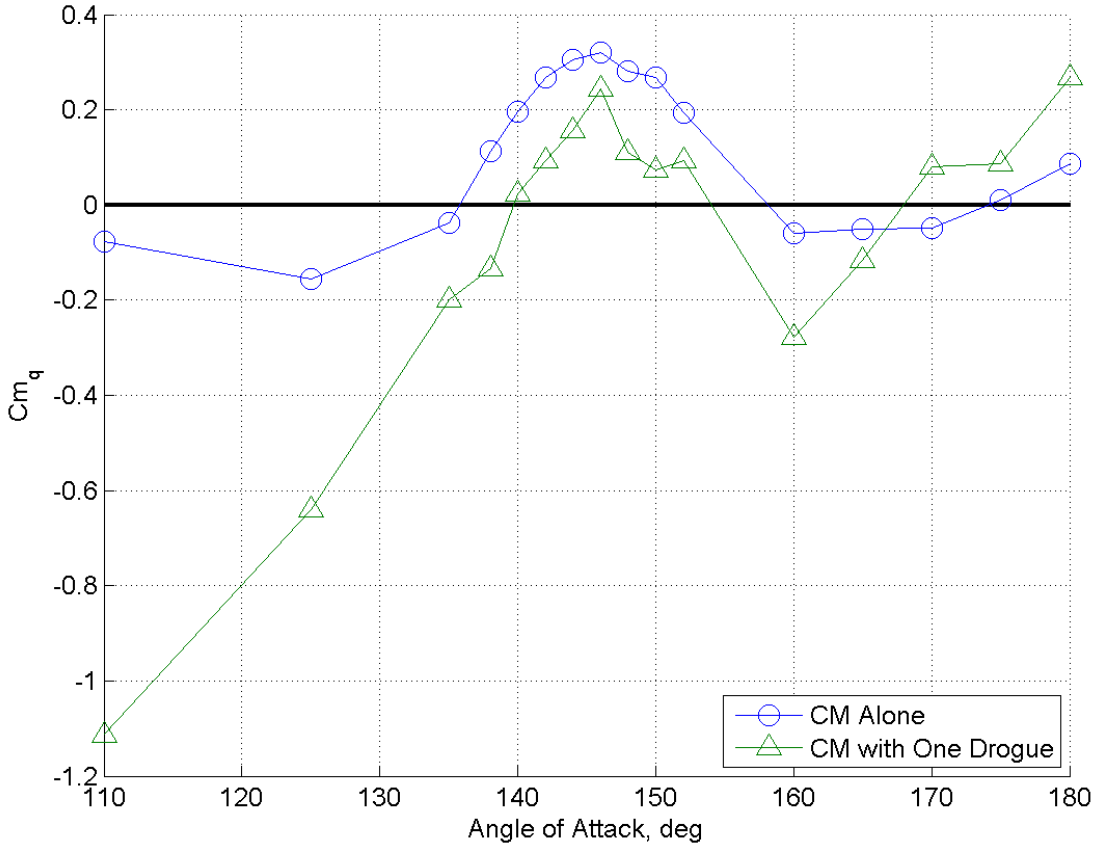

Figure 3-3: Effect of Drogue Out (k = 0.091, $\hat{q}_{max}$ = 0.016).

3.1.2.3 Effects of Oscillation Frequency on Pitch Damping Derivatives

Vehicle aerodynamic damping is dependent on oscillation frequency [14]. The natural oscillation frequency of the CM is primarily dependent on the vehicle inertia and $Cm_{\alpha,}$ with minimal dependence on damping. Frequencies observed in VST free-flight tests

with a dynamically scaled model were 1.4 Hz (k = 0.091) with one drogue parachute and 2 Hz (k = 0.123) with two drogue parachutes. The effect of reduced frequency on damping of the CM-drogue system is shown in Figure 3-4. The maximum non-dimensional angular rate (q_{max}) was held constant at 0.030. A negligible effect is seen for reduced frequencies (k) of 0.087 and 0.130. For a reduced frequency of 0.044, damping becomes highly unstable for the angle-of-attack range between 145° and 180°. A similar plot of frequency dependence for the CM alone is shown in Figure 3-5. Frequency dependence is much more evident for this configuration. In the trim region for the CM alone, about 167° angle of attack, damping becomes more unstable as frequency decreases. In the trim region for the CM with drogues, about 151° angle of attack, damping has the opposite trend of decreasing stability as frequency increases.

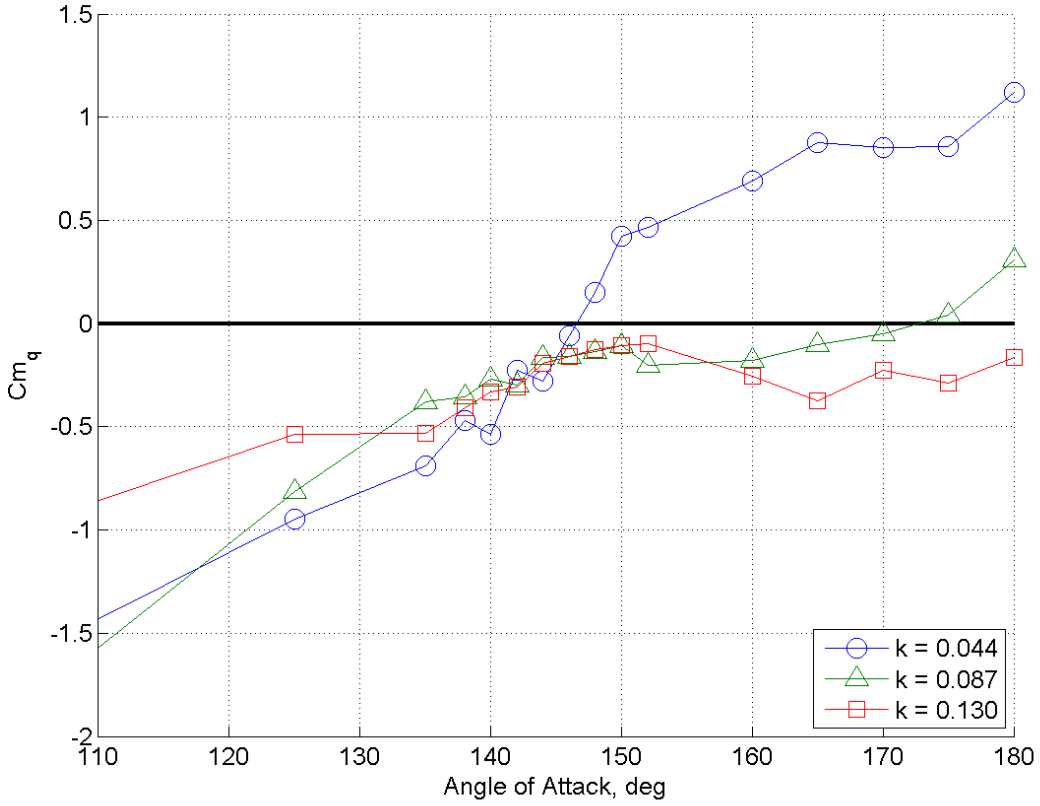

Figure 3-4: Effect of oscillation frequency for CM with two drogues, $\hat{q}_{max}$=0.030.

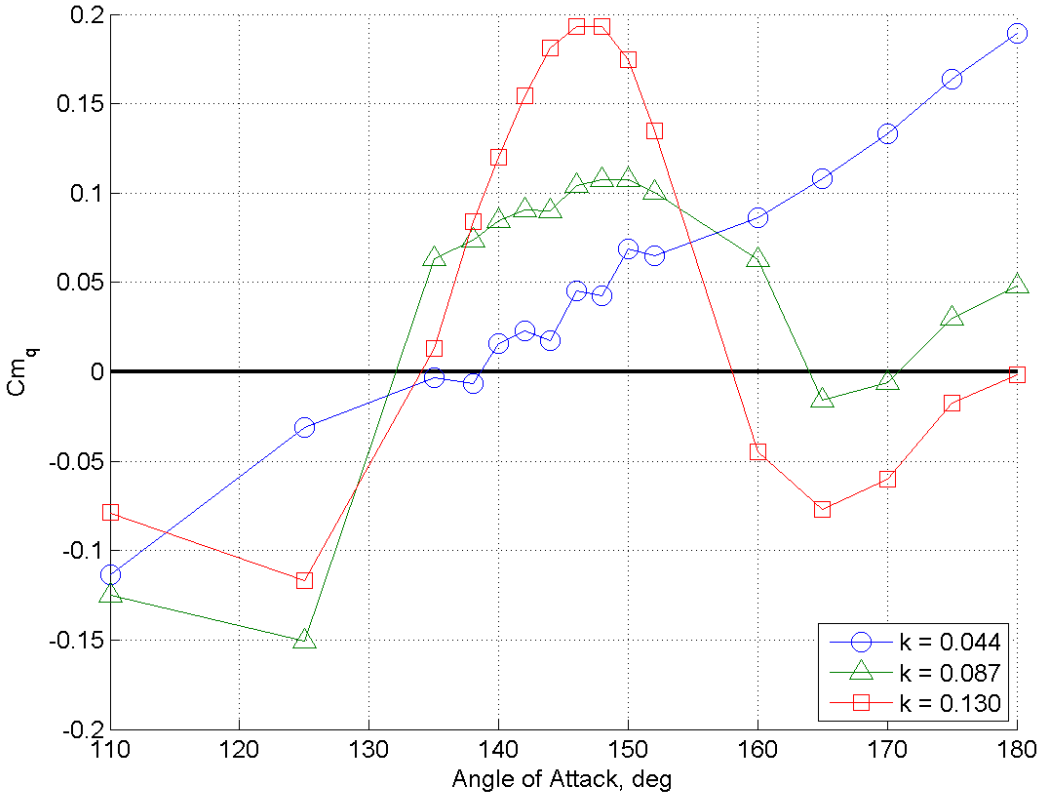

Figure 3-5: Effect of oscillation frequency for CM alone, $\hat{q}_{max}$=0.030.

These figures show a dependence of damping values on oscillation frequency, verifying the importance of capturing dynamic derivative values at the correct reduced frequency in order to match motions observed in free flight to motions predicted by simulations.

3.1.2.4 Effects of Pitch Rate on Pitch Damping Derivatives

An alternative orientation of an angle of attack time history trace from a VST free-flight run is shown in Figure 3-6. The figure shows the time in model scale (MS) versus the angle of attack of the CM. The angle of attack time history is shown this way to more easily visualize the amplitude change in motion over time. Initially, amplitudes of ±40°

are seen. This range justifies the range of angle of attack used to take data and shows that the entire Cm_q table is used when simulating these types of runs.

The effect of maximum angular rate ($\hat{q}_{max}$) on damping of the CM-drogue system is shown in Figure 3-7. Reduced frequency was held constant at 0.044. The frequencies and amplitudes chosen to capture the effects of reduced frequency and angular rate were limited by the capability of the forced oscillation rig. It should be noted, however, that the rig was capable of oscillating the model at the desired frequency to match free-flight motion in earlier VST tests. In the region of trim for the CM with drogue parachutes, the total system damping becomes less stable (the damping derivative increases in the positive direction) as the angular rate increases at this frequency. This trend reverses at angles of attack less than about 145° and greater than 170°. The same effect of angular rate is shown for the CM alone in Figure 3-8. In the trim region for the CM alone, the vehicle is more damped as pitch rate increases at this frequency. In the trim region for the total CM-drogue system, the trend is reversed in that the vehicle is less damped as pitch rate increases. Also, the angles of attack at which these trends reverse are 135° and 155°, which are different than the angles of attack for trend reversal for the total CM-drogue system.

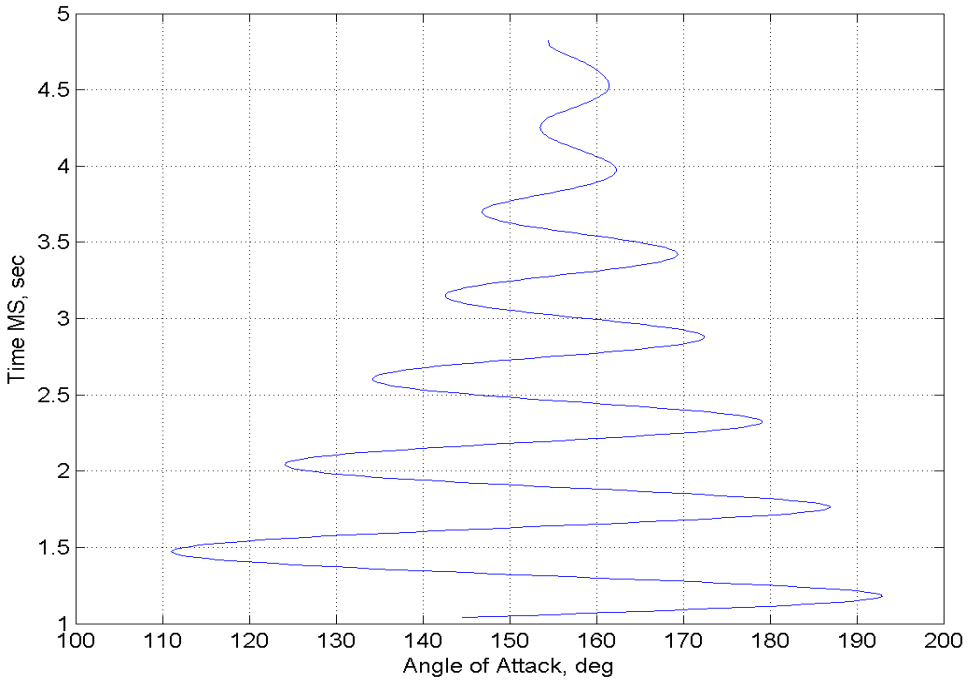

Figure 3-6: VST free-flight angle of attack versus time.

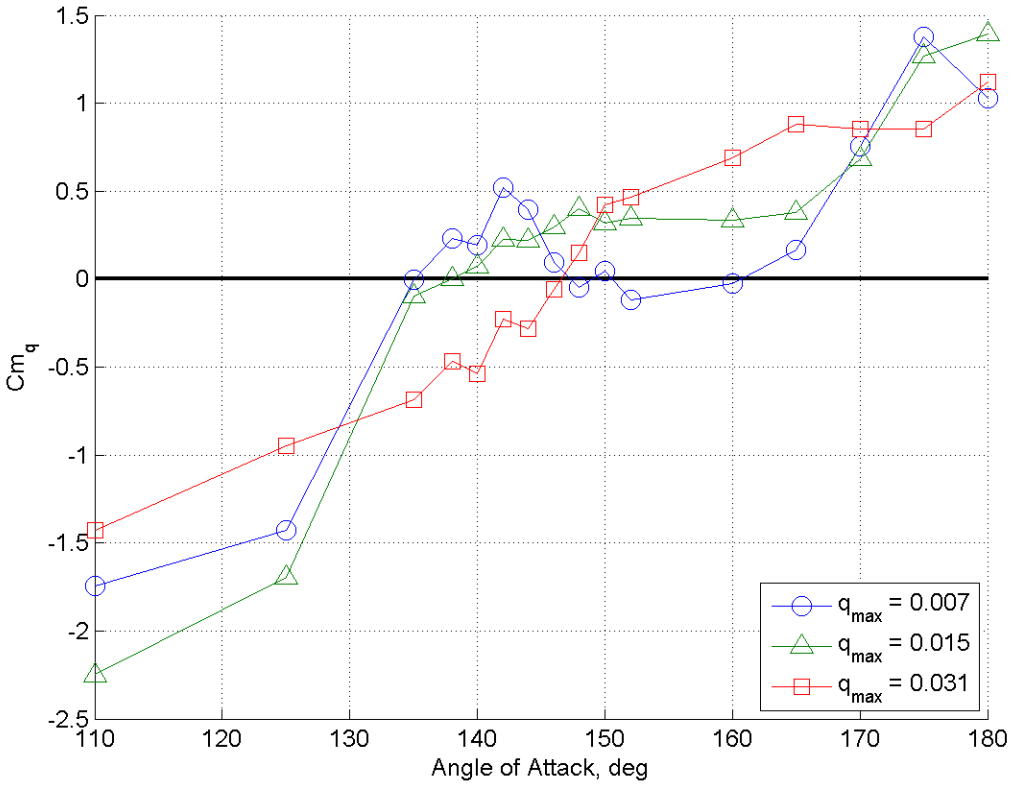

Figure 3-7: Effect of pitch rate for CM with drogues, k = 0.044.

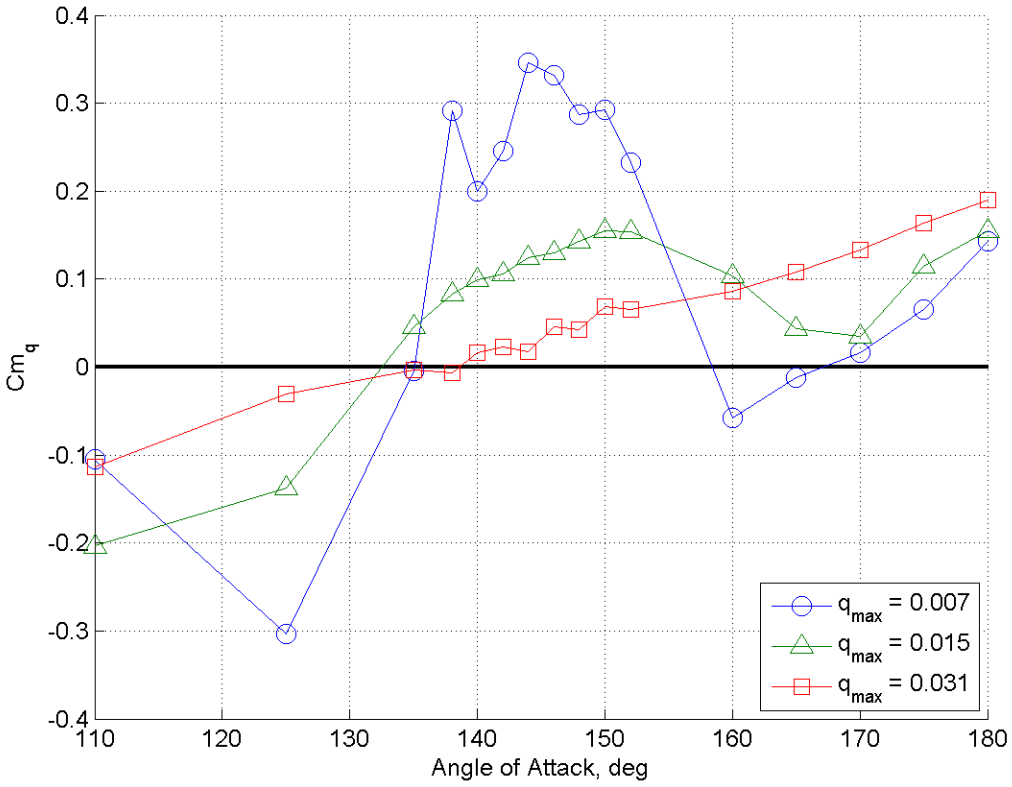

Figure 3-8: Effect of pitch rate for CM alone, k = 0.044.

The dependence of the dynamic derivatives on pitch rate has been previously identified for this vehicle and is currently being modeled in the CM aerodatabase. Capturing the effect of rate for the CM-drogue system may aid in simulation modeling of the system, although not directly since the rate effect at the flight frequency could not be captured in this test.

3.1.2.5 Yaw Damping Characteristics

Although the vehicle primarily oscillates in pitch, there is some oscillation in yaw, so yaw damping was briefly examined. A non-zero sideslip angle, β, of 10°, which is a

reasonable amount of sideslip for a nominal flight, causes an insignificant change in drogue line force, as illustrated by the C_D versus α data in Figure 3-9. The drag values of the parachutes are not symmetric about angle of attack of 180°. This is due to the offset drogue attach point on the vehicle. The chutes are in different wake regions on either side of 180°. The total system pitch damping with respect to sideslip angle is shown in Figure 3-10. An insignificant change is noted here also. Due to the unsteady nature of the drogue parachutes in the CM wake, these values are within the repeatability bounds of the CM-drogue system.

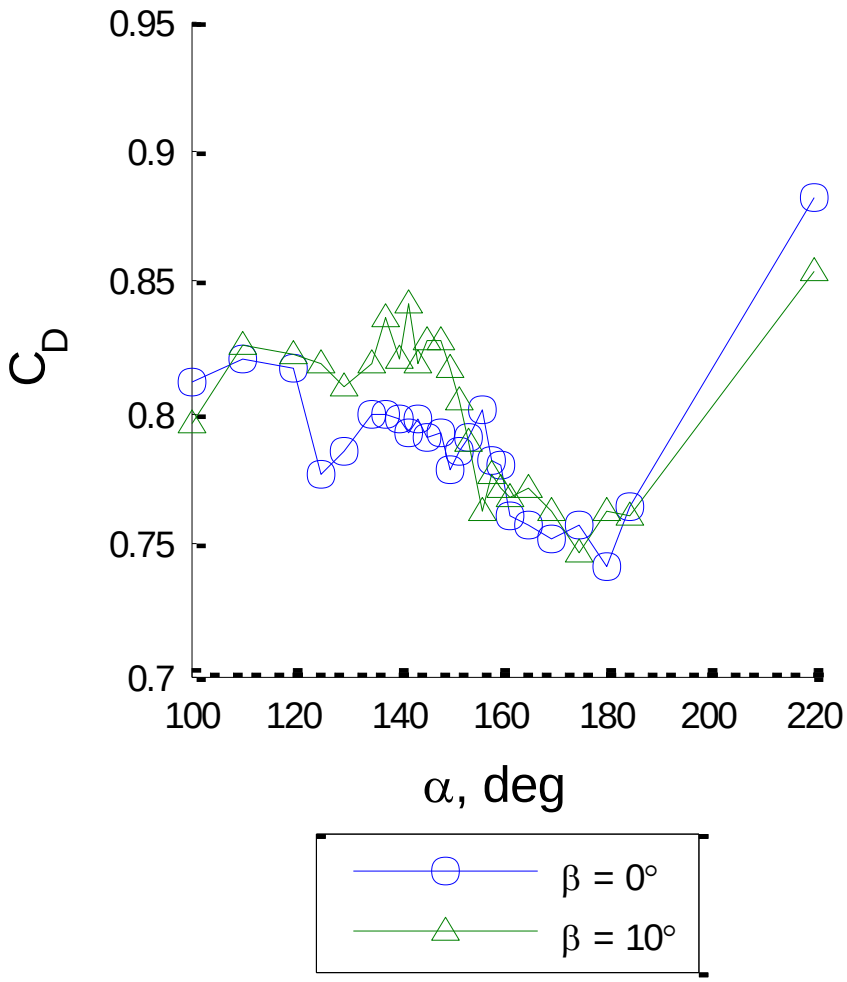

Figure 3-9: Effect of sideslip on drogue line force for two drogues.

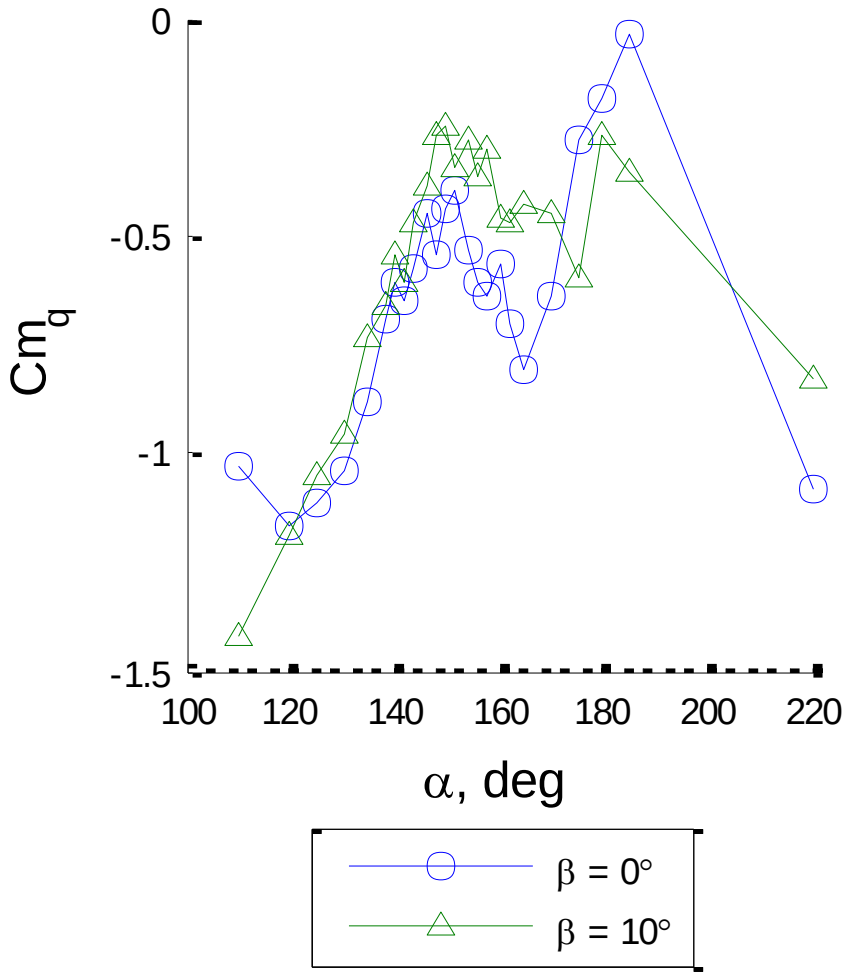

Figure 3-10: Effect of sideslip on longitudinal dynamic stability

(k = 0.125, $\hat{q}_{max}$ = 0.022).

Figure 3-11 shows the effect of angle of attack on yaw damping. Little effect is noted. For sideslip angle of near 0°, damping is less stabilizing at the minimum angle of attack of 130°. A comparison of Cn_r (at $\alpha = 180°$) to Cm_q (at $\beta = 0°$) is shown in Figure 3-12. Pitch and yaw damping values are similar near trim attitude ($\beta = 0°$, $\alpha = 151°$). However,

pitch damping dramatically increases as angle of attack departs from trim, whereas yaw damping only slightly increases. This difference is due to the drogues being attached on the axis of rotation for the yaw damping measurements and offset from the axis of rotation for the pitch damping measurements.

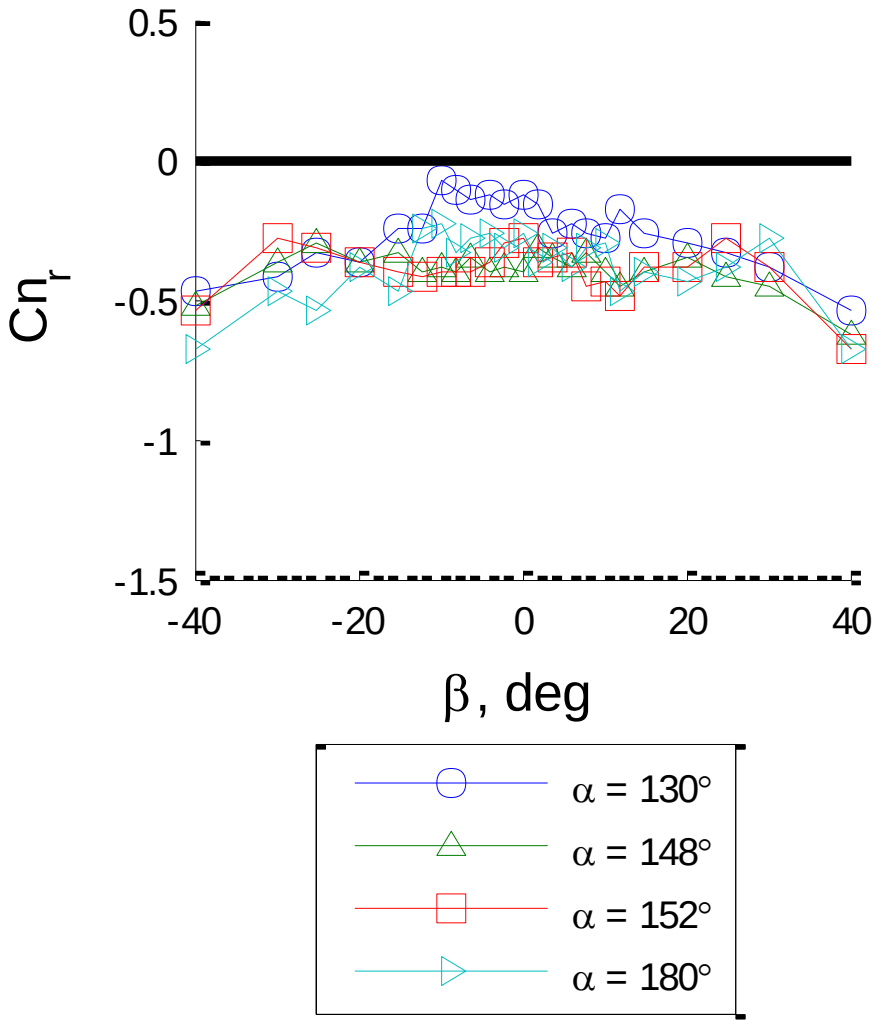

Figure 3-11: Effect of angle of attack on yaw damping (k = 0.133, $\hat{q}_{max}$ = 0.023).

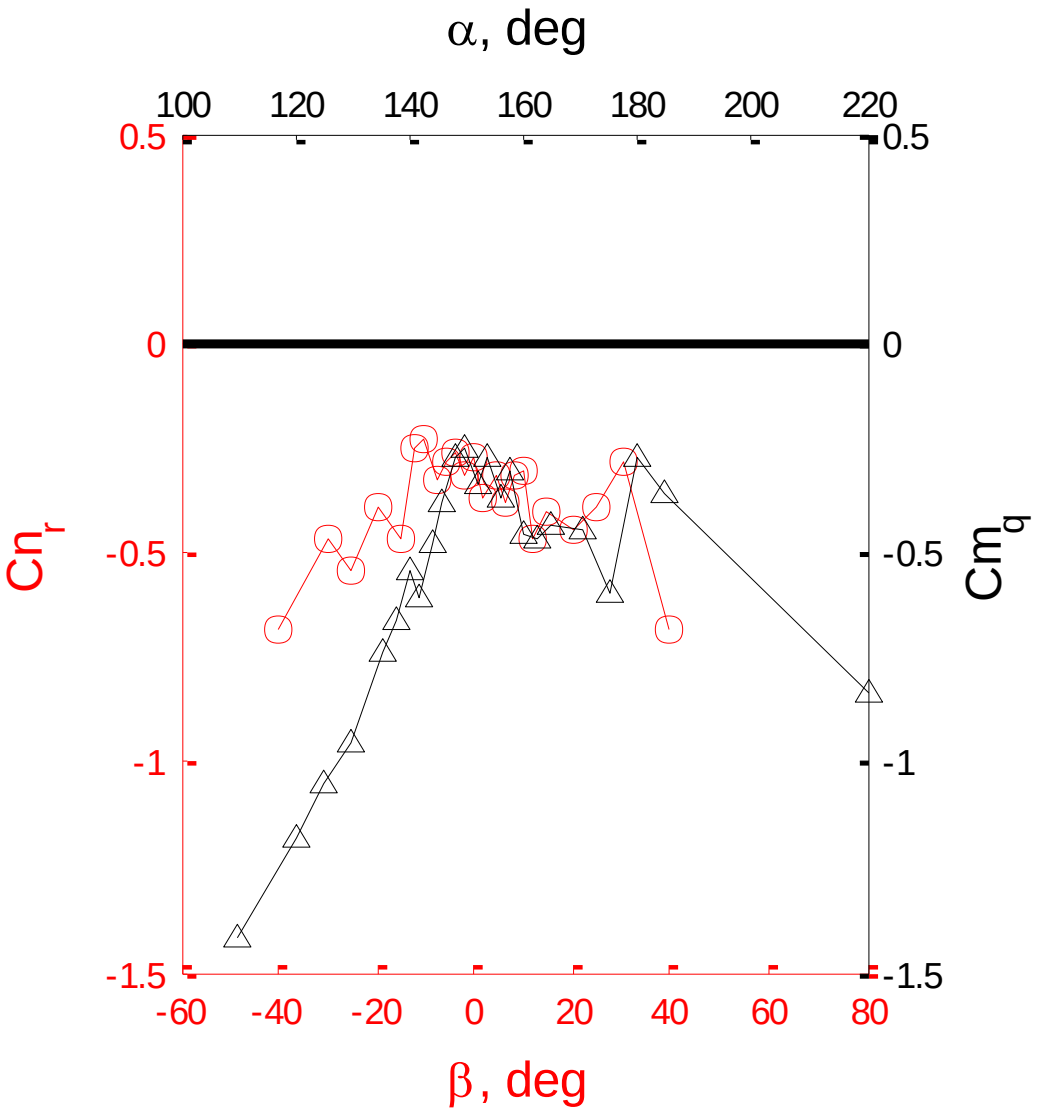

Figure 3-12: Yaw damping at 180° angle of attack compared to pitch damping at 0° sideslip angle.

3.2 Upstream Influence of Drogue Parachutes on CM Aerodynamics

One possible explanation for inaccurate simulation predictions of the CM-drogue system is an upstream influence of the drogue parachutes on the CM that is not being modeled in the simulations. The hypothesis is that the parachutes are far enough away from the CM to not induce significant aerodynamic effects on the CM. Since the data presented in Figure 3-13 and Figure 3-14 indicate similar aerodynamic forces and moments for the *CM Alone with Drogue Sting* and *CM with Two Drogues Mounted to Drogue Sting* configurations, there is no evidence (at the resolution of the instruments used in this test) of the drogue parachutes inducing upstream aerodynamic effects on the CM.

Since the drogue sting is an additional object inserted into the flow between the CM and the drogues, there was some concern that the drag produced by the drogues would be affected. Comparing the *CM with Two Drogues* and *CM with Two Drogues and Drogue Sting* configurations reveals that the drogue sting had a negligible effect on both static and dynamic forces and moments, as shown in Figure 3-13 and Figure 3-14.

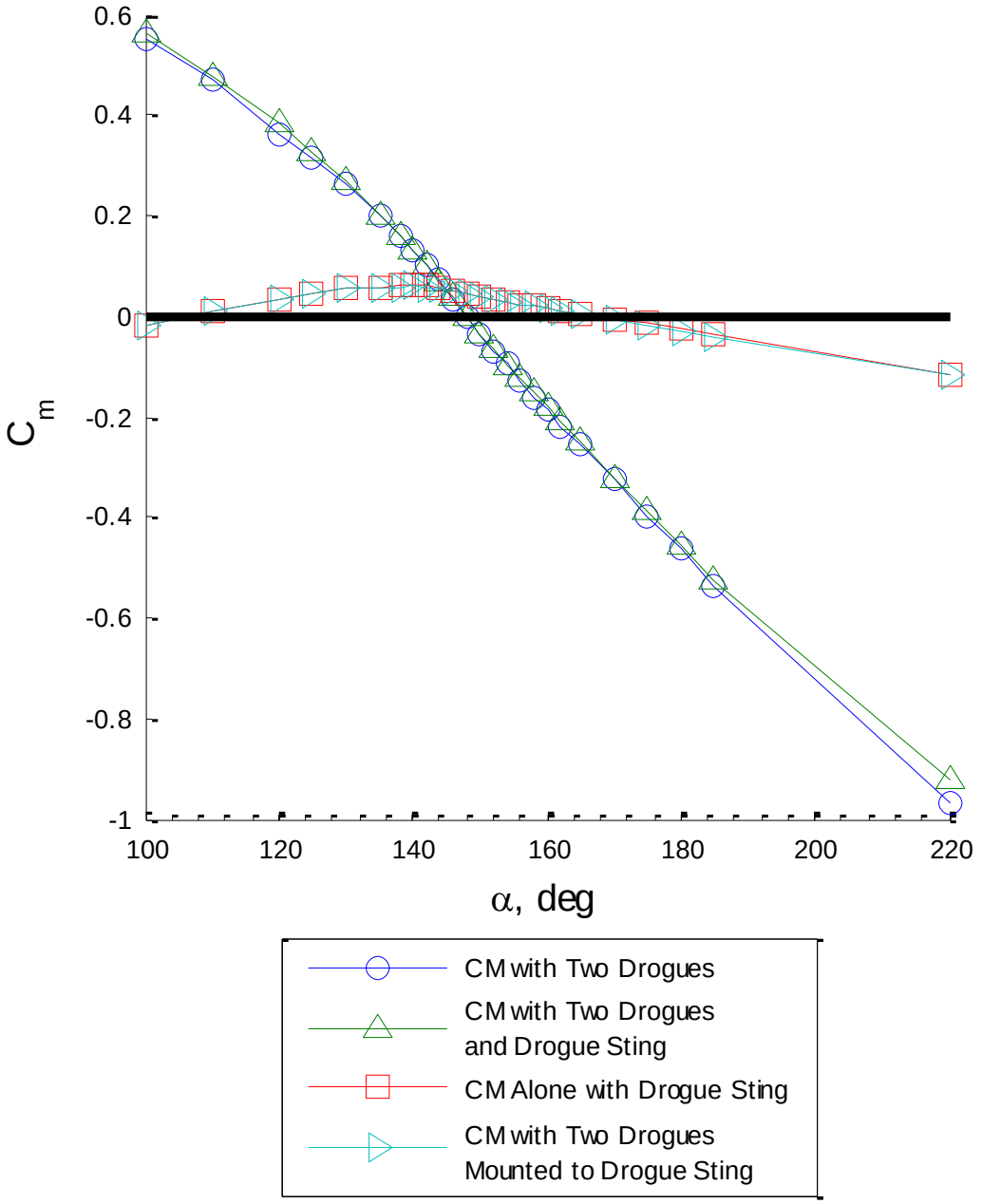

Figure 3-13: Static stability for four configurations.

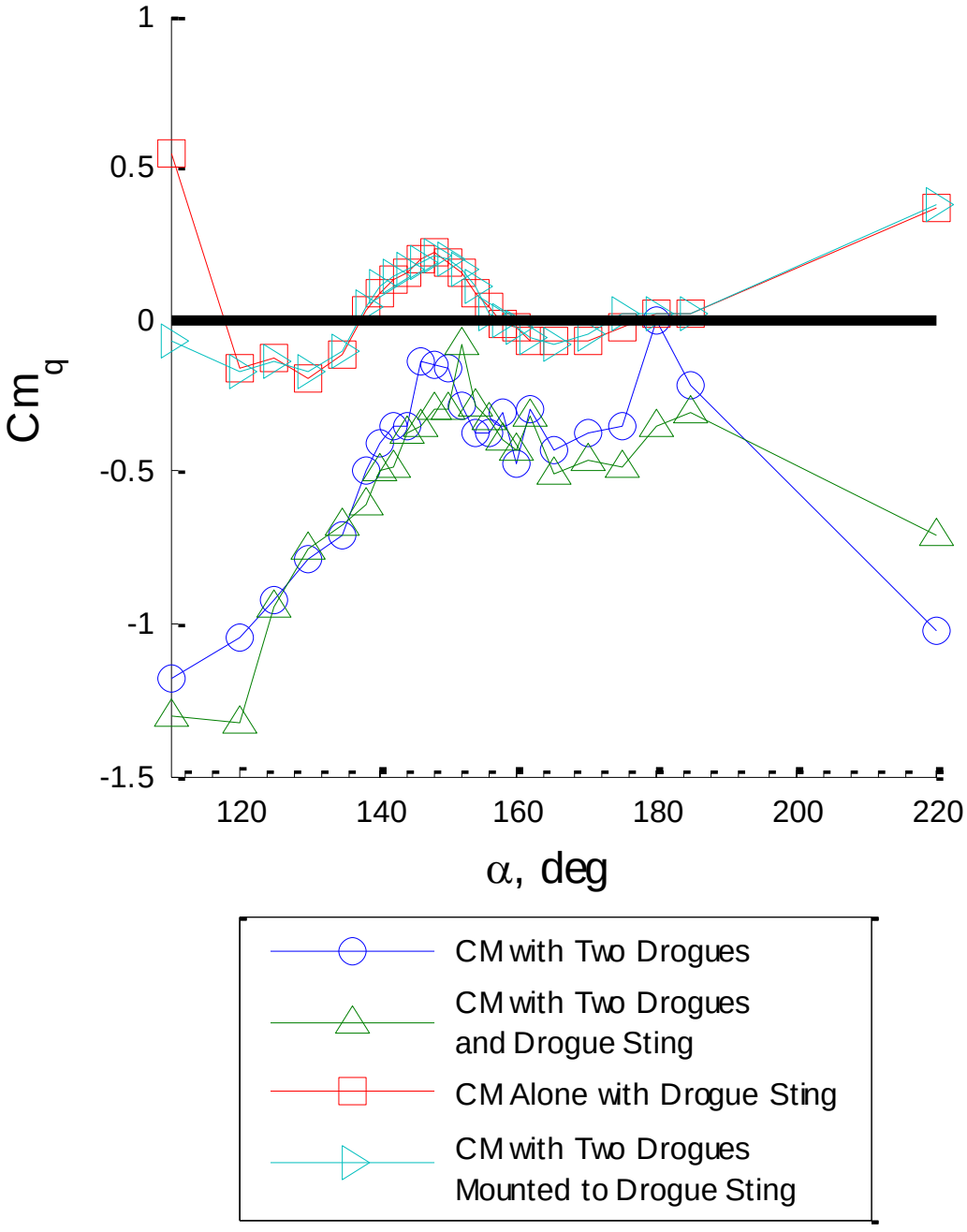

Figure 3-14: Dynamic stability for four configurations (k = 0.125, $\hat{q}_{max}$ = 0.022).

3.3 Drogue Parachute Drag Reduction Due to CM Wake Deficit

The drogue parachute drag (non-dimensionalized with drogue parachute parameters) for a static CM is plotted in Figure 3-15. The drogue parachute drag without the CM wake is shown, as well as the drag for one and two parachutes. The dynamic pressure due to the CM wake decreases by 2-15% for two parachutes versus one. These values are similar to the 10% reduction predicted by Knacke [16]. The Pressure Recovery Fraction (PRF) for one parachute versus two parachutes is shown in Figure 3-16. PRF is calculated by dividing the drag of the parachutes in the wake of the CM, C_D, by the drag of the parachutes in clean flow, $C_{D\infty}$. The CM wake causes a maximum drag reduction of approximately 15% for one drogue parachute and approximately 20% for two drogue parachutes. These maximum drag reductions occur at an angle of attack of 170°. Near the trim angle of attack around 151°, the wake deficit is about 6% for one drogue and 14% for two drogues. The drag reduction for a single parachute is less than the measured 12.4% drag reduction described in Ref. [17] for the CM at 160° angle of attack and less than the approximately 40% predicted by CFD [17]. The PRF measurement is significant because the PRF variation with angle of attack used in simulations is not anchored to test data [18]. The data collected in this test may be able to aid in anchoring those values in simulations. Knacke reports a PRF of 0.82 from Apollo drop tests [16]. This is shown by the line at PRF = 0.82 spanning the angles of attack from 150° to 160°, the approximate trim region for the Apollo vehicle under drogue parachutes. The maximum parachute drag is in the angle of attack range between 140° to 150°. The back shell angle of the CM is 32.5°. This means the flow will start to attach to the back shell

around an angle of attack of 147°, meaning a less turbulent wake behind the CM and a higher freestream velocity at the parachutes. The attachment of flow to the backshell angle could occur at lower angles of attack due to the large should radius on the CM.

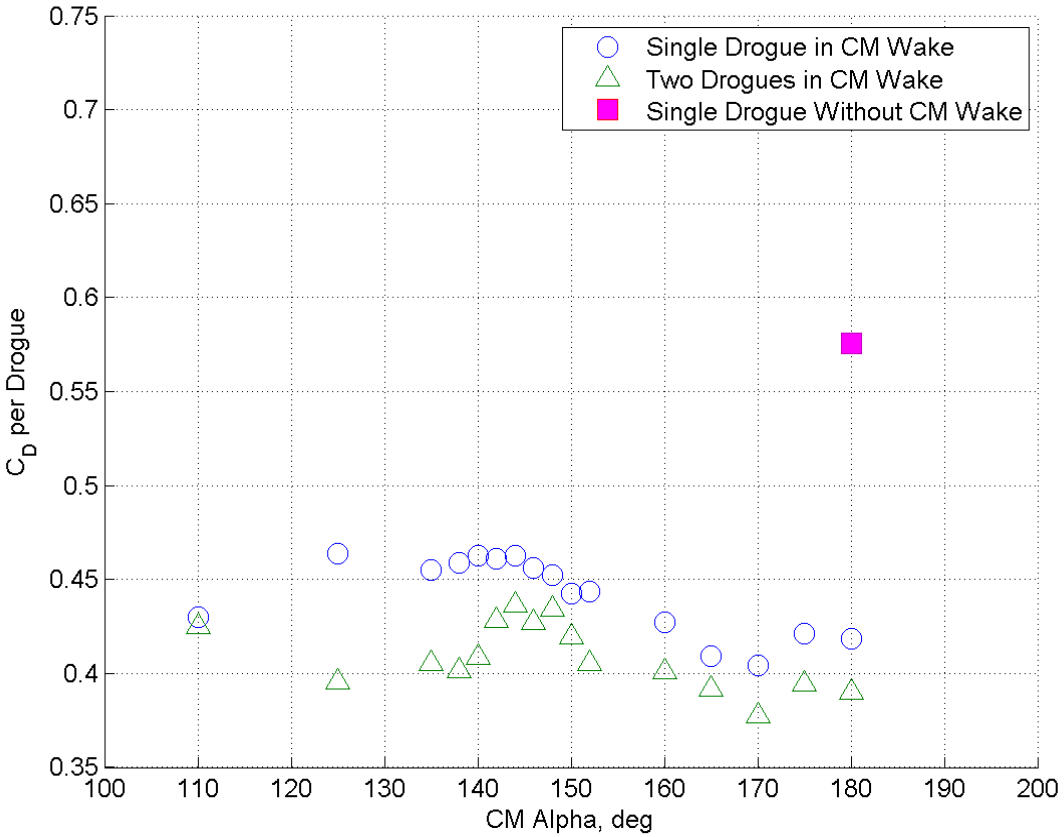

Figure 3-15: The drogue parachute drag wake deficit versus CM angle of attack.

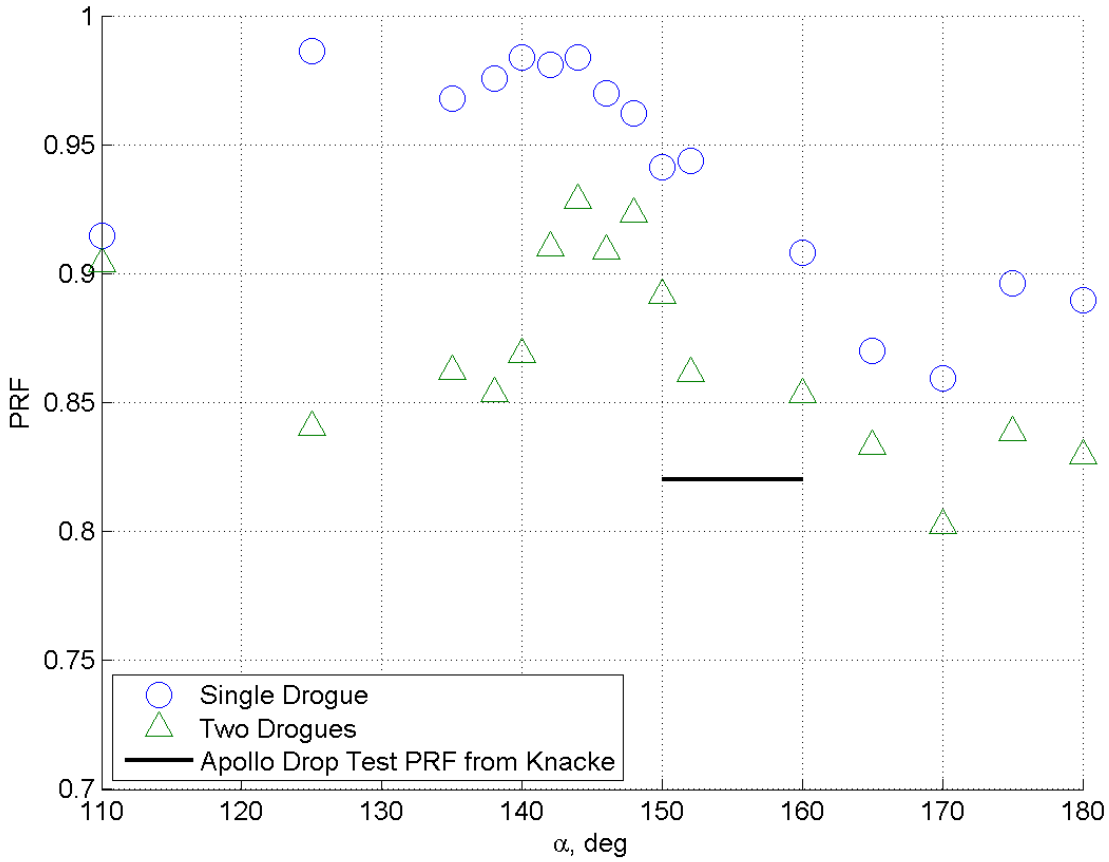

Figure 3-16: Pressure Recovery Factor (PRF), drag loss in CM wake, $C_D/C_{D\infty}$.

Chapter 4

Experimental Results Compared to Apollo Drogue Model Predictions

The experimental results are compared to the Apollo drogue model predictions, and possible explanations for differences between the predicted values and experimentally obtained values are discussed. The damping derivative variation due to unsteady parachute forces is discussed, and the error of the riser line force vector angle due to balance accuracy is computed using the root-sum-square formula for combining errors in overall system-accuracy calculations.

4.1 Predicted Versus Experimental Static and Dynamic Pitching Moments

The static pitching moment coefficient, C_m, for both the Apollo model predictions, as in (1.6), and the experimental wind tunnel test are shown in Figure 4-1. The data from the wind tunnel test for the CM alone, drogue contribution, and the total CM-drogue system are shown. The Apollo drogue model approximation for the drogue contribution is shown in red. The Apollo drogue model approximation for the CM with drogues, shown in cyan, is calculated by adding the drogue contribution to the experimentally obtained CM alone value. C_m for the drogue contribution was calculated from Cm_α in (1.6) by accounting for the parachute wake deficit ($\bar{q}_{chute}/\bar{q}_{CM}$) variation with angle of attack and using the experimentally obtained trim angle of attack for the CM-drogue system. Figure 4-2 shows the experimental pitching moment for one versus two drogues, along with the

Apollo model approximation. The values for the drogue contribution and CM-drogue system compare very well, validating the Apollo drogue model approximation for the Cm_{α} contribution from the drogue parachutes.

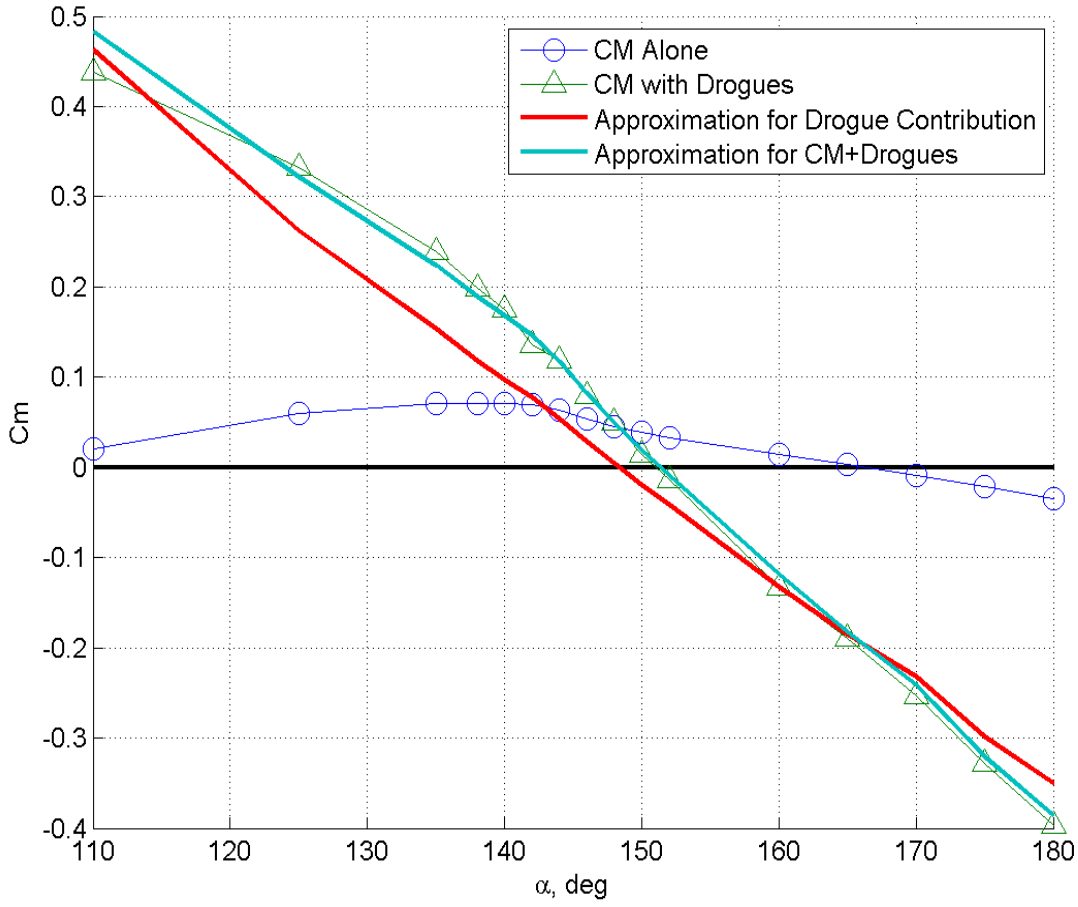

Figure 4-1: Apollo drogue model predicted versus experimental static pitching moment.

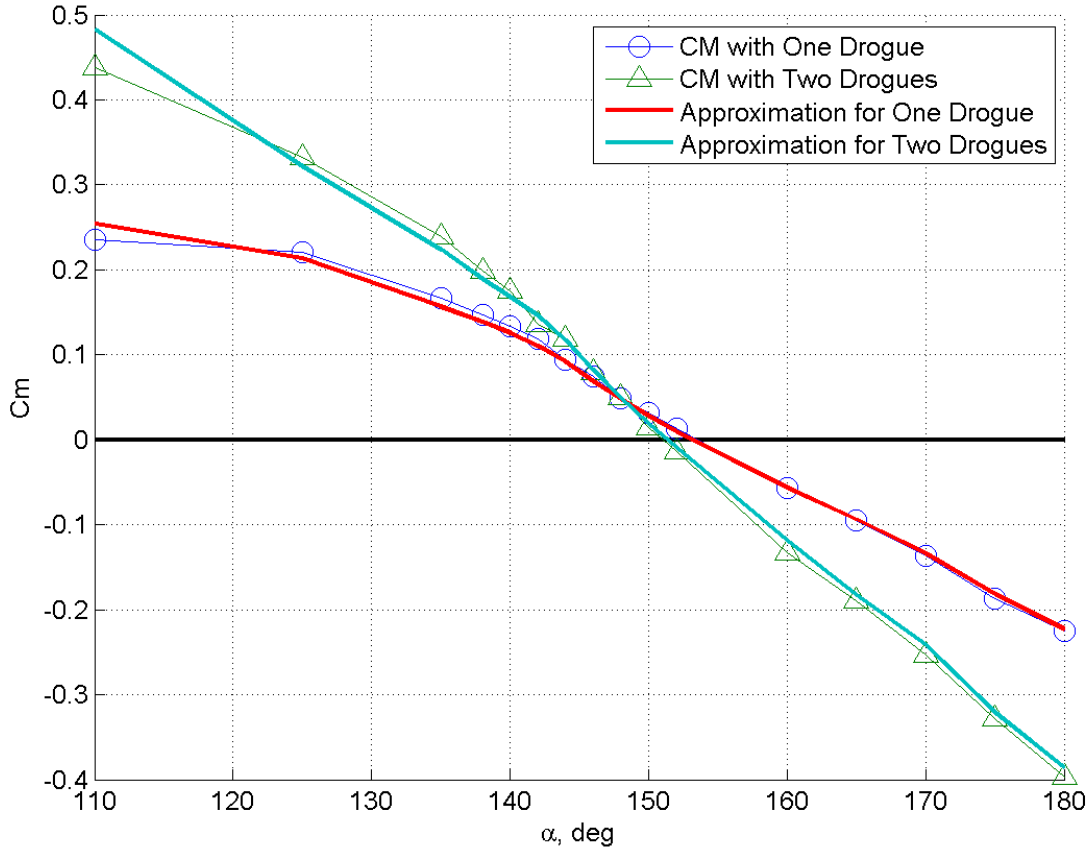

Figure 4-2: Apollo drogue model predicted versus experimental static pitching moment for one versus two drogue parachutes.

The pitch damping for both the Apollo model predictions, as in (1.7), and from the experimental wind tunnel test are shown in Figure 4-3. The data from the wind tunnel test for the CM alone, drogue contribution, and CM with drogues are shown. The Apollo drogue model approximation for the drogue contribution is shown in red. The Apollo drogue model approximation for the CM with drogues, shown in cyan, is calculated by adding the drogue contribution to the experimentally obtained CM alone value. Cm_q for the drogue contribution took the parachute wake deficit variation with angle of attack into account. The Cm_q values are limited to ±25° about trim due to limitations of the small

angle theorem in the derivation of Cm_q. The Apollo drogue model predicts a much more dynamically stable system than experimentally obtained. The drogue contribution to damping measured in the wind tunnel test does not provide the level of dynamic stability indicated by the Apollo model.

Assuming that the CM alone pitch damping measurements are correct, the drogue riser line force vector should be examined in detail. The fourth goal of the wind tunnel test was to measure this force vector, both the magnitude and direction, or angle with respect to the freestream velocity. These data are shown in the next section.

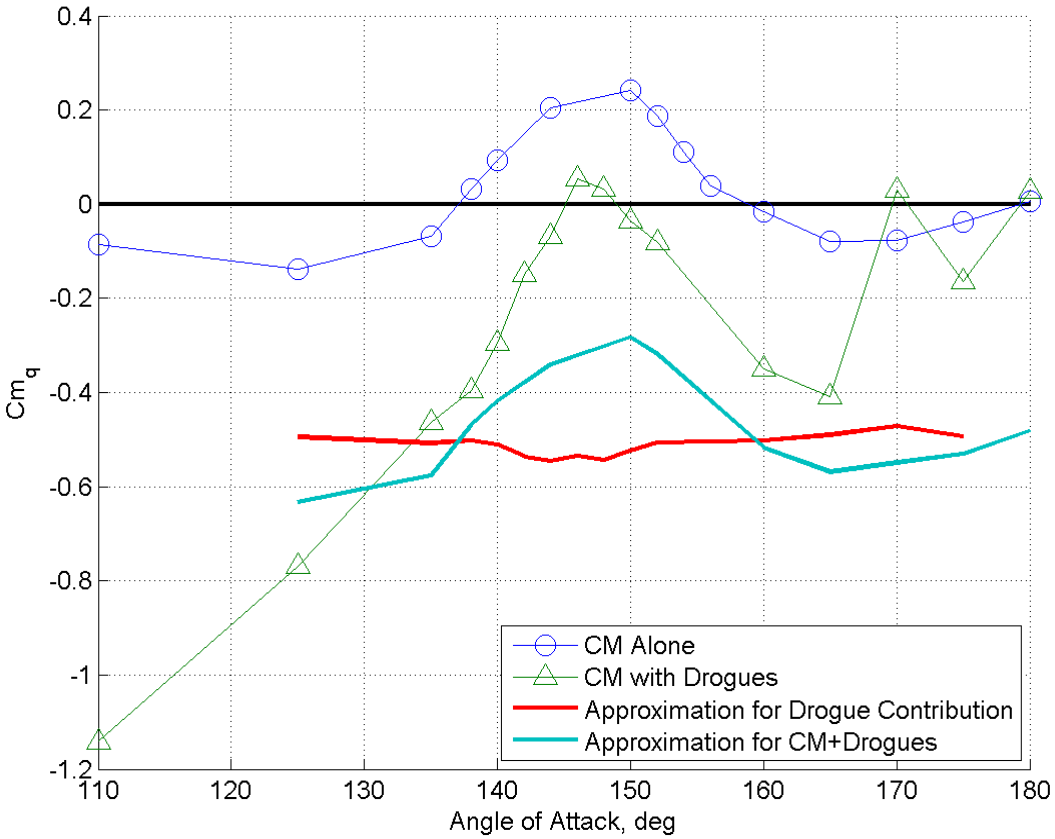

Figure 4-3: Apollo drogue model predicted versus experimental pitch damping.

4.2 Riser Line Force Vector

A major objective of this wind tunnel test was to measure the riser line force vector, both magnitude and direction. The magnitude of the force vector, or parachute drag, was discussed above in Chapter 3. The direction, or angle of the force vector from the freestream velocity vector, is discussed in this section. This angle directly affects the total system pitch damping. The Apollo model approximations do not match the experimentally obtained pitch damping values for the CM-drogue system, as shown in Figure 4-3. This indicates that the major assumption of the Apollo drogue model of the drogue riser line force vector aligning with the velocity vector at the drogue attach point is incorrect. In this section, this angle as measured in the wind tunnel test is shown and compared to the Apollo model assumption.

As a reminder of the definitions of the $\Delta\alpha$ and $\Delta\theta$ angles, Figure 4-4 shows a diagram of the CM-drogue system. The CM coordinate system is shown, along with the positive directions of the drogue attach point forces as measured by the drogue balance at the attach point.

The predicted $\Delta\theta$ is defined as in (1.4). The experimental $\Delta\theta$ is defined as in (4.1). The arctangent of the ratio of normal force to negative axial force gives the drogue line force angle with respect to capsule vertical. The angle of attack of the CM, α, subtracted from 180° gives the CM angle of attack with respect to vertical, or the angle of the freestream

velocity vector with respect to vertical. Subtracting these two angles gives the drogue force vector with respect to the freestream velocity vector, or Δθ.

$$\Delta\theta_{experimental} = \text{atan}\left(\frac{NF_{drogues}}{-AF_{drogues}}\right) - (180 - \alpha) \tag{4.1}$$

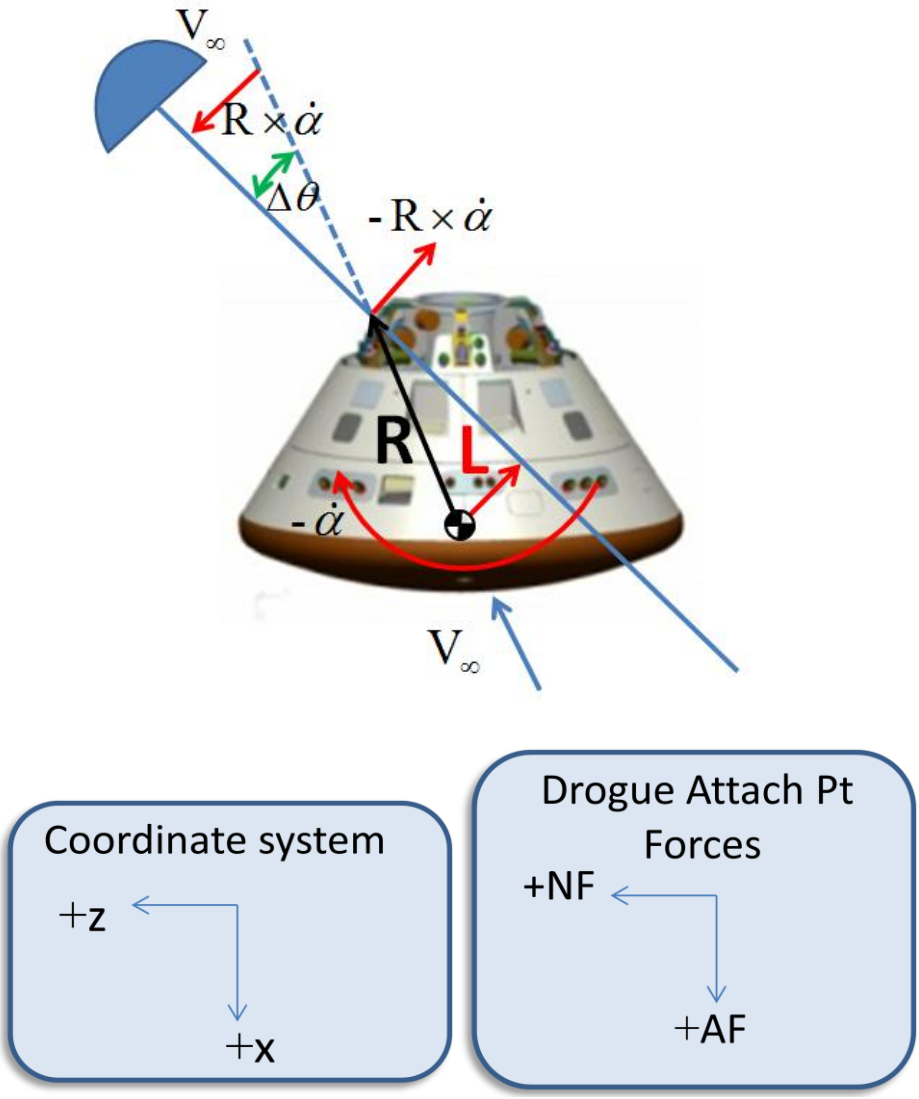

Figure 4-4: Diagram of CM-drogue system with coordinate system and drogue force coordinate system.

A comparison of Δθ angle as predicted by the Apollo drogue model assumption and the experimentally obtained angle is shown in Figure 4-5. This is a time history of data collected from a forced oscillation run where the model was oscillating at 2 Hz with a 10°-amplitude about 152° angle of attack (k = 0.123, $\hat{q}_{max}$ = 0.021). Noticeable in this time history is a bias in the angle and frequency content other than 2 Hz, which is the CM oscillation frequency for this particular run. The extra frequency content is attributable to the unsteady wake behind the CM, perhaps an indication of wake shedding frequency, and possible fluctuations in tunnel flow. The frequency content sources were not thoroughly investigated as they were assumed to have little bearing on the overall damping qualities of the parachutes. According to the Apollo drogue model hypothesis, the drogue parachute force vector should be oscillating about the freestream velocity vector as the CM oscillates about that vector. Therefore, as the predicted Δθ values show, the drogue force vector should be oscillating about zero. The experimental data show an obvious bias of the parachutes from the freestream velocity vector.

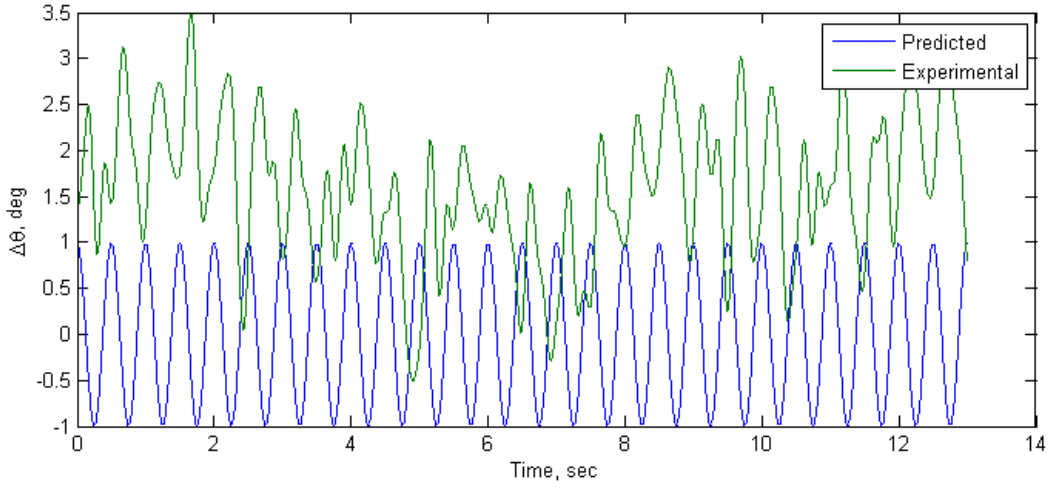

Figure 4-5: Predicted versus experimental drogue chute Δθ time history.

In Figure 4-6, Δθ is plotted versus the CM angle of attack. The bias becomes very apparent in this figure. Also noticeable, is an additional lag in the force vector. If you introduce a lag in the predicted Δθ, you achieve a slanted hysteresis loop as seen in Figure 4-6.

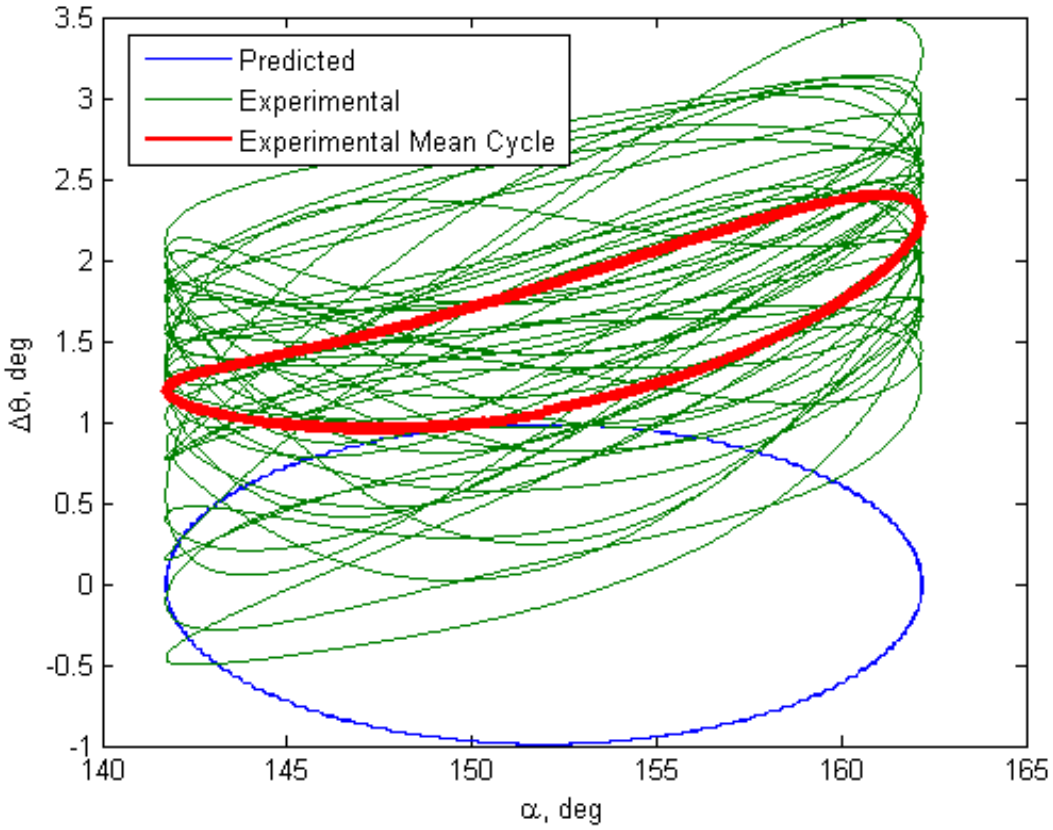

Figure 4-6: Δθ versus CM angle of attack.

The cycles from the time history are averaged to obtain a mean cycle, as shown by the red line in Figure 4-6. The mean cycles of Δθ for each angle of attack that the model was oscillated about are shown in Figure 4-7 versus the Apollo model predictions. The bias away from the freestream velocity vector varies with CM angle of attack. Also, based on

the change in the shape of the mean cycles, the additional lag of the drogue force vector is varying with angle of attack.

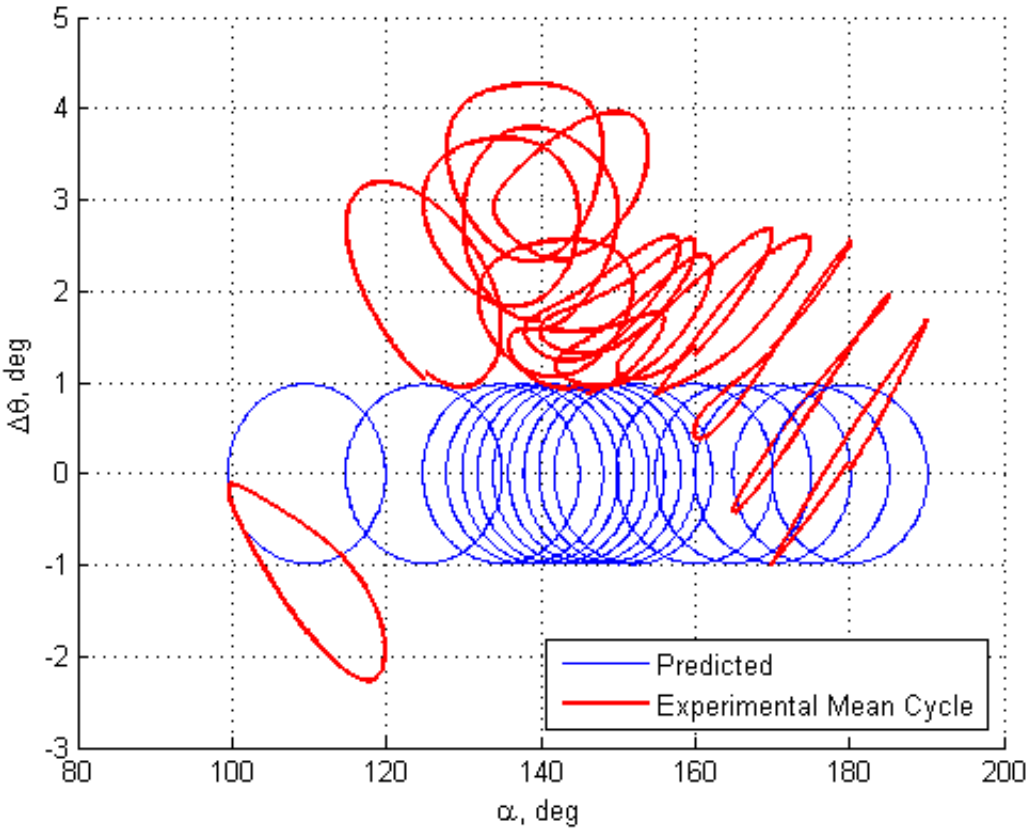

Figure 4-7: Predicted versus experimental Δθ mean cycles.

Modifications to the predicted Δθ were empirically made to closely replicate the experimental Δθ. There are three necessary modifications: 1) time shift, 2) bias, and 3) scale factor. These parameters are similar to a steady-state error, gain, and phase shift that are obtained from analyzing the frequency response of a linear time invariant system. The modified predicted Δθ is shown in equation form in (4.2).

$$\Delta\theta_{pred}^{mod} = \Delta\theta_{pred}^{Shift} * ScaleFactor + Bias \tag{4.2}$$

The time shift is introduced to the predicted Δθ to imitate the additional time lag in the force vector that is seen in the experimental data. The time shift is achieved by merely shifting the data over with respect to time until the slope of the hysteresis loop matches that of the experimental data. This step is shown in Figure 4-8. The predicted Δθ loops are now slanted in the same manner as the experimental Δθ. A bias is then introduced to the predicted Δθ to imitate the bias seen in the experimental data. The effects of time shift and bias are shown in Figure 4-9. The final modification is a scale factor adjustment. The scale factor is primarily required around the trim angle of attack to reduce the magnitude of the loops. An increase in magnitude was also necessary near 180° angle of attack. The result of applying all three modifications, time shift, bias, and scale factor, are shown in Figure 4-10.

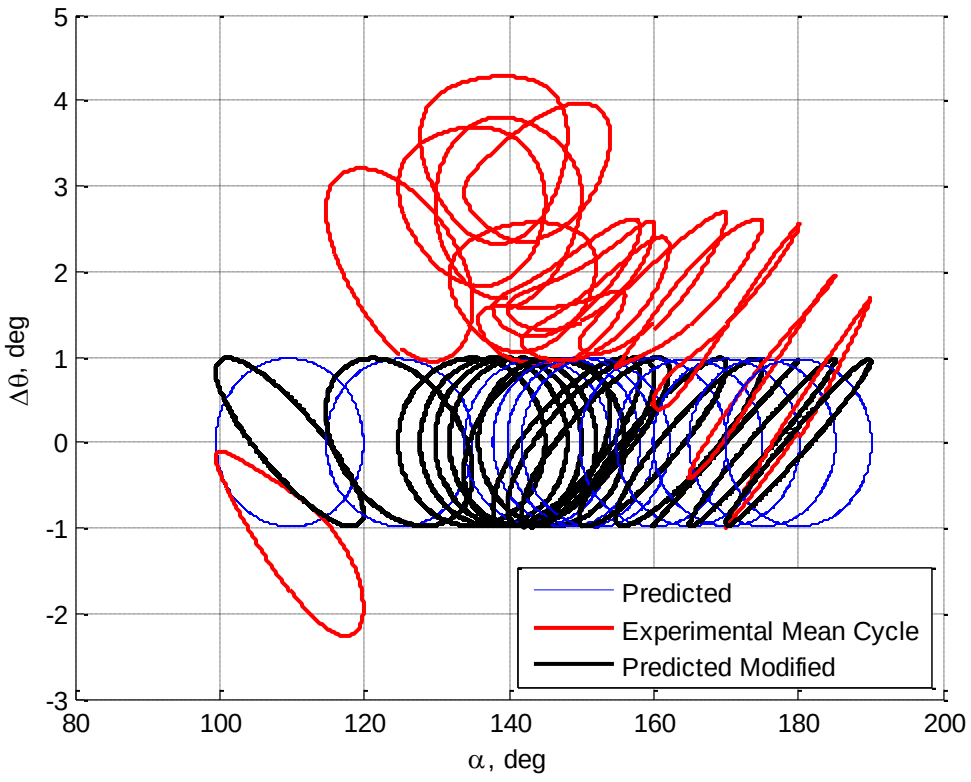

Figure 4-8: Time shift in predicted Δθ to replicate experimental Δθ.

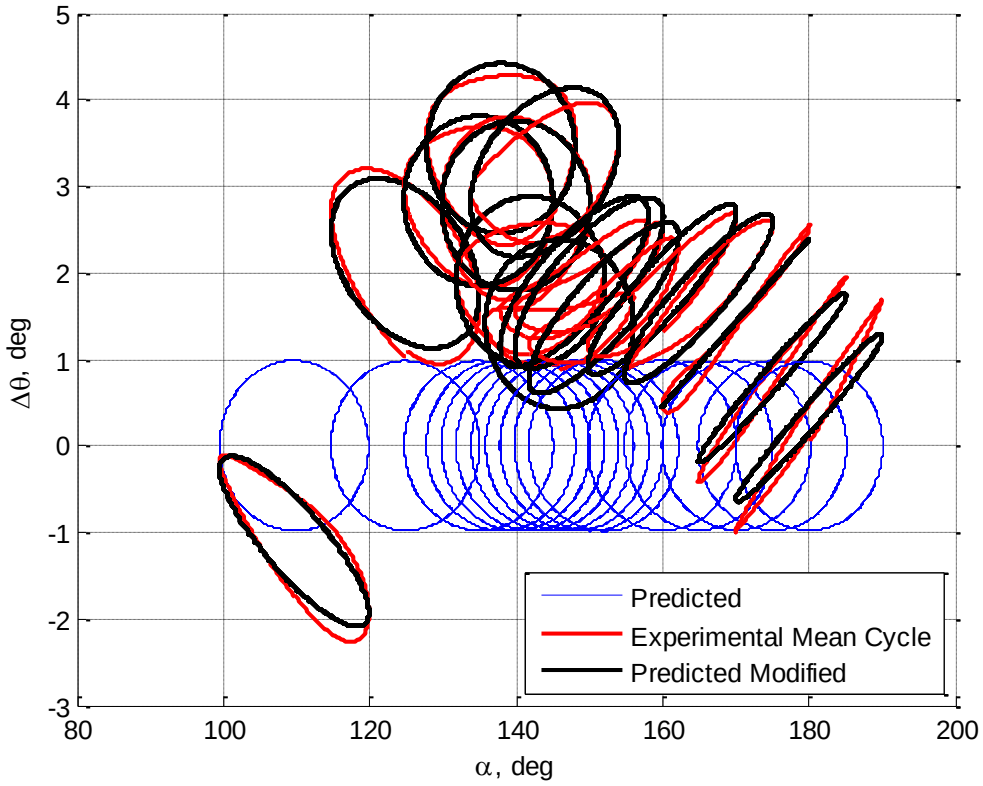

Figure 4-9: Time shift and bias in predicted Δθ to replicate experimental Δθ.

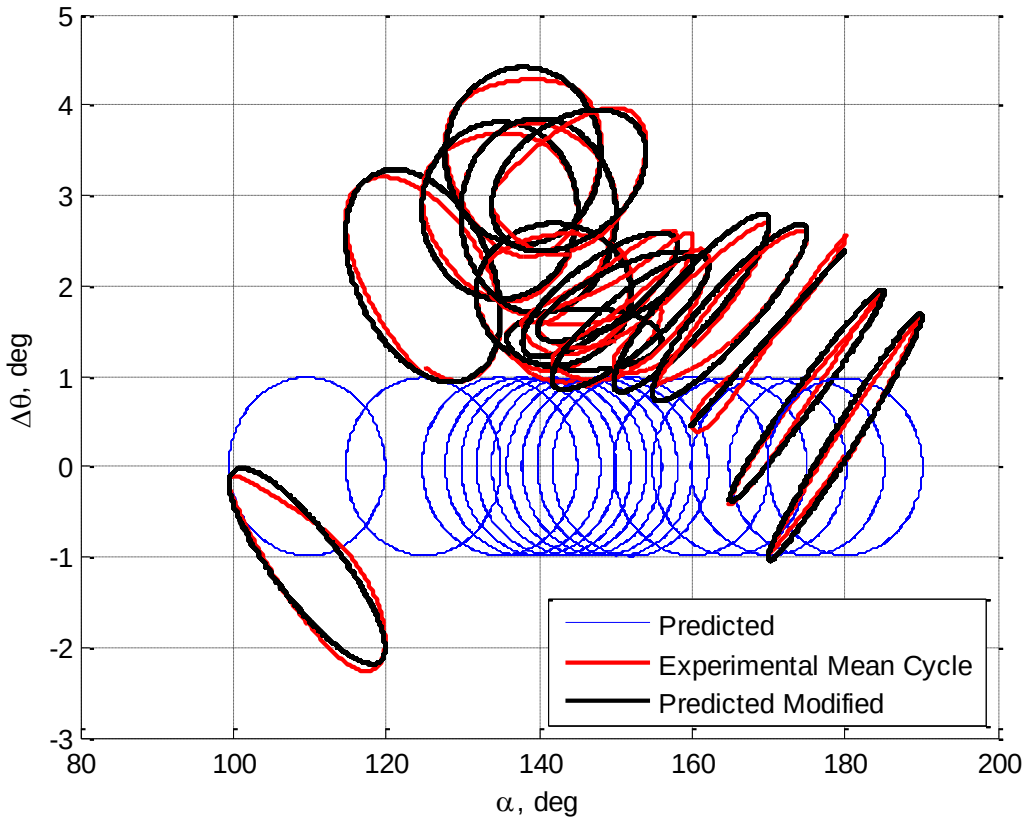

Figure 4-10: Time shift, bias, and scale factor in predicted Δθ to replicate experimental Δθ.

The time shift, bias, and scale factor values are shown versus CM angle of attack in Figure 4-11. The time shift values increase from a CM angle of attack of 180° to 110°. There is a necessary time shift of about 0.17 seconds at the trim angle of attack to match the experimental data, which is about a half of the oscillation cycle of the CM. The Δθ angle is scaled down in the angle of attack range of 140° to 152° to match the experimental data, and is scaled up near an angle of attack of 180 °. The bias values are mostly positive with the exception of one negative value at 110° angle of attack. The

bias appears to be several degrees, between 2° and 4° for the most of the angle of attack range tested, decreasing to 0° very close to an angle of attack of 180°.

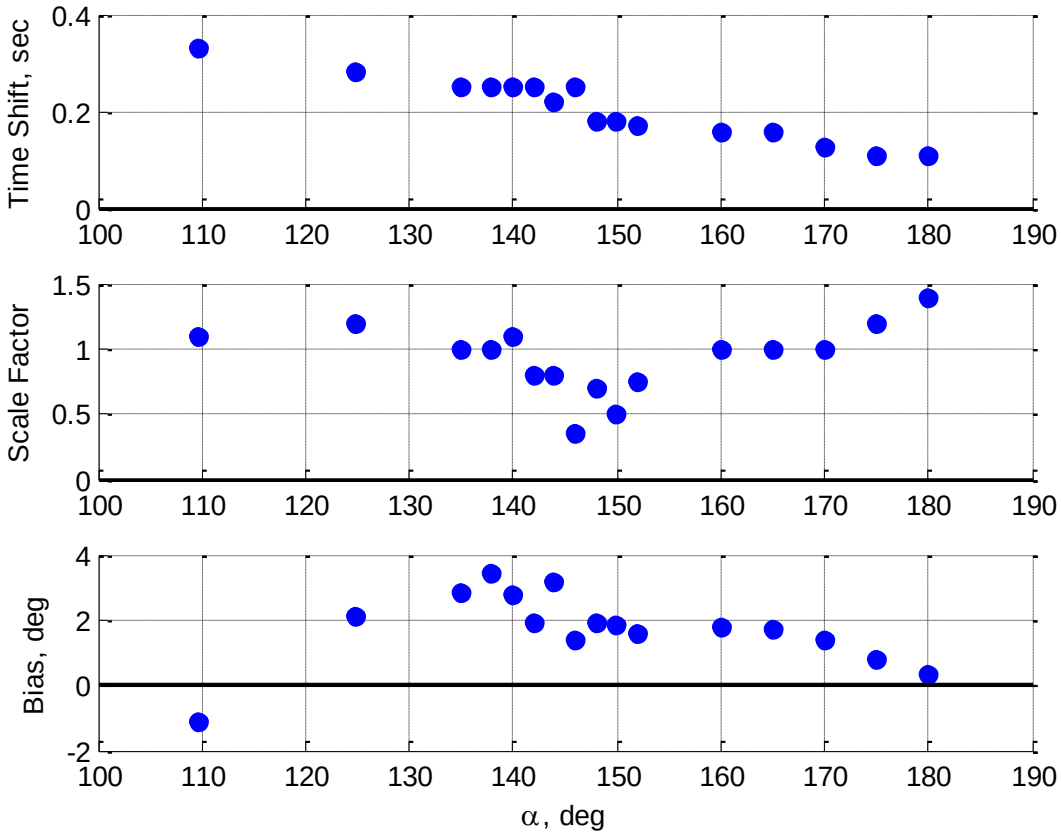

Figure 4-11: Time shift, bias, and scale factor parameters versus angle of attack.

The bias from the freestream velocity vector for a static run is shown in Figure 4-12. The bias shows a similar trend to the bias seen in a forced oscillation run. At 110° angle of attack, the bias is near zero, but at the rest of the angle of attack range, the bias trends from 4° down to 1° at 180° angle of attack. In general, the bias for a static vehicle has a positive increment over the bias for an oscillating vehicle.

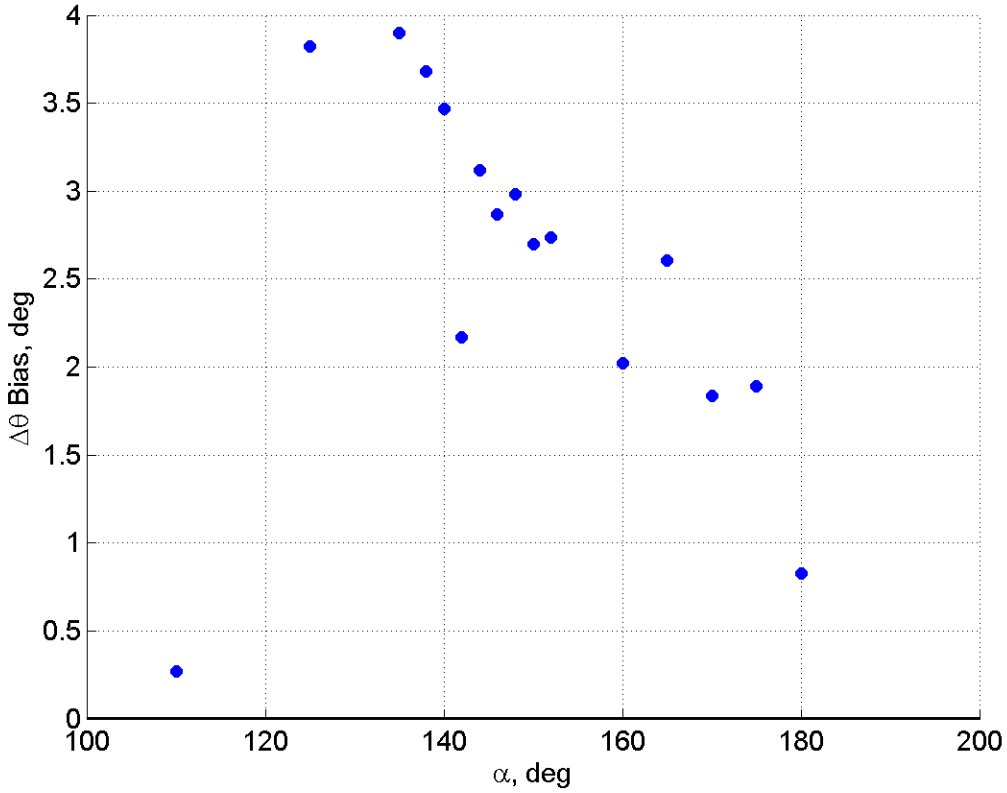

Figure 4-12: Bias from freestream velocity vector for a static run.

Evidence of this bias was seen in both the PA-1 test flight and the VST free-flight tests. Recall that in the simulation matching to the PA-1 test flight data, a 7° magnitude bias, or pitch angle bias, correction was needed [8]. In the simulation matching of the VST free-flight test, slight adjustments were made to the drogue attach point location to achieve a proper trim angle of attack. A bias in the parachute force vector will also have this effect on trim angle of attack. There is sufficient evidence that the wake behind the CM is biasing the parachute force vector away from the freestream velocity vector, indicating that a bias variation with CM angle of attack may need to be modeled in the simulation.

The scale factor can be correlated to PRF, as shown in Figure 4-13. As the drag of the drogue parachutes increases, the predicted maximum and minimum values of Δθ need to be decreased in order to match the experimental Δθ. The same relationship is evident in (1.4). As the velocity is increased in the denominator of the equation, Δθ decreases. This indicates that the angle of the riser line is also a function of velocity in the wake of the CM, not only the freestream velocity of the CM.

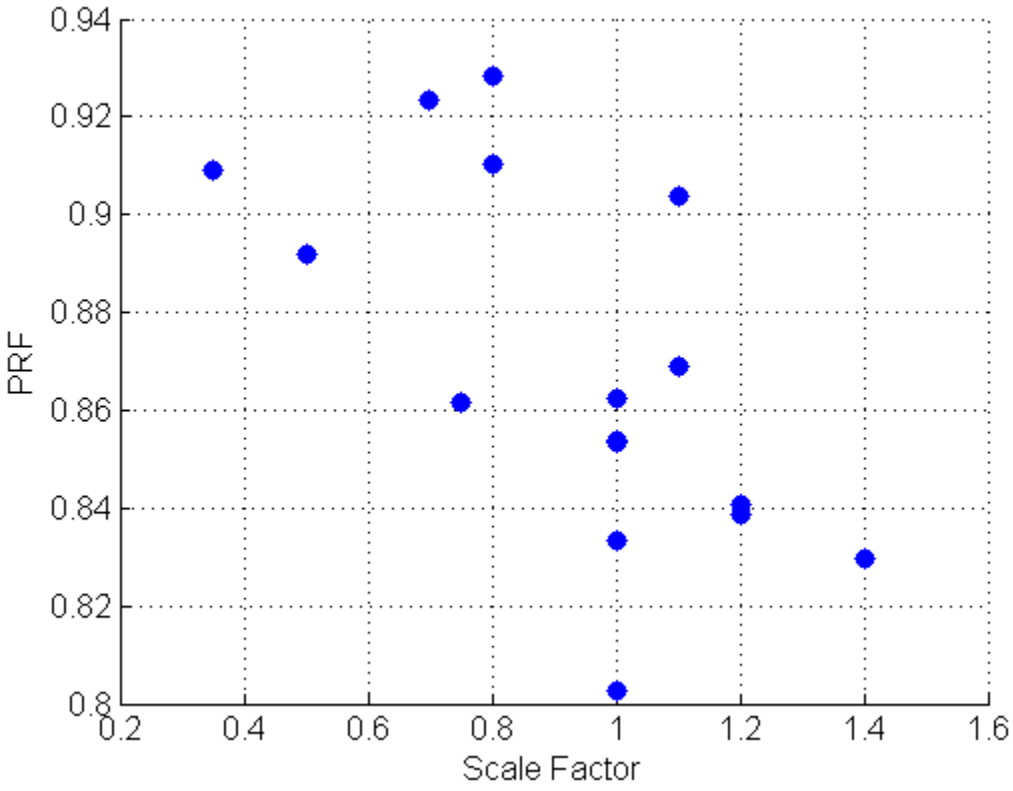

Figure 4-13: Scale factor correlation to PRF.

Similar to the plot shown in Figure 4-7, Figure 4-14 is another plot of a different forced oscillation run for k = 0.042 and $\hat{q}_{max}$=0.007. A similar bias is noted, but the mean cycles have different slopes. This provides further evidence that the bias is due to wake

changes at various CM angles of attack. The different slopes of the mean cycles between Figure 4-7 and Figure 4-14 indicate that the lag is a function of oscillation frequency or pitch rate.

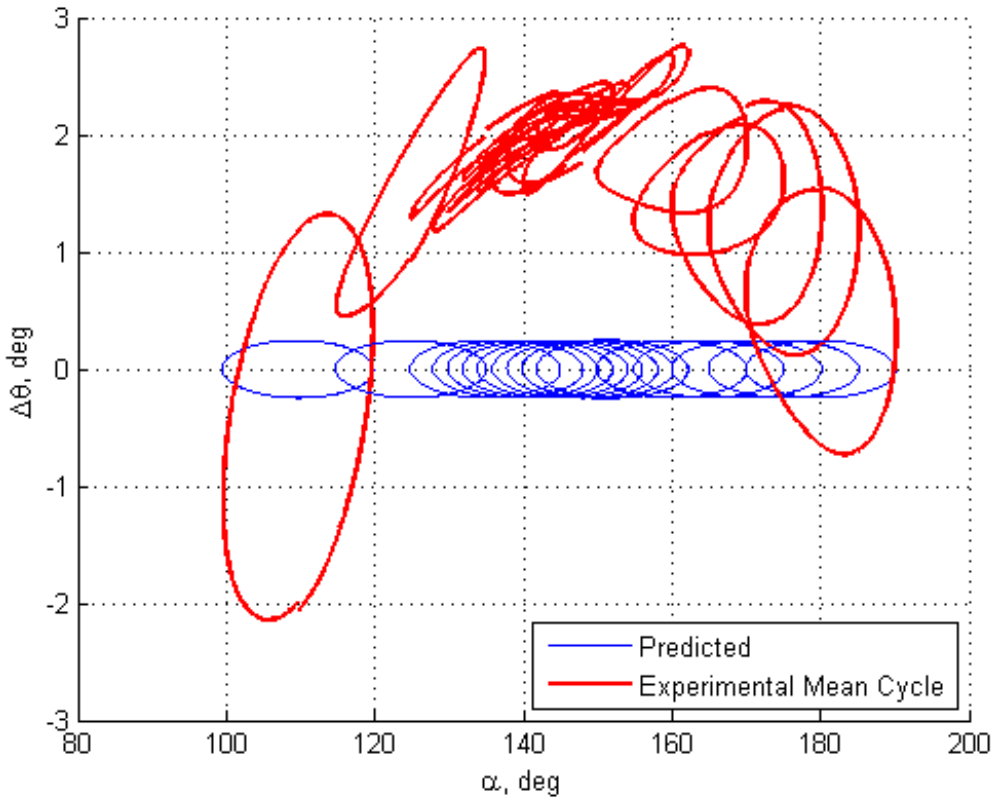

Figure 4-14: Predicted versus experimental Δθ mean cycles for k = 0.042, $\hat{q}_{max}$ = 0.007.

Examining the Δθ mean cycles at a CM angle of attack of 180° for various combinations of frequency and pitch rate produces the plot shown in Figure 4-15. The shapes of the loops show a clear dependency on oscillation frequency. As the frequency of CM oscillation increases, so does the slope of the hysteresis loop, indicating an increased time lag of the drogue force vector over what is predicted by the Apollo drogue model.

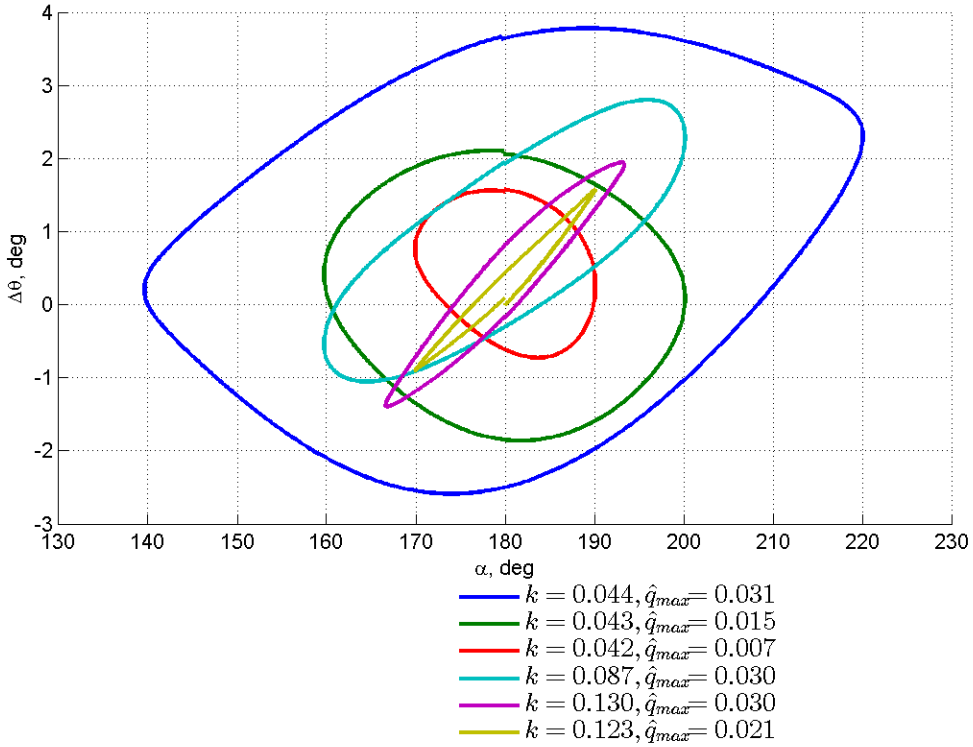

Figure 4-15: Δθ mean cycles for varying frequency-rate combinations at 180° angle of attack.

The time lag, converted to phase shift notation, over all angle of attack values for various vehicle oscillation frequencies is shown in the plot in Figure 4-16. The lag is clearly dependent on vehicle angle of attack and oscillation frequency. The angle of attack dependency is most likely due to varying wake effects at different CM angles of attack. In Ref. [8], a small time lag in the riser line angle relative to the vehicle was also noted in the PA-1 flight test data. The additional, unpredicted phase shift effect with frequency indicates that parachute motion relative to the CM is not completely described by the Apollo model.

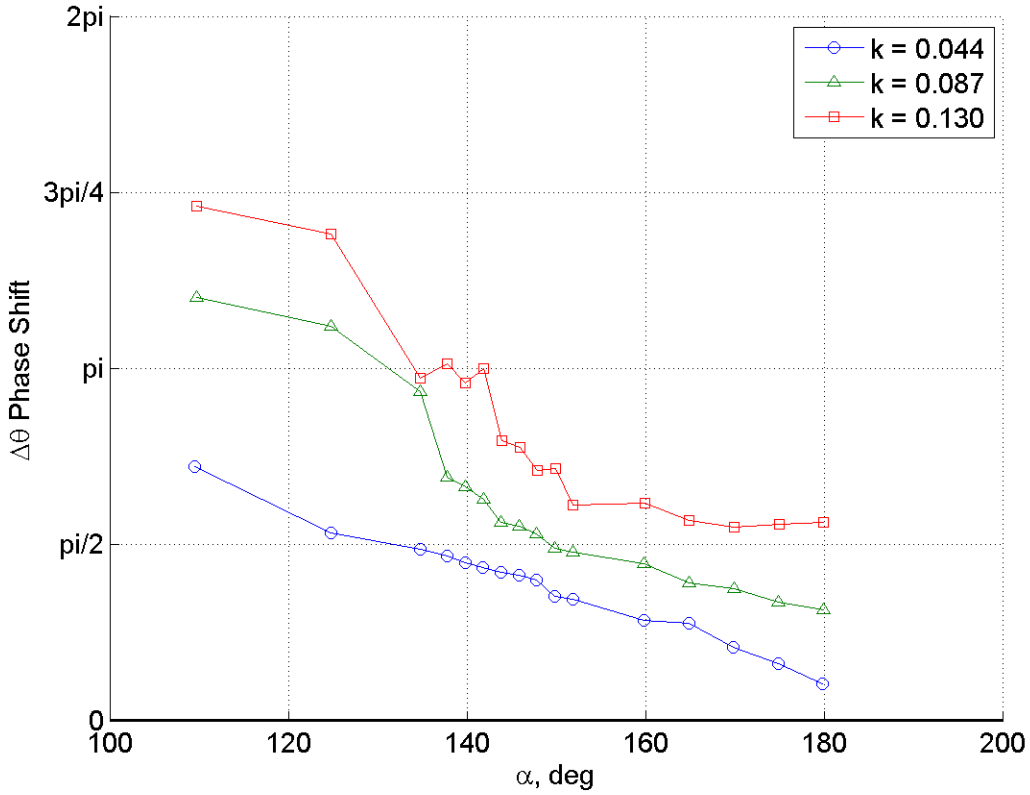

Figure 4-16: Phase shift, or additional lag, as function of oscillation frequency and angle of attack, $\hat{q}_{max} = 0.030$.

4.3 Riser Line Force Vector for Single Drogue

The bias from the freestream velocity vector for one drogue parachute is shown in Figure 4-17. This bias is increased from the bias for two drogue parachutes by about 0.5°. This difference is caused by the single parachute settling into a region of the wake that is least turbulent. When two parachutes are in the wake, one of them will be pushed out of the region with less turbulent flow and cause the resultant force vector to align more with the freestream velocity of the CM. Evidence of this behavior was seen in the wind tunnel

test in VST. One parachute remains relatively stationary in the CM wake, while the other oscillates at the same frequency as the CM.

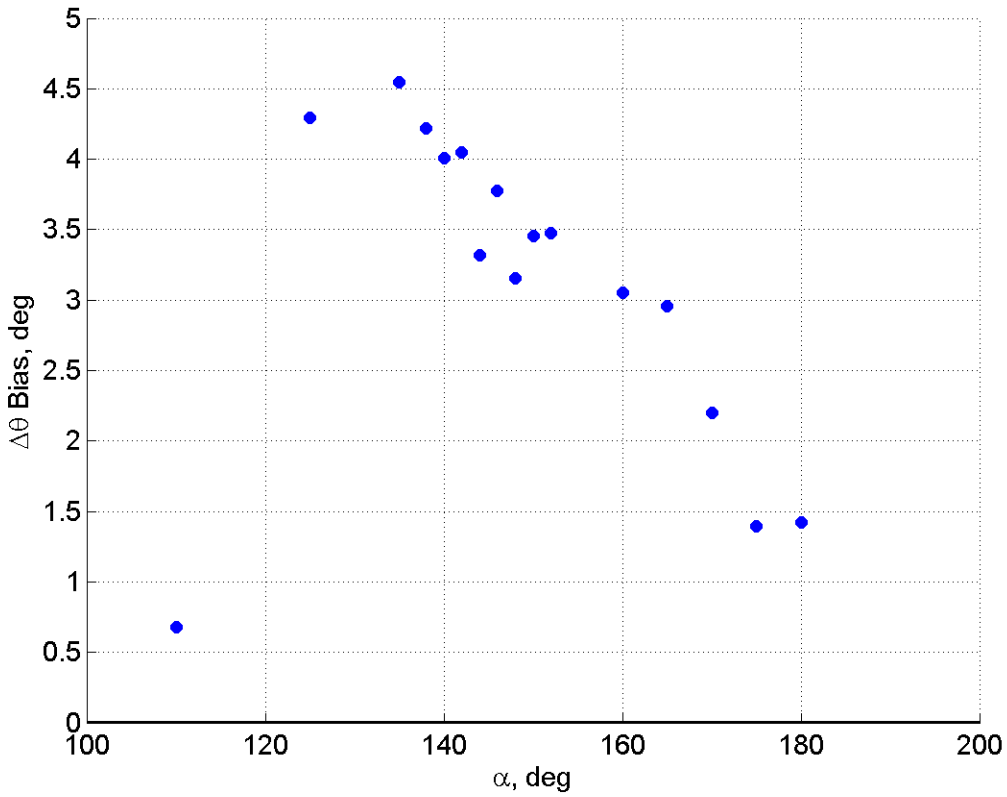

Figure 4-17: Bias from freestream velocity vector for a static run with one drogue parachute.

The phase shift from the Apollo-predicted $\Delta\theta$ is shown in Figure 4-18. These values are very similar to the phase shift for two drogue parachutes. A strong dependence on CM angle of attack and oscillation frequency are noted.

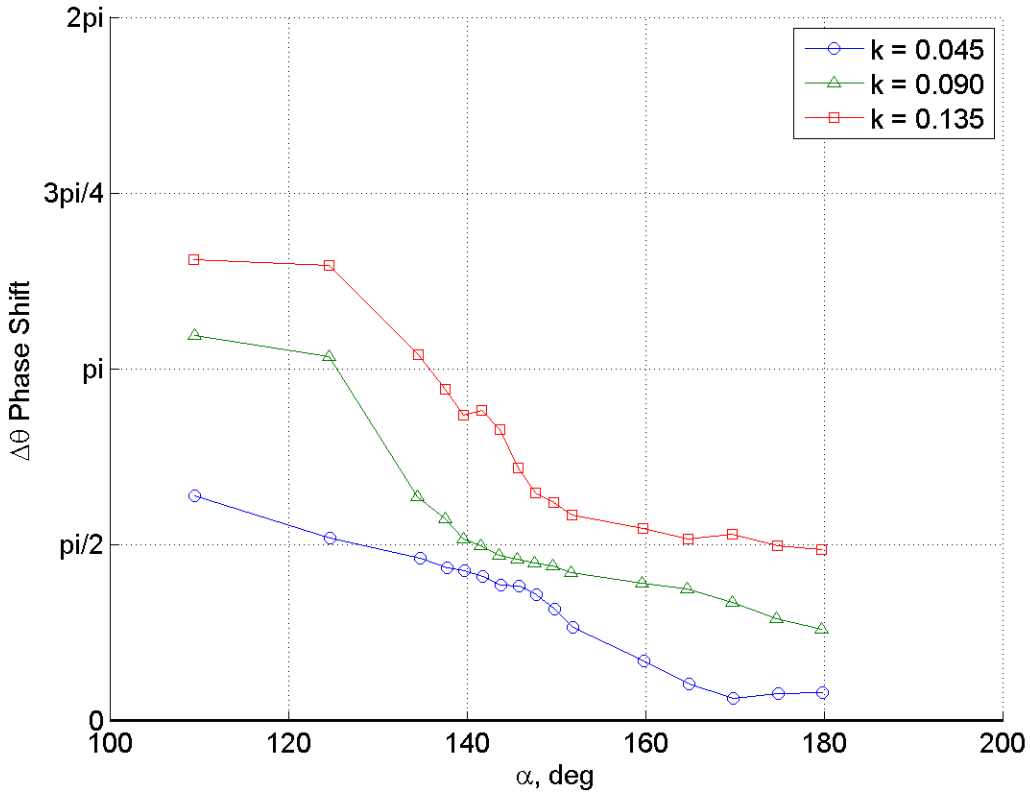

Figure 4-18: Phase shift, or additional lag, as function of oscillation frequency and angle of attack for one drogue parachute, $\hat{q}_{max} = 0.031$.

4.4 Hysteresis in Parachute Force Magnitude

The Apollo drogue model assumes a constant drag on the drogue parachutes even as they are traversing through the wake of an oscillating CM. Figure 4-19 shows the drag of two drogue parachutes versus the CM angle of attack for an oscillating CM. The drag is computed only in the pitch plane of the CM because the focus is Cm_q. The force component in the yaw plane is neglected. The drag exhibits a hysteresis effect. The effect is a function of the wake variation with CM angle of attack and the acceleration experienced by being pulled back and forth by the oscillating CM.

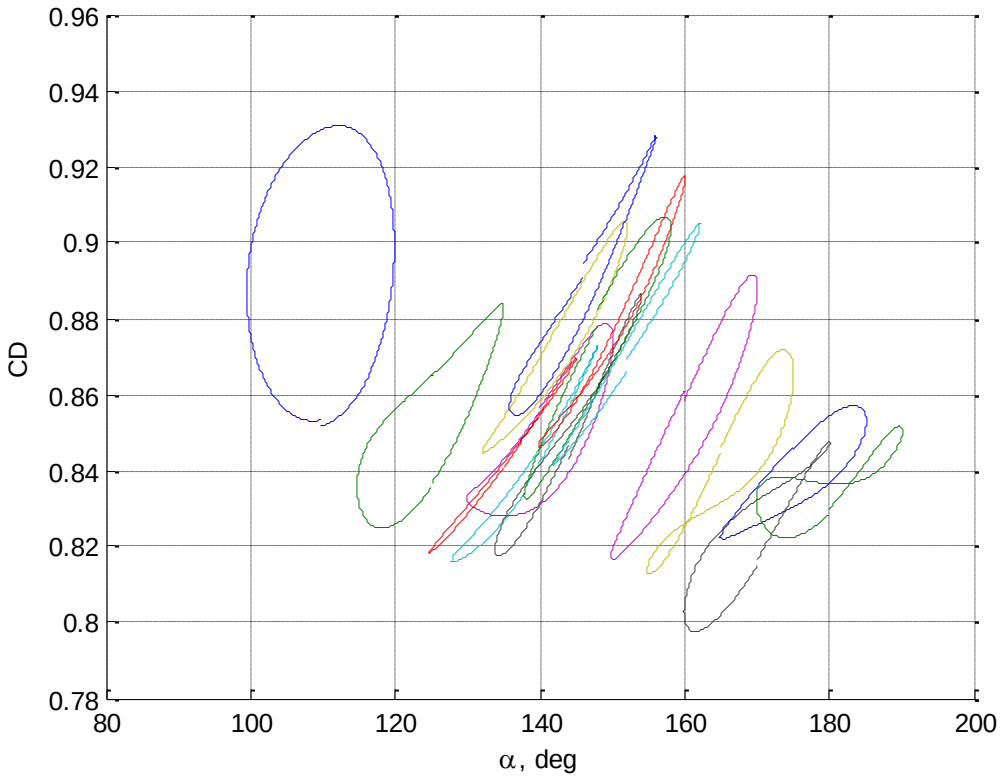

Figure 4-19: Drogue parachute drag versus CM angle of attack.

4.5 Cm_q Variation Due to Unsteady Drogue Parachute Forces

The unsteady nature of the drogue parachute forces in the CM wake produces a rather large variation of calculated Cm_q values per cycle in the forced oscillation method. Many cycles are measured about one angle of attack point, and then the pitching moment is averaged to obtain a mean cycle from which to derive the Cm_q value for that mean angle of attack. The pitching moment coefficient produced by the drogue parachutes (non-dimensionalized with CM reference area and length) versus angle of attack for a complete set of cycles is shown in Figure 4-20. The average, or mean cycle, is shown in

red. The standard method of computing Cm_q is to use the mean cycle. However, if each cycle is used individually to compute Cm_q, the trend of Cm_q with cycle number is shown in Figure 4-21. The blue line shows the result of averaging each individual Cm_q value, and the red line shows the result of using the mean cycle to calculate Cm_q. The difference between these two methods does not appear large for this angle of attack condition. However, the variation of Cm_q values per cycle is fairly large.

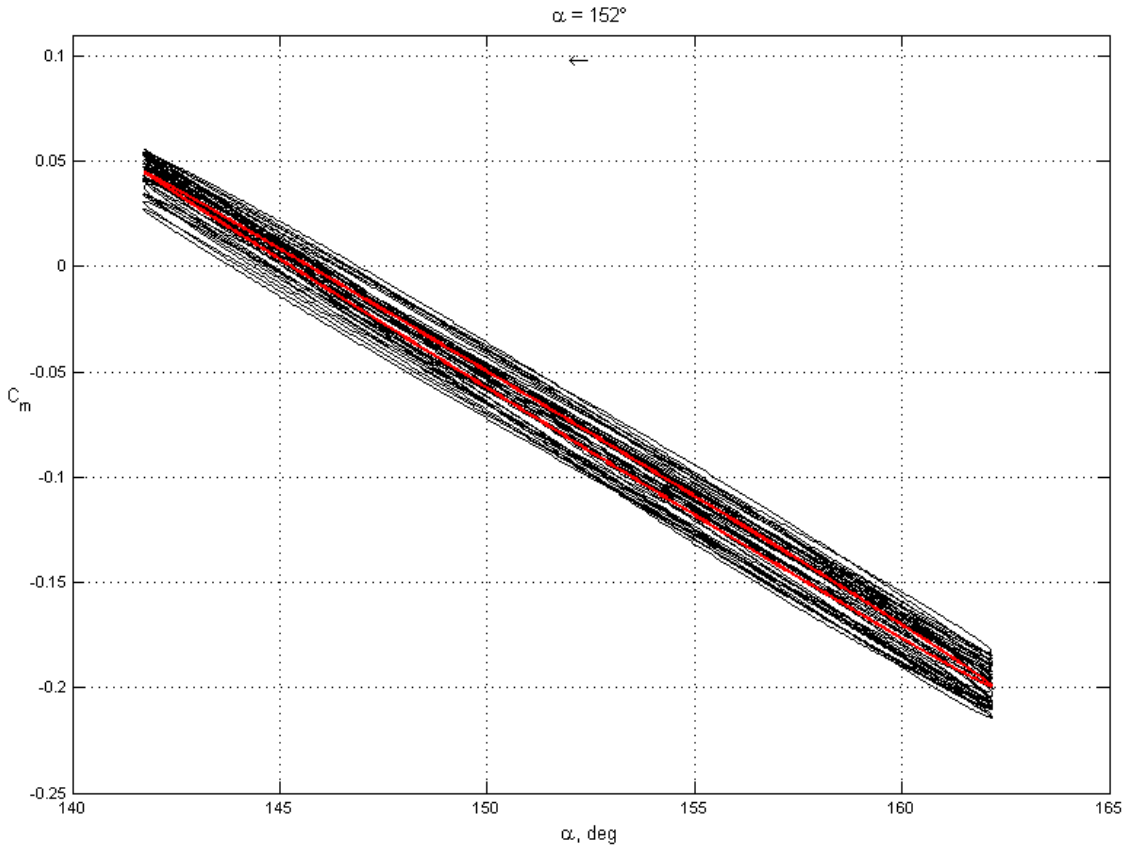

Figure 4-20: Pitching moment coefficient produced by drogue parachutes for a complete set of cycles.

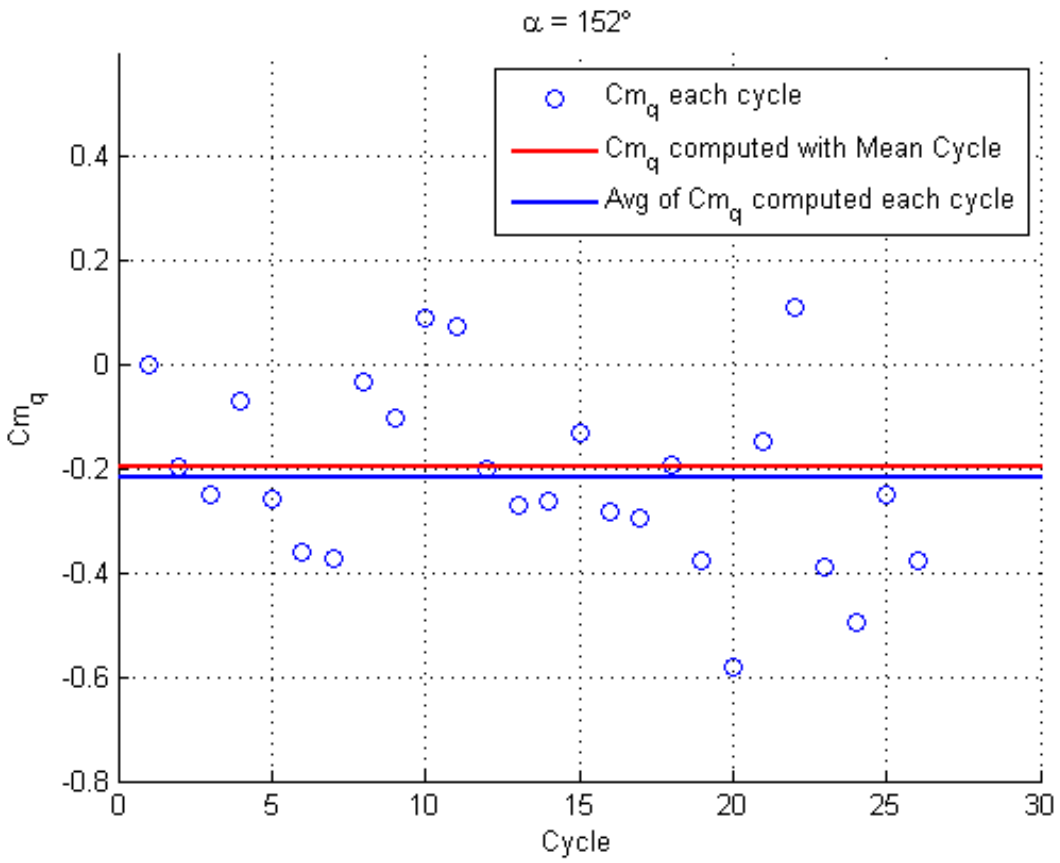

Figure 4-21: Cm_q per cycle for drogues.

A similar method can be applied to all angle of attack values in a forced oscillation run, and the plot in Figure 4-22 is produced. The black dots indicate the Cm_q values per cycle for a given angle of attack. The blue circles are the average of those individually-computed Cm_q values, and the red circles are the Cm_q values computed with the mean cycle. The variation of Cm_q values is quite large for most angle of attack values. The Apollo model predicts Cm_q values of approximately -0.5 near the trim angle of attack of 151°. The most negative values of Cmq in this region do reach this value. If uncertainties were added to the calculated Cmq values to cover this broad range of possible values, the level of damping predicted by the Apollo model would be included in

the range. If a Monte Carlo type analysis was used to cover this range of possible values, the overall performance of the system would still be evaluated relative to a mean damping that is less damped than predicted by the Apollo model but still stable.

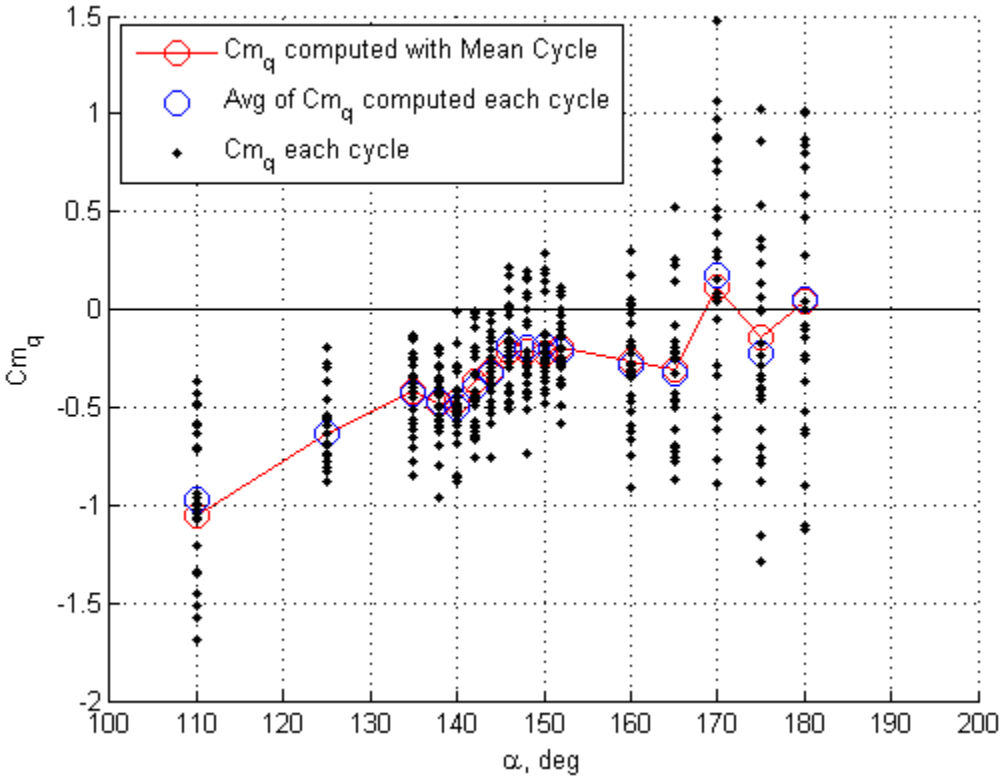

Figure 4-22: Cm_q contribution from drogues per cycle.

4.6 Error of Δθ Computed From Balance Accuracy Statistics

One more potential error is discussed in this section: the error of Δθ due to balance accuracy. The root-sum-square (RSS) formula for combining of component error in overall system-accuracy calculations is used to calculate potential errors from balance accuracy [19]. First, consider a quantity *y* that is a function of *n* independent variables, as in (4.3). Using a Taylor series expansion of this equation to account for small changes in

the independent variables, the uncertainty of *y* can be derived as in (4.4) to be a function of the uncertainties of the independent variables. This equation provides a 95% confidence interval for the dependent variable *y*, since U_y is computed from individual uncertainties that are 95% confidence intervals.

$$y = f(x_1, x_2, x_3, \dots x_n) \tag{4.3}$$

$$U_y \approx \sqrt{\left(\frac{\partial f}{\partial x_1} \cdot u_{x1}\right)^2 + \left(\frac{\partial f}{\partial x_2} \cdot u_{x2}\right)^2 + \cdots + \left(\frac{\partial f}{\partial x_n} \cdot u_{xn}\right)^2} \tag{4.4}$$

The equation to calculate Δθ from the experimental data is shown in (4.5). In this case, Δθ is the dependent variable, and drogue normal and axial force ($NF_{drogues}$, $AF_{drogues}$) and α_{CM} are the independent variables. Taking the partial derivative of this equation with respect to $NF_{drogues}$ and $AF_{drogues}$ and multiplying those partial derivatives by the 95% confidence interval of those variables gives (4.6). Uncertainties for $NF_{drogues}$ and $AF_{drogues}$ come from the calibration of the drogue balance and are provided in terms of standard deviations. Assuming these variables are Gaussian, multiplying the standard deviation by 2 gives the 95% confidence interval needed in the RSS formula.

$$\Delta\theta_{experimental} = atan\left(\frac{NF_{drogues}}{-AF_{drogues}}\right) - (180° - \alpha_{CM}) \tag{4.5}$$

$$U = \pm\sqrt{\left[\left(\frac{-AF}{AF^2 + NF^2}\right) \cdot (2 \cdot 0.002)\right]^2 + \left[\left(\frac{NF}{AF^2 + NF^2}\right) \cdot (2 \cdot 0.004)\right]^2} \tag{4.6}$$

The uncertainty on Δθ from the drogue balance is computed for a forced oscillation at an angle of attack of 180°, k of 0.123, and $\hat{q}_{max}$ of 0.021. Δθ versus angle of attack with the uncertainty bounds is shown in Figure 4-23. Just the uncertainty versus angle of attack is shown in Figure 4-24. The same two plots for a different forced oscillation run at an angle of attack of 180°, k of 0.044, and $\hat{q}_{max}$ of 0.031 are shown in Figure 4-25 and Figure 4-26. The uncertainties are very small compared to the magnitude of the angle measurement, and, therefore, not a concern as far as compromising the drogue riser line vector measurement.

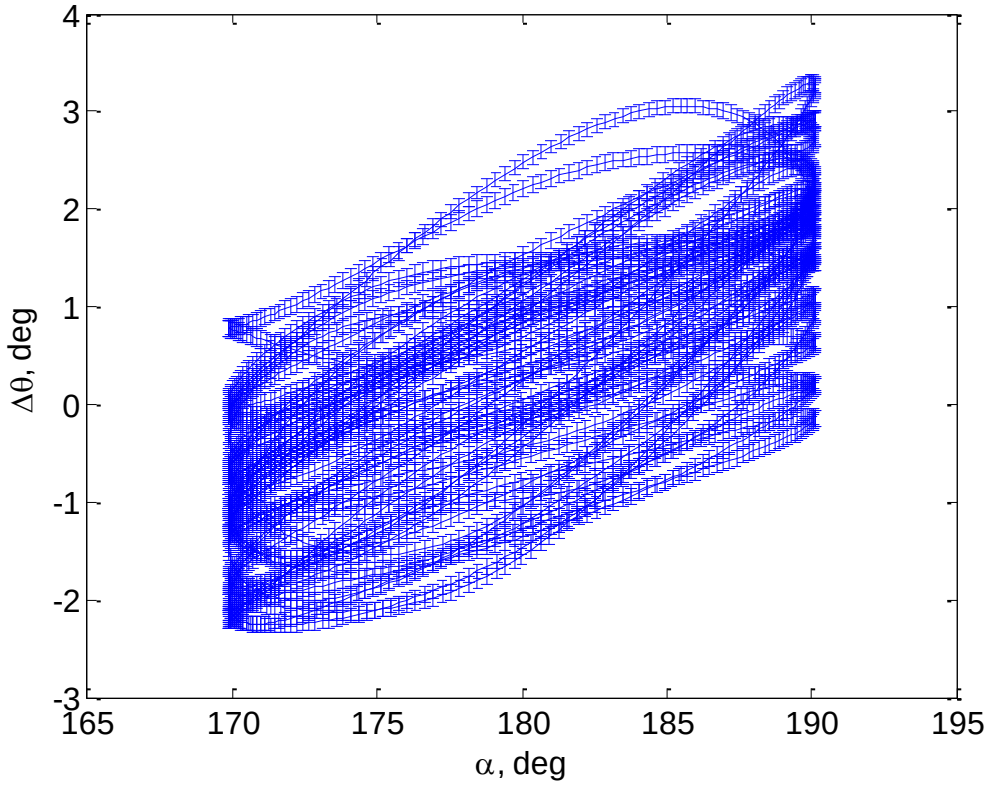

Figure 4-23: Δθ versus angle of attack with positive and negative uncertainties.

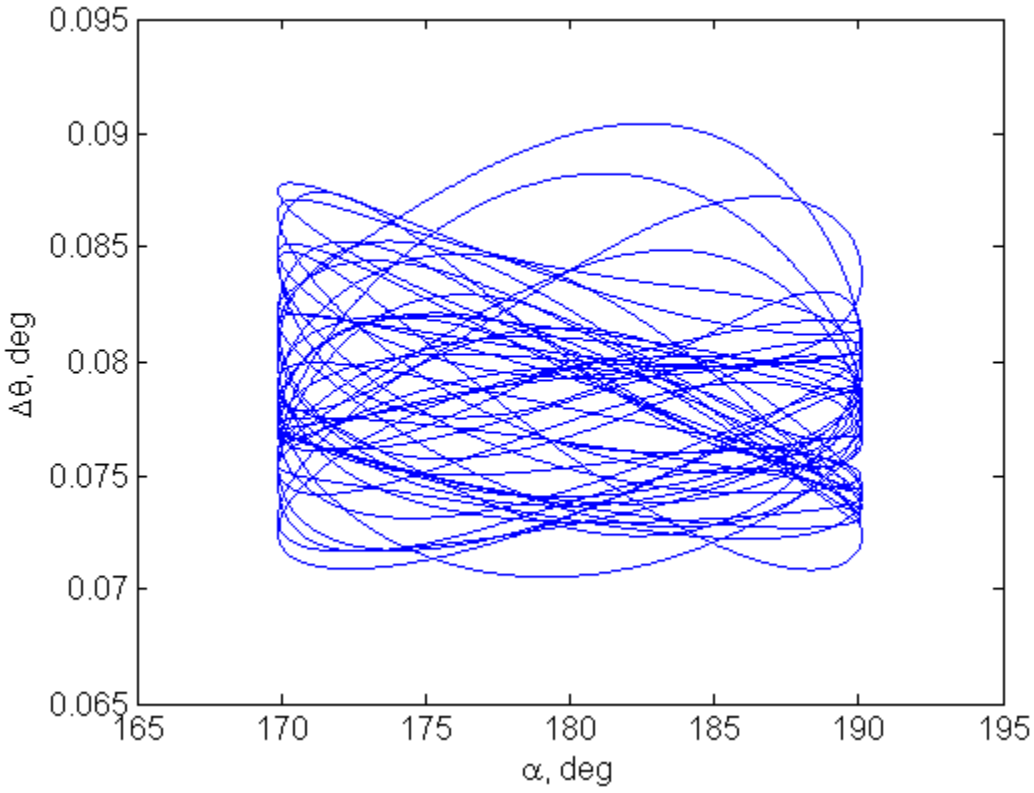

Figure 4-24: Uncertainty of Δθ versus angle of attack.

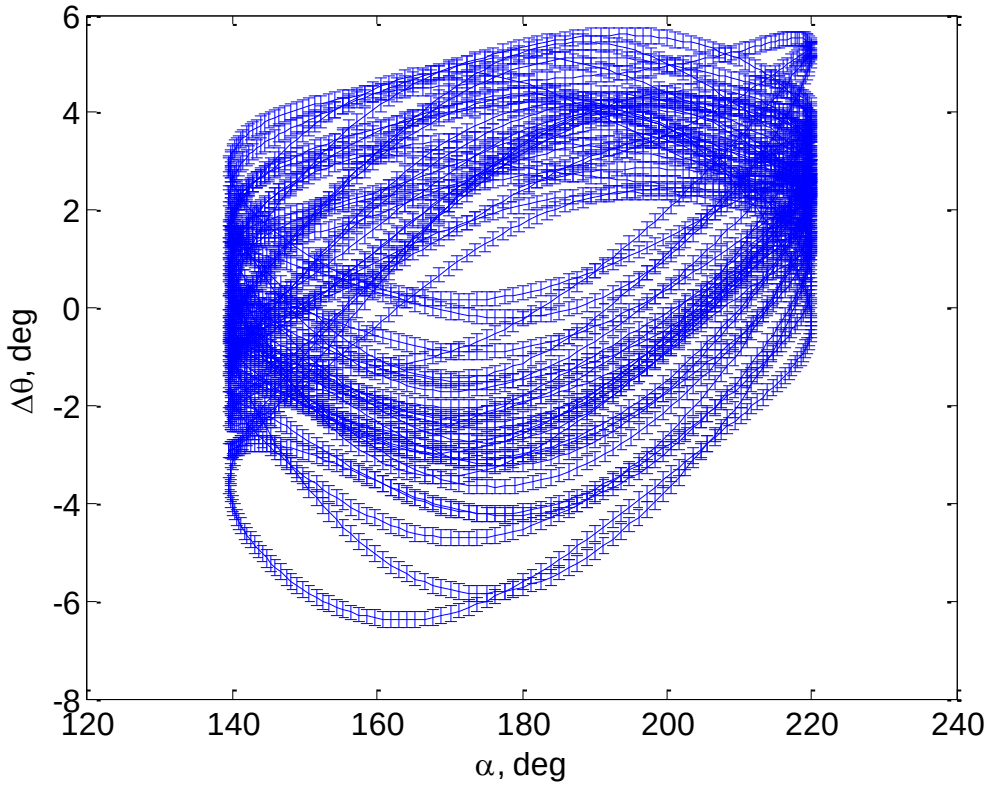

Figure 4-25: Δθ versus angle of attack with positive and negative uncertainties.

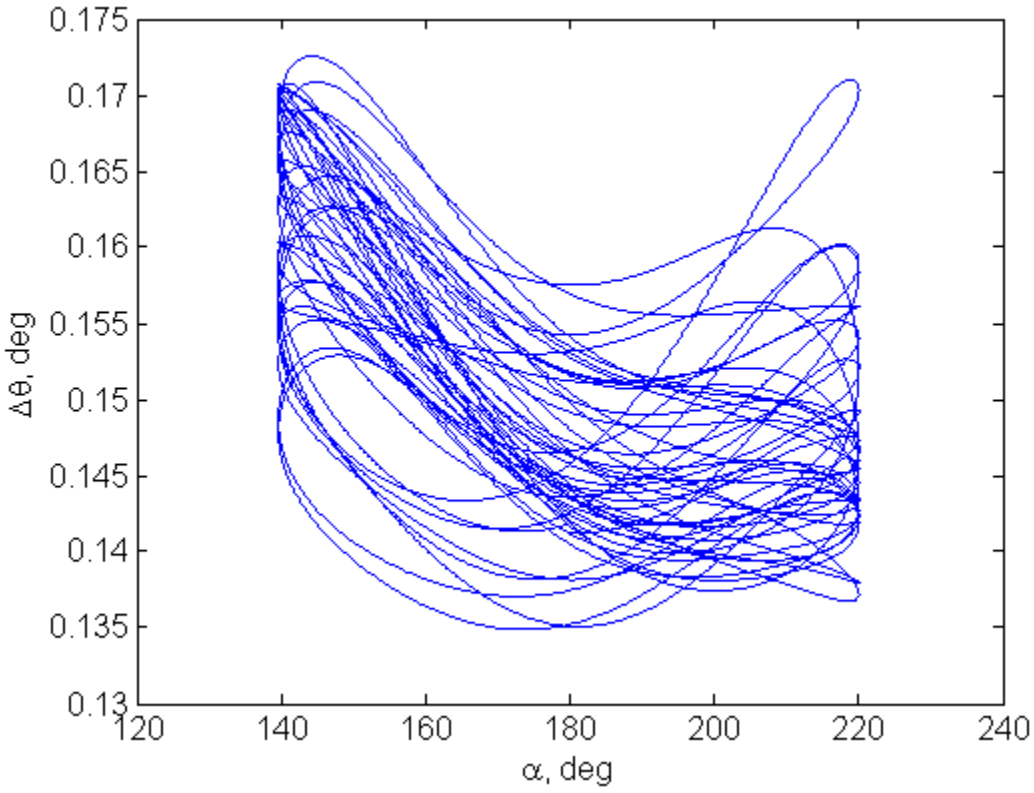

Figure 4-26: Uncertainty of Δθ versus angle of attack.

Chapter 5

Summary and Conclusions

Currently, simulation predictions using DSS and other high-fidelity simulations of the Orion Crew Module (CM) with drogue parachutes deployed are under-predicting the amount of damping as compared to free-flight tests. The Apollo Legacy Chute Damping model has been resurrected and applied to the Orion system. A key hypothesis in the Apollo legacy drogue damping analysis is that the drogue parachutes' net load vector aligns with the CM drogue attachment point velocity vector. This assumption is physically reasonable and produces good results, but has never been quantitatively proven. A forced oscillation test of the CM with parachutes was conducted in the NASA Langley 20-Ft Vertical Spin Tunnel (VST) to gather additional data to validate and refine the Apollo legacy drogue model. A second loads balance was added to the original Orion VST model to measure the drogue parachute loads independently of the CM.

The wake of the CM influences the drogue parachutes, which makes performance predictions of the parachutes difficult. Significant interactions exist between the CM and the drogue parachutes, which vary with CM angle of attack. Many of these effects are not currently modeled in the simulations, and what is modeled is not anchored to test data. The objective of the test was to identify the contribution of the drogues to CM damping and provide additional information to quantify wake effects and the interactions

between the CM and parachutes. The rate damping characteristics of the CM-drogue chute system were quantified in the form of dynamic derivatives using the forced oscillation technique. The riser line force vector was also measured to directly compare to the Apollo drogue model assumptions. It is believed that this is the first time since the Apollo program that dynamic aerodynamics of an integrated capsule-drogue system have been measured directly.

The wind tunnel test results show that the CM-drogue system is dynamically stable at most combinations of frequency and amplitude. The drogues have a relatively constant damping effect from an angle of attack of 144° to 180°. Below 144°, the drogues significantly increase their damping capability. Aerodynamic damping decreases from one drogue versus two, as expected. The data show the importance of capturing dynamic derivatives at the correct oscillation frequency and angular rate, as the damping values are impacted by those dynamic scaling parameters. A non-zero sideslip angle of 10° causes an insignificant change in drogue line force and total system damping. Pitch and yaw damping values are similar near trim attitude, but pitch damping dramatically increases as angle of attack departs from trim, whereas yaw damping only slightly increases. This difference is due to the drogues being attached on the axis of rotation for yaw motion and offset from the axis of rotation for pitch motion. Additionally, it was shown that the drogues have little upstream influence on CM aerodynamics (either statically or dynamically).

The wake of the CM reduces the drogue riser line force due to the reduced wake dynamic pressure by approximately 14% near the trim angle of attack for two drogues and 6% for one drogue. The drag reduction is a strong function of CM angle of attack. The parachute drag loss measurements obtained in this test are significant because the drag loss variation with angle of attack used in simulations are not currently anchored to test data. These results may be used to aid in anchoring those data tables. Also, the drag loss affects the restoring moment provided by the drogue parachutes, so it is important to accurately model that force.

The experimentally-obtained static pitching moment contribution from the drogue parachutes compares very well to the Apollo drogue model predictions. However, the magnitude of the damping derivatives obtained experimentally does not match the Apollo drogue model prediction. The Apollo drogue model predicts Cm_q values near -0.5 for the drogue parachute contribution. The wind tunnel test data shows values closer to -0.2 near the CM trim angle of attack.

Inspection of the drogue parachute riser line force vector revealed differences between the predicted vector and the experimentally obtained vector. The predicted angle of the riser line force vector relative to the freestream velocity vector, $\Delta\theta$, was modified using three parameters, time (or phase) shift, bias, and scale factor, in order to match the experimental data. These parameters are similar to a steady-state error, gain, and phase shift that are obtained from analyzing the frequency response of a linear time invariant system. These parameters indicate that the system is not entirely described by the Apollo

model equation. Potentially, a system identification technique could be used to further define the parachute behavior in terms of the CM motion.

A bias is evident in the forced oscillation and static wind tunnel data, and the bias is a function of angle of attack of the CM. The bias for one drogue parachute is greater than the bias for two drogue parachutes. This difference is caused by the single parachute settling into a region of the wake that is least turbulent. When two parachutes are in the wake, one of them will be pushed out of the region with less turbulent flow and cause the resultant force vector to align more with the freestream velocity of the CM. Evidence of this behavior is seen in video of the CM with two parachutes in the VST. One parachute remains relatively stationary in the CM wake, while the other oscillates at the same frequency as the CM. Evidence of this bias was seen in both the PA-1 test flight and the VST free-flight tests. The time lag, or phase shift, of the riser line angle relative to the freestream velocity is a function of CM angle of attack and oscillation frequency. The trend in phase shift is similar for one drogue parachute versus two. The scale factor trend is correlated to PRF, indicating that the angle of the riser line is a function of velocity in the wake of the CM, not the freestream velocity of the CM.

The drag of the drogue parachutes also exhibits a hysteresis effect. This effect is neglected in the Apollo drogue damping model, which assumes a constant drag of the parachutes. The effect is a function of the wake variation with CM angle of attack and the acceleration experienced by traversing the wake of the oscillating CM.

The variation and uncertainty of the Cm_q values was examined based on the unsteady nature of the drogue parachutes and the error due to balance accuracy. Uncertainty due to balance accuracy was determined to be negligible. However, the variation of Cm_q values due to the unsteady nature of the drogue parachutes does include the Apollo model predicted values, although marginally. If an uncertainty range was added to the experimentally obtained values that covered this variation, the Apollo values would lie within that range.

The drogue parachutes were shown to provide damping from both a drag hysteresis effect and out-of-phase riser line angle relative to the freestream velocity. Both the force and the angle are highly dependent on the CM wake characteristics. Based on these wind tunnel data, the Apollo Legacy Chute Damping model was determined to be a sufficient approximation of the parachute dynamics in relationship to the CM dynamics for preliminary entry vehicle system design. More wake effects should be included to better model the system.

These results will be used to improve simulation model fidelity of CM flight with drogues deployed, which has been identified by the project as key to a successful Orion Critical Design Review. The results could also be used to improve the preliminary design equations for reentry vehicles under drogue parachutes derived from the Apollo model. The understanding of CM wake effects on the drogue cluster was enhanced and will contribute to the reentry parachute community's knowledge base.

Appendix

Single Point Method of Calculating Rate Damping

Rate damping derivatives presented in this paper were calculated using the single point method on aerodynamic data collected with the forced oscillation technique. In the forced oscillation technique, the model is oscillated with a sinusoidal pattern at a given frequency and amplitude about a certain angle of attack. A strain gauge balance mounted in the model provides the forces and moments measured during these oscillations. In order to extract the forces and moments due to aerodynamic forces only, both a wind-off and wind-on run must be made. The wind-off run is called a tare. The tare captures the weight and inertia effects on the balance readings. The wind-on run contains the weight, inertia, and aerodynamic forces. At each angle of attack, the model is oscillated through a number of cycles. The balance signal is averaged over these cycles to obtain a mean cycle. The mean cycles from the wind-off tare and wind-on run are subtracted to isolate the aerodynamic forces needed to calculate the rate damping derivatives.

Figure A-1 shows the static aerodynamic pitching moment versus angle of attack and the forced oscillation pitching moment versus angle of attack. The model was oscillated about an angle of attack of 160° with an amplitude of 10°. The figure shows the rate-induced aerodynamics creates a hysteresis loop.

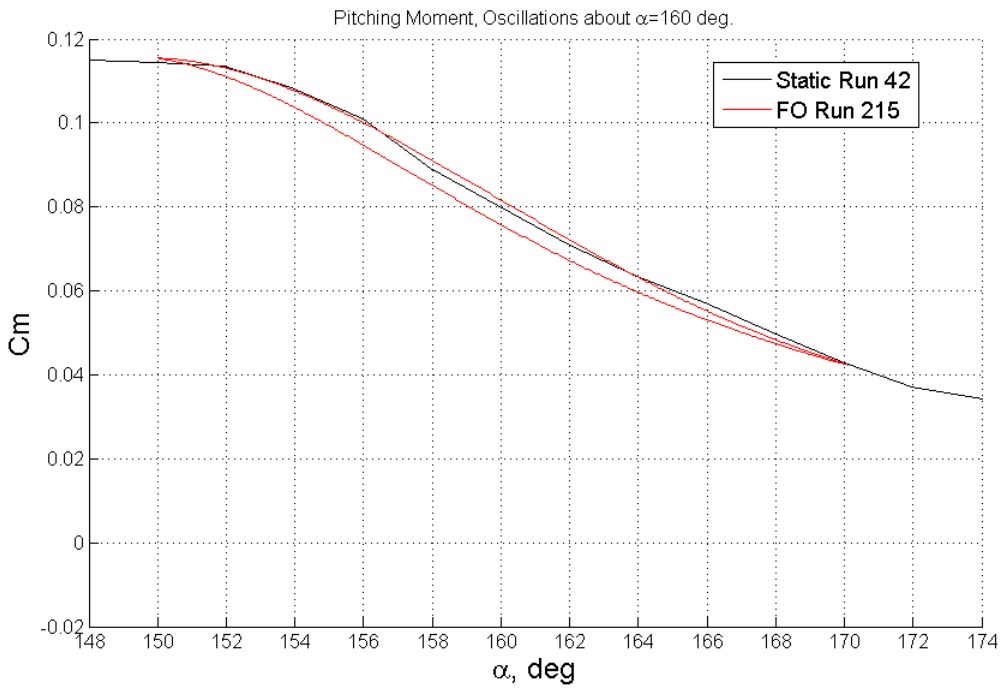

Figure A-1: Pitching moment for static and forced oscillation.

The single point method of calculating rate damping derivatives is based on the premise that the damping derivative can be calculated from linearizing the pitching moment from a forced oscillation run. This linearization concept is commonly used for stability and control characterization. The linearization is taken at the point of zero angular acceleration and the extrema of angular rate so that the damping derivative is due only to angular rate and not due to angular acceleration of the flow. For a sinusoidal motion, this occurs at the angle of attack the model is being oscillated about. In Figure A-1, this would be at an angle of attack of 160°. The damping derivative is calculated as in (A.1). The rate damping derivative is the summation of the aerodynamic forces due to the rate of change of angle of attack and pitch rate of the vehicle. These values are assumed to be the same in the wind tunnel. Points 1 and 2 represent the points of maximum and minimum angular rate and are shown in Figure A-2. $\hat{q}$ is the non-dimensional angular

rate, or $\frac{qL_{ref}}{2V}$. Since a delta is being taken, the static contribution to the aerodynamic pitching moment would be the same for each point, and, therefore, would cancel each other if included in the above equation.

$$\overline{C_{m_q}} = C_{m_{\dot{\alpha}}} + C_{m_q} = \frac{C_{m_2} - C_{m_1}}{\hat{q}_2 - \hat{q}_1} \tag{A.1}$$

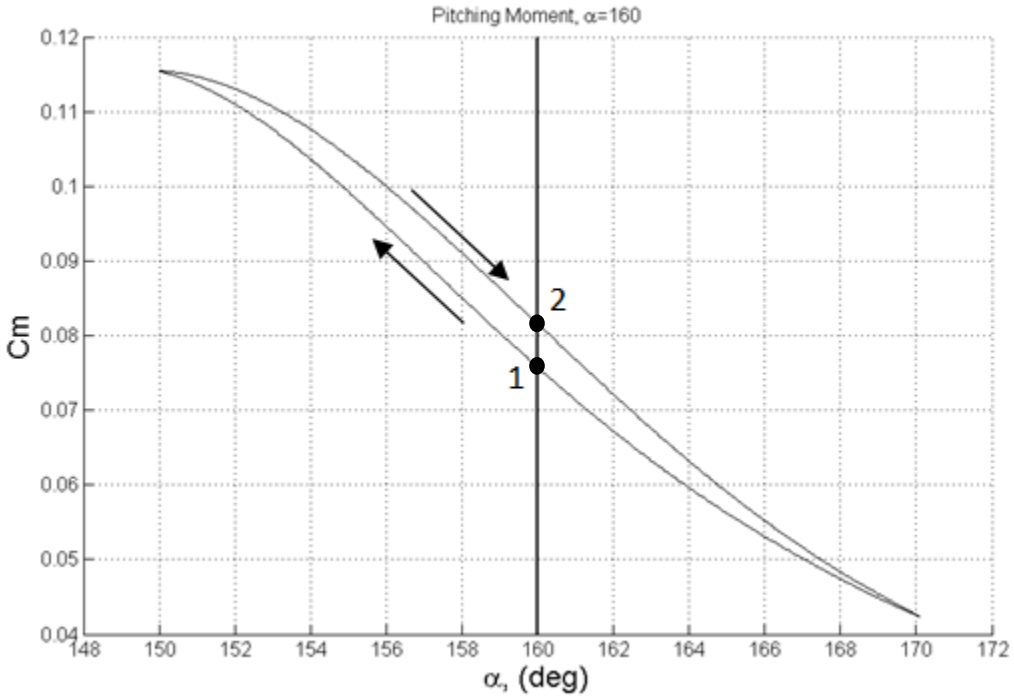

Figure A-2: Pitching moment hysteresis loop for single point method.

Bibliography

[1] "Exploration Systems Architecture Study Final Report," NASA TM-2005-214062, Nov. 2005.

[2] "Crew Exploration Vehicle Architecture Design Document," NASA CEV Document Number: CxP-72140, Jan. 2007.

[3] C. M. Fremaux, "Final Report for CEV Test 48-CD: Low Subsonic Dynamic Stability Test of the Orion Crew Module," NASA CEV Aerosciences Project Document Number: EG-CAP-08-122, June 2008.

[4] D. E. Hahne and C. M. Fremaux, "Low-Speed Flight Dynamic Tests and Analysis of the Orion Crew Module Drogue Parachute System," AIAA-2008-6391, Aug. 2008.

[5] D. B. Owens, S. E. Riddick, D. A. Matz and C. M. Fremaux, "IDAT Drogue Parachute Assessment in the NASA LaRC Vertical Spin Tunnel (VST) (Test 109-CD)," NASA CEV Aerosciences Project, 2010.

[6] P. A. Cuthbert, "A Software Simulation of Cargo Drop Tests," AIAA 2003-2132, May 2003.

[7] J. Idicula, P. S. Williams-Hayes and R. Stillwater, "A Flight Dynamics Perspective of the Orion Pad Abort One Flight Test," AIAA 2009-5730, Aug. 2009.

[8] K. M. Currin, J. D. Gamble, D. A. Matz and D. R. Bretz, "Evaluation of Drogue Parachute Damping Effects Utilizing the Apollo Legacy Parachute Model," AIAA 2012-3227, June 2012.

[9] "Data Report for Low Speed Wind Tunnel Tests of a 0.10-Scale Apollo Model (FDC-1) to Determine Dynamic Stability Characteristics of the Command Module and Drogue Parachute Combination," NASA CR-116641, Aug. 1963.

[10] D. B. Owens and D. Tomek, "18-CD Subsonic-Transonic Crew Module Dynamic Stability Test in the NASA LaRC Transonic Dynamics Tunnel," NASA CEV Aerosciences Program Document Number: EG-CEV-06-23, Feb. 2009.

[11] "20-Foot Vertical Spin Tunnel," NASA, 16 April 2008. [Online]. Available: http://www.aeronautics.nasa.gov/atp/facilities/vst/. [Accessed 27 April 2013].

[12] Orion Vehicle Simulation Data Book, CEV-MA-10-012: Orion Mission Analysis Department of Lockheed Martin Space Systems Company - Human Space Flight, 2010.

[13] K. J. Murphy, K. L. Bibb, J. B. Gregory, M. N. Rhode, D. B. Owens, D. T. Chan, E. L. Walker, J. H. Bell and T. M. Wilson, "Orion Crew Module Aerodynamic Testing - Invited," AIAA-2011-3502, June 2011.

[14] D. B. Owens and V. V. Aubuchon, "Overview of Orion Crew Module and Launch Abort Vehicle Dynamic Stability," AIAA-2011-3504, June 2011.

[15] D. B. Owens, J. M. Brandon, M. A. Croom, C. M. Fremaux, E. H. Heim and D. D. Vicroy, "Overview of Dynamic Test Techniques for Flight Dynamics Research and NASA LaRC," AIAA-2006-3146, June 2006.

[16] T. W. Knacke, Parachute Recovery Systems Design Manual, Santa Barbara, CA: Para Publishing, 1992.

[17] J. Becker, S. Johnson and T. T. Yechout, "Investigation of NASA Orion Wake Effects on Drogue Chute Aerodynamic Characteristics," AIAA 2011-2539, May 2011.

[18] "Capsule Parachute Assembly System (CPAS) Engineering Development Unit Operating Modeling Parameters Version 9," NASA Johnson Space Center, DRD CEV-G-036, JSC 65914 Revision D, April 2012.

[19] E. O. Doebelin, Measurement Systems: Application and Design, New York: McGraw-Hill, 2004.